CONSIDERATION OF STRUCTURAL AGEING IN THE DEVELOPMENT OF ANALYTICAL FRAGILITY FUNCTIONS

by

Onur Çevik

B.S., Civil Engineering, Istanbul University, 2020

Submitted to the Kandilli Observatory and Earthquake Research Institute in partial fulfillment of the requirements for the degree of

Master of Science

Graduate Program in Earthquake Engineering

Boğaziçi University

2023

ACKNOWLEDGEMENTS

I would like to express my gratitude to Professor Hancılar for his support, generosity, and patience throughout my studies. It was a unique experience being guided by him.

I would like to thank my former academic advisor, Dr. Karin Şeşetyan for her kindness, and guidance throughout my graduate education.

Lastly, I would like to thank The Scientific and Technological Research Council of Türkiye, 2211 national graduate scholarship program for their support.

ABSTRACT

CONSIDERATION OF STRUCTURAL AGEING IN THE DEVELOPMENT OF ANALYTICAL FRAGILITY FUNCTIONS

This study investigates the ageing effects led by the corrosion of structural materials on the fragility functions analytically derived for reinforced concrete moment-resisting frame type buildings which is the predominant typology in Türkiye. First, in situ and laboratory material testing results for 175 reinforced concrete buildings located in Istanbul, constructed between 1962 and 2004 with different heights and plan features are examined in order to better understand the level of corrosion and its spread in structural members. The level of corrosion and different ways it occurs is then implemented in structural analyses by altering the mechanical properties and constitutive models of materials with the data obtained from the experimental and numerical results in the literature. For this purpose, three-dimensional finite element models for low- and mid-rise buildings designed in accordance with the provisions of the 1975, 1997 and 2018 Turkish earthquake codes are elaborated. The responses of pristine and aged buildings are studied through nonlinear dynamic analyses under strong ground motion acceleration recordings selected and scaled to represent the level of seismic hazard in Istanbul. Multiple-stripe analysis and maximum likelihood method are implemented for the derivation of fragility functions. The results show that the behavior of structures aged by the effects of corrosion is a significant reduction in structural capacity and thus yields higher damage probability estimates by the derived fragility curves.

ÖZET

ANALİTİK KIRILGANLIK FONKSİYONLARININ TÜRETİLMESİNDE YAPISAL YAŞLANMANIN DİKKATE ALINMASI

Bu çalışma, Türkiye'de baskın yapı tipi olan moment aktaran çerçeve tipi betonarme binalar için türetilen analitik kırılganlık eğrileri üzerindeki yapısal malzemelerin korozyonunun yol açtığı yaşlanma etkilerini araştırmaktadır. İlk olarak, İstanbul'da bulunan ve 1962 ile 2004 yılları arasında inşa edilmiş farklı yapısal plan ve bina yüksekliğine sahip olan 175 binanın malzeme incelemesi yerinde ve laboratuvarda yapılan değerlendirmelerin sonuçlarından korozyonun seviyesi ve yapısal elemanlardaki dağılımı anlaşılmaya çalışılmıştır. Bu korozyon seviyesi ve oluşma şekli daha sonrasında deneysel olarak bulunan sonuçlar ile literatürdeki öneriler doğrultusunda malzemelerin mekanik ve yapısal modelleri değiştirilerek yapısal analizlerde kullanılmıştır. Bu amaç için, az ve orta katlı binaların sonlu eleman modelleri Türkiye Bina Deprem Yönetmeliği'nin 1975, 1997, ve 2018 versiyonları kullanılarak tasarlanmıştır. Yaşlanmış ve yaşlanmamış binaların incelenmesi ise İstanbul'daki deprem tehlike seviyesi düşünülerek seçilen ve ölçeklendirilen deprem ivme kayıtları altında doğrusal olmayan dinamik analizler ile yapılmıştır. Kırılganlık eğrilerini elde etmek için ise çoklu şerit analizi ve maksimum olasılık yöntemi uygulanmıştır. Sonuçlar, korozyon etkileri ile yaşlandırılmış yapıların yapısal kapasitelerinde önemli azalma göstermektedir, ve bu durum türetilen kırılganlık eğrilerinde yaşlanmış yapılar için daha yüksek hasar tahminleri vermiştir.

TABLE OF CONTENTS

LIST OF FIGURES

LIST OF TABLES

LIST OF SYMBOLS

a_0	Time constant
a_1	Time constant
b_f	Section width after corrosion cracking
b_o	Pristine section width
d_s	Diameter of corroded reinforcing bar
D_{Top}	Top (roof) displacement
D_u	Ultimate displacement
D_y	Yield displacement
$\mathbf{d}$	Diameter of pristine reinforcing bar
E_c	Modulus of elasticity of concrete
f_c^*	Peak concrete compressive strength after corrosion
f_{ck}	Characteristic compressive strength of concrete
f_y^*	Strength of corroded reinforcing bar
f_{yk}	Characteristic yield strength of steel
G_c	Shear modulus of concrete
$\mathbf{g}$	Gravitational constant
$\mathbf{k}$	Stiffness matrix
M_w	Moment magnitude
$\mathbf{m}$	Mass matrix
n_{bars}	Number of compression bar
p_{Sa}	Pseudo-spectral acceleration
Q_{corr}	Corrosion percentage of reinforcement
R_{JB}	Joyner-Boore distance
S_a	Spectral acceleration
S_d	Spectral displacement
u_{icorr}	Opening of each single corrosion attack
V_{s30}	Average shear wave velocity to a depth of 30 meters
w_{cr}	Total crack width

w_{rs}	Ratio of volumetric expansion
$\mathbf{w}$	Natural angular frequency
$\mathbf{X}$	Depth of corrosion attack
β_N	Newmark's integration factor
β	Dispersion of the intensity measure (standard deviation)
γ_N	Newmark's integration factor
ϵ_1	Average tensile strength
ϵ_{co}	Concrete strain corresponding peak compressive stress
ϵ^*_{co}	Post-corrosion concrete strain corresponding peak compressive stress
ϵ_u	Ultimate strain of pristine reinforcing bar
ϵ_{u^*}	Ultimate strain of corroded reinforcing bar
θ	Median of the fragility function
ν_c	Poisson's ratio
ξ	Damping ratio
ϕ	Standard normal cumulative distribution function

LIST OF ACRONYMS/ABBREVIATIONS

3D	Three Dimensional
EDP	Engineering Demand Parameter
IM	Intensity Measure
MIDR	Maximum Inter-story Drift Ratio
MRF	Moment-Resisting Frame
MSK	Medvedev–Sponheuer–Karnik
PGA	Peak Ground Acceleration
PGV	Peak Ground Velocity
TBEC	Turkish Building Earthquake Code
TS	Turkish Standards

1. INTRODUCTION

What are the fundamental causes that lead reinforced concrete structures to deteriorate over the years? Are the structures capable to meet performance criteria as they get aged? Although there are few answers to these questions, uncertainties on that topics increase attention. Reinforced concrete structures experience significant differences in their lifetime due to external or internal chemical effects, and there are many experimental studies showing that there is a degradation in the mechanical properties of materials in reinforced concrete buildings or structural members such as called in the literature "ageing" [1, 2].

Yet several effects are affiliated with ageing (e.g., freeze-thaw attack, the reactivity of aggregate, acid action, etc.), there is a consensus that corrosion (e.g., carbonation or chloride induced) negatively affects the durability of structures, and it is significantly higher than those, and the relationship of these two words, corrosion, and ageing, develops each other's cause-and-effect relationship as time progresses [3].

To evaluate and explain the impact of ageing for reinforced concrete structures, nonlinear modeling methodologies are available in the literature for the mechanical properties of materials [4-6], and time-dependent seismic assessments are conducted considering the degradation mechanisms of structural elements with models suggested [3]. As ages structure, deterioration begins clearer, and the process becomes irreversible. For reinforced concrete structural members, the corrosion process rests on three stages [1].

(i) Initiation stage,
(ii) Propagation stage,
(iii) Deterioration stage.

Corrosion initiation starts after the embedment of reinforcing bars into the concrete, and the progress ratio depends on corrosion type [1]. Corrosion propagation phase on the other hand, depends on corrosion types which are pitting corrosion, and uniform corrosion developing in the reinforcing bars [7]. There are a few studies concentrated on pitting and uniform corrosion effects on structural behavior in the literature [8, 9], but the analysis results show that the difference between the results is almost the same. Therefore, in this study, I focus on only uniform corrosion in this topic since in-situ and laboratory material tests are done for corroded reinforcing steel that all assumed and quantified their cross-sectional area were reduced uniformly. The reduction of area in reinforcing steel has numerous effects such as cracking of unconfined concrete, and decreasing ductility of confined concrete. The deterioration phase contains these secondary effects, and fragility analyses are performed along with probability-based earthquake demand assessments to analyze the modeled structures using nonlinear material models to investigate the ageing effects and to understand their behavior.

Fragility assessment is an essential instrument to represent the probability of reaching or exceeding a damage state for a given level of ground motion intensity and to understand the extent of nonlinear seismic demand such as maximum inter-story drift ratio, roof displacement, or plastic rotation. The most common examples of intensity measures (IM) are the peak ground acceleration (PGA), peak ground velocity (PGV), and the 5% damped spectral acceleration and displacement at the structure's first-mode period ($S_a(T_1,5\%)$, $S_d(T_1,5\%)$). In this study, multiple stripe analysis which is a wide-range nonlinear demand estimation practice and maximum likelihood method [10] are used to derive fragility functions for study buildings representing low-rise and mid-rise reinforced concrete buildings under selected ground motion excitation scaled to spectral acceleration and displacement values.

Moreover, as time passes, ageing is not seen as the only criterion causing decreased durability for structures since the design criteria become more complex and formidable leading to higher performance necessities, thus the buildings designed according to the earthquake-resistant building philosophy and theories of that day may

have difficulty meeting performance objectives. To investigate the effects of different design approaches, and understand better the behavior of study buildings, 1975, 1997, and 2018 provisions of Turkish Building Earthquake Codes are utilized in this study [11-13].

1.1. Evolution of Turkish Earthquake Code Regulations and Hazard Maps

Türkiye's first official earthquake design code was published in 1945, and with improvements, it is revised and published in 1947 after the destructive Erzincan earthquake occurred in 1939. The 1945 earthquake hazard map (Figure 1.1, after [14]) was promulgated in this period, and prepared according to the conditions of that time, but due to the insufficient historical seismicity information available or misinterpretation of the seismicity history, the earthquake map was divided into 3 regions considering possibly destructive earthquakes [14].

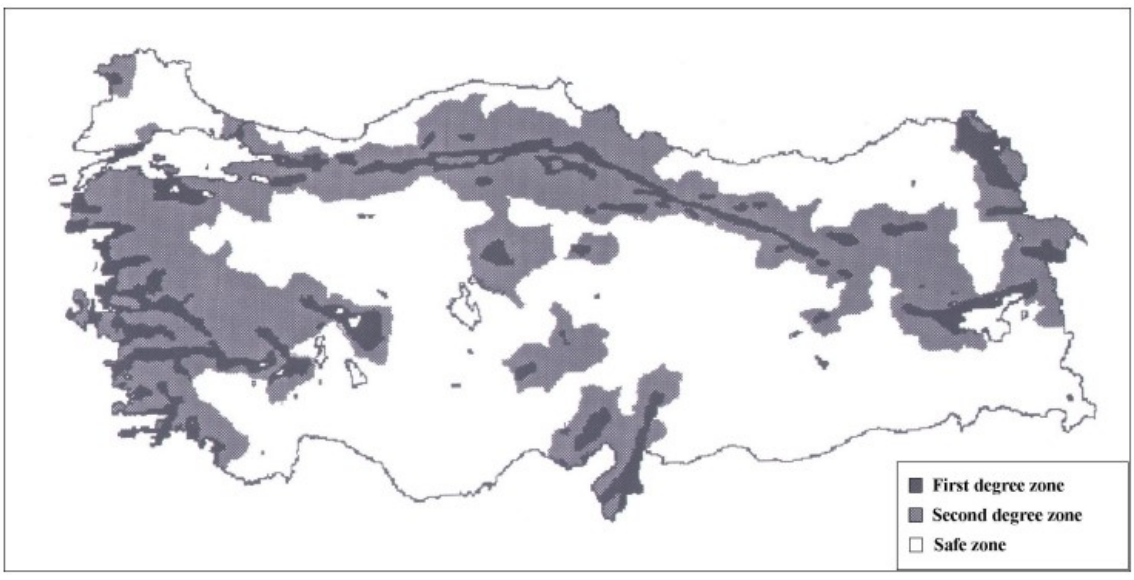

Figure 1.1. Seismic zonation map of Türkiye, 1945 [14].

After 1947, the earthquake code was revised in 1953 and 1961 with new rules such as load combinations and load coefficients. Using new earthquake data and seismotectonic maps, a second official earthquake zoning map (Figure 1.2, after [14]) that classifies Türkiye into 4 hazard zones was published in 1963 and used in the 1968 earthquake code. 4 hazard zones were defined according to the MSK scale [15] with maximum intensities greater than VIII (first zone), VII (second zone), equal to VI (third zone), and less than V (no hazard zone) [14].

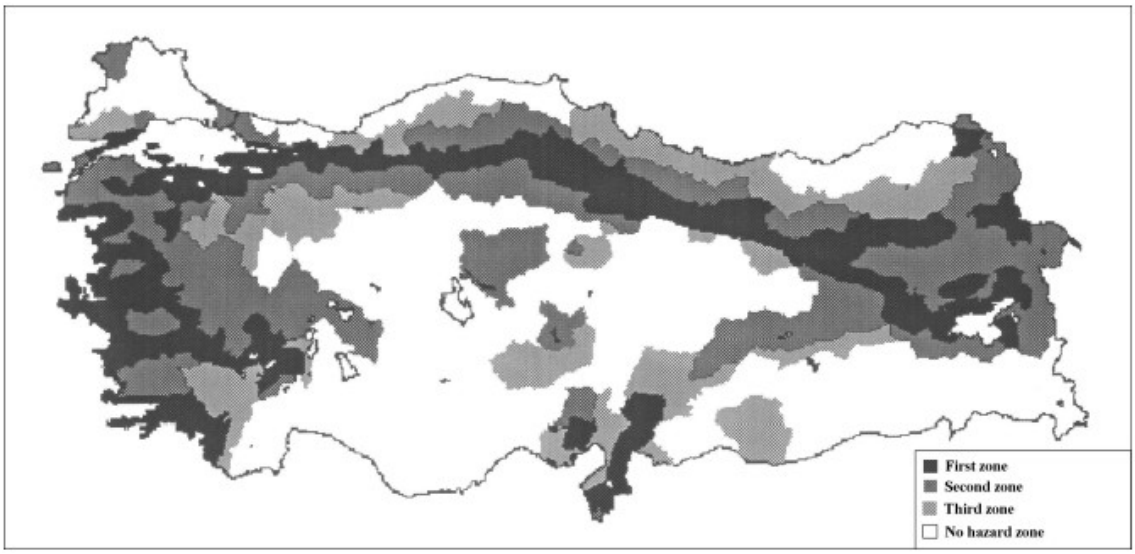

Figure 1.2. Seismic zonation map of Türkiye, 1963 [14].

At the 1968 Strasbourg meeting of the European Seismological Commission, the preparation of the third zoning map is determined due to the presence of discontinuities in areas, the occurrence of earthquakes in no-hazard zones, and abnormalities with the resolutions [14].

After 4 years, the 1972 zonation map (Figure 1.3, after [14]) was organized as 5 zones in terms of earthquake hazard. In the first-degree hazard zone, the maximum intensity (MSK) is higher than or equal to IX, in the second-degree hazard zone equal to VIII, in the third degree equal to VII, in the fourth degree equal to VI, and in the fifth degree no hazard zone equal to V [14].

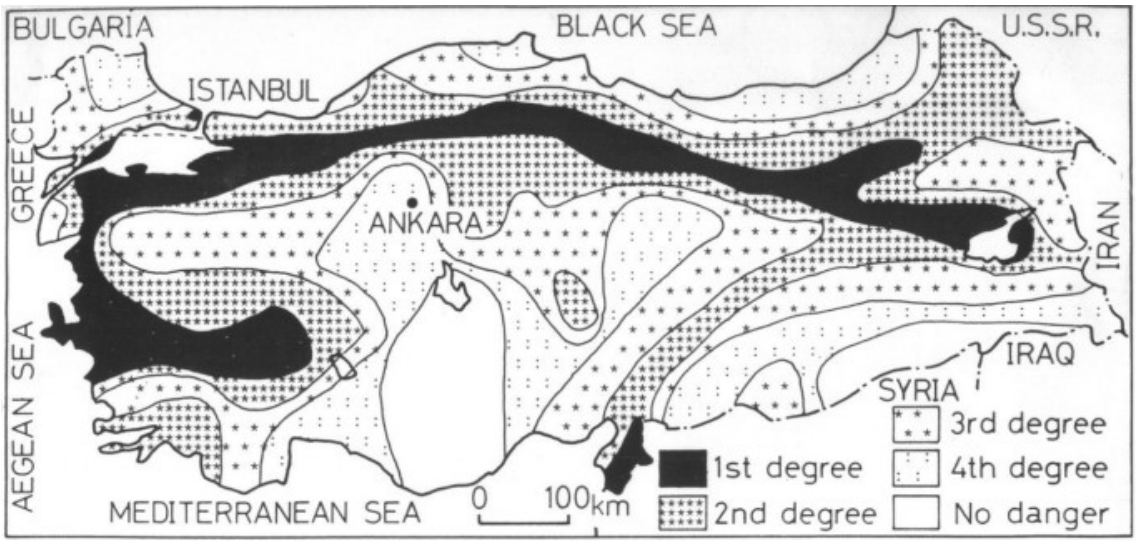

Figure 1.3. Seismic zonation map of Türkiye, 1972 [14].

In 1975, a new earthquake code was promulgated as "Specifications for Structures to be Built in Disaster Areas" (TBEC-1975). 1975 earthquake code is considered as the first modern earthquake code of Türkiye including more articulated necessities and approaches such as building importance factor, minimum cross-sectional dimensions for structural members for buildings built in earthquake-prone areas, minimum material strengths, minimum transverse reinforcement ratio and reinforcement placement for more detailed confinement to resist lateral loads, earthquake load distribution rules, soil effects in strong ground motion, and earthquake design spectrum and engineering calculations for nonstructural components.

The previous seismic hazard map of Türkiye was introduced in 1996, and it is also a zonation map dividing the country into five hazard zones considering PGA intervals. The fifth zone represents a PGA value lower than 0.1 g, the fourth zone represents a PGA value equal to 0.1 g and between 0.1 g and 0.2 g, the third zone represents a PGA value between equal to 0.2 g and 0.2 g and 0.3 g, second zone represents PGA value between equal to 0.3 g and 0.3 g and 0.4 g, and first zone represents PGA value between equal to 0.4 g and 0.4 g and 0.6 g [16]. 1996 seismic zonation map of Türkiye illustrated in Figure 1.4 [17].

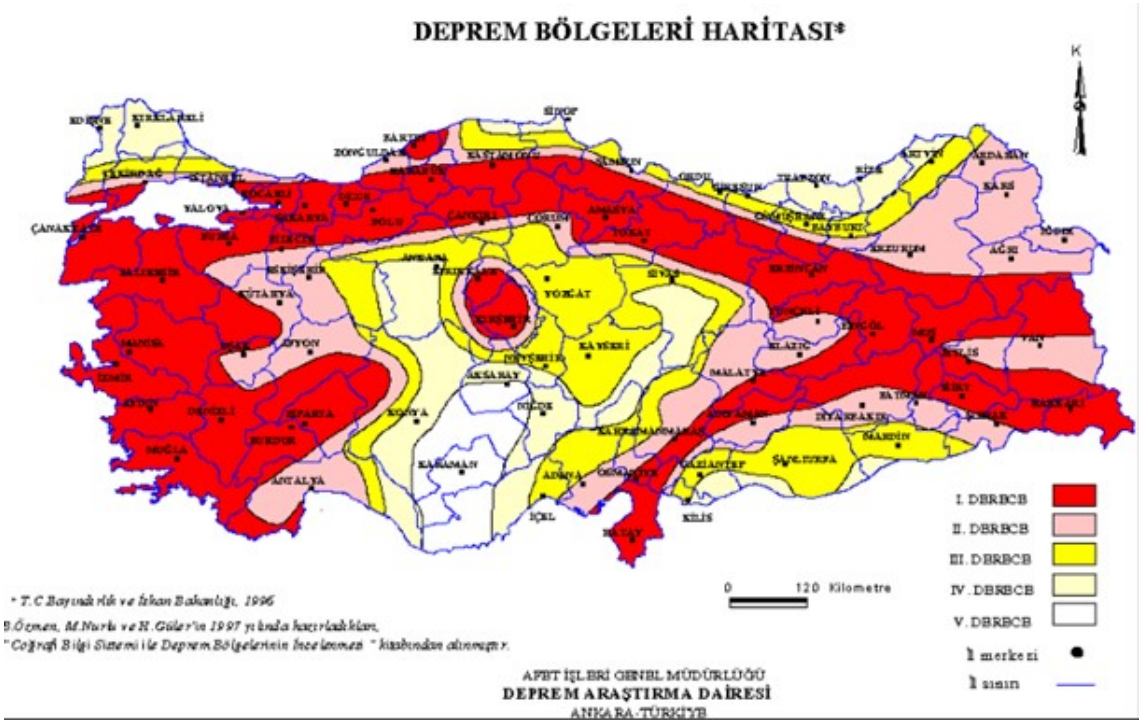

Figure 1.4. Seismic zonation map of Türkiye, 1996 [17].

After the 1996 hazard map was introduced, the new Turkish Earthquake Code was published as "Specifications for Buildings to be Built in Disaster Areas" in 1997 (TBEC-1997). 1997 earthquake code was more detailed including state-of-the-art rules by considering its time. New approaches include more complex rules such as capacity design principles, new design spectrum under given hazard level, earthquake load reduction factor, ductile design principles, over-strength factor, structural behavior factor, and new rules for confinement and reinforcement placing in beam-column joints.

The 1997 earthquake code was followed by the 2007 Turkish Earthquake Code as a provision of the 1997 code. The strengthening of existing buildings, nonlinear static and dynamic analysis procedures, and performance-based evaluation of buildings are example topics for improvement.

The current Turkish Seismic Hazard Map (Figure 1.5, after [18]) was introduced in 2018 in correlation with Turkish Building Earthquake Code-2018 (TBEC-2018). The

new seismic hazard map is a coordinate-based map, not a zoning map, and the hazard is expressed as a spectral value, not a PGA. The lateral elastic design spectrum can be obtained also for various options in terms of hazard levels, such as different earthquake return periods, and for different soil types. In addition, the lateral elastic design spectrum does not have a peak value of 1 g as the spectra introduced in other regulations. Current earthquake-resistant design code provides wide area options for building design ranging from low-rise to high-rise buildings with heights over 105 meters, different building performance levels, design performance targets, and design procedures, stiffness modifiers for structural elements, nonlinear design procedures and options, base-isolated building design are some examples.

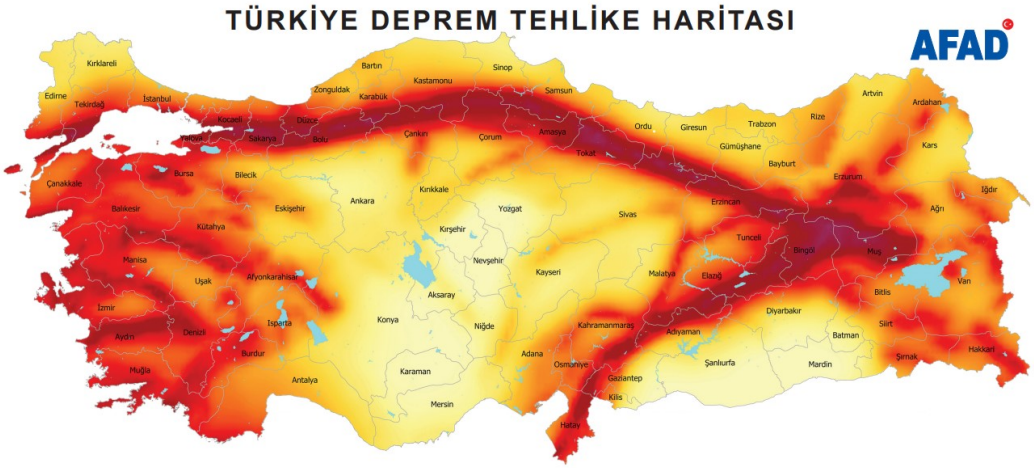

Figure 1.5. Seismic hazard map of Türkiye, 2018 [18].

1.2. Seismic Fragility Relationships

Fragility curves represent the cumulative probability of reaching or exceeding a certain damage state for different levels of a ground motion intensity measure. There are 4 types of fragility functions which are judgemental, empirical, analytical, and hybrid to assess the relationship. Judgemental fragility functions depend on the expert's opinion when analytical or observational data are not available. It relies on the engineer's expertise, and it should be emphasized the functions obtained accordingly

depend on this proficiency [19].

Empirical fragility functions, on the other hand, depend on observational data from earthquakes to estimate structures' performance for future events. Since empirical fragility functions are based on observational data acquired after earthquakes, they are significantly useful approaches that can be used to understand future results [19].

As can be understood by the name, hybrid fragility assessment is an evaluation method based on the use of certain methods together, the simultaneous analysis of empirical data with analytical data, the observation of a real building, and the understanding of the analytical results resulting from the numerical modeling of that structures [19].

Analytical fragility functions are built upon the mathematical models and give area to work on the different types of structural form. To assess the fragility of buildings, analytical fragility functions involve computational effort substantially, however; it decreases uncertainties if it is compared to other methods by using engineering-based modeling methodologies [19]. Moreover, it can be used for various and complex structures; thus, it allows to assess different types of buildings designed with different material types (e.g., ageing structures).

However, it is also known that there are a lot of uncertainties when deriving analytical fragility functions. Uncertainties in this regard are usually those arising from the ground motion selection and scaling, analysis methodologies and their validity, and the response of structures [20]. Especially capacity levels of structures and their damage state estimations for analytical models have been complicated issues in this regard. Although the appraisal of the capacity of the structures is largely understood today, it is still the subject of research the selection of the convenient damage measures for limit states for the evaluation is important for performance objectives in performance-based evaluation procedures [21].

In addition, the dynamic analysis methods which can be categorized into narrow-range and wide-range for obtaining analytical fragility functions and their verifications still contain uncertainties [21]. Narrow-range methods measure the demand over a small area of intensity measure values in contrast to wide-range methods. For example, single-stripe analysis, and cloud analysis can be mentioned. Single stripe analysis is a dynamic analysis method with a certain level of IM level with a set of ground motions. Cloud analysis, on the other hand, is a procedure where the structure is subjected to different IM levels corresponding to the first period of structure with certain ground motion records [21].

Wide range analysis methods, conversely, is a process to estimate the demand and response of structures over a wide range of IM levels with a set of ground motion records [21]. Wide-range analysis procedures can be classified into two as multiple-stripe analysis and incremental dynamic analysis [22]. Multiple-stripe analysis is a dynamic analysis procedure using a wide range of IM levels (e.g., spectral acceleration) and a set of ground motions to scatter structures' responses to provide statistical information. To do that, ground motions are scaled into a first or desired period of structures in certain IM levels.

Incremental dynamic analysis, on the other hand, can be described as dynamic pushover analysis addressing the capacity and demand of structures. In the incremental dynamic analysis procedure, each ground motion record is scaled to multiple IM levels, and the resulting maximum engineering demand parameter (EDP) (e.g., inter-story drift ratio) is calculated in each case to observe the collapse situation of the structure [21].

1.3. Structural Limit States

Structural limit states are threshold levels for different damage cases (Figure 1.6, after [28]) (e.g., slight, moderate, extensive, collapse) for structural behavior defined in different ways. State variables are generally chosen as a displacement-based structural

response representing structures' dynamic and nonlinear behavior (e.g., roof displacement, maximum inter-story drift ratio) [21].

There are various options to estimate threshold levels to understand structural behavior based on pushover analysis or capacity spectrum method. Damage estimation from pushover and capacity curves generally depends on element-based approaches measuring plastic rotation or concrete and steel strain in structural members. Yet, there are few suggestions in the literature to understand damage threshold levels from the global behavior of structure [11,12], [23-30].

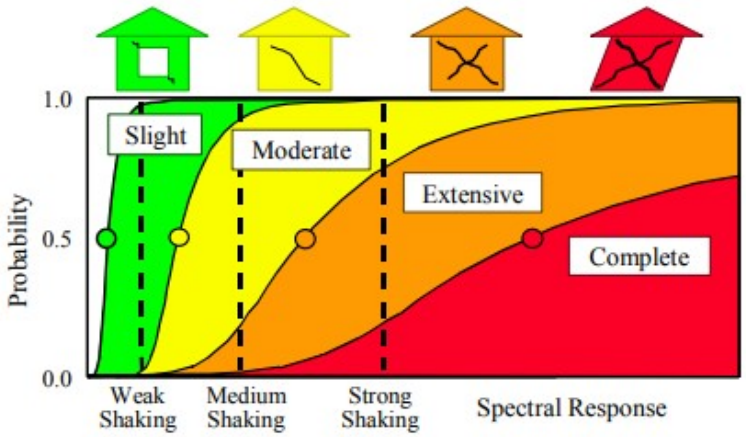

Figure 1.6. General damage levels for structures [28].

1.4. The Scope of the Thesis

General objectives of the thesis are:

(i) To develop low-rise and mid-rise structural systems designed with different earthquake design philosophies,

(ii) To investigate the design methodologies for ageing structures and model them according to literature's suggestions,

(iii) To implement nonlinear static and dynamic analyses procedures to understand the global performance of structural systems,

(iv) To derive analytical fragility functions to assess the behavior of pristine and ageing structures,

(v) To reach conclusions on the effectiveness of the methodologies conducted in this research, and suggest new directions from findings.

1.5. Thesis Outline

This study includes seven chapters. Chapter 1 presents a general introduction and a brief overview of the Turkish Building Earthquake Code evolution. Terminology about ageing mechanism and its effects on structural materials is given in Chapter 2. Studied buildings, design and modeling methodologies, and nonlinear modeling details are provided in Chapter 3. Chapter 4 presents the ground motion selection and scaling process in detail. The details of the probabilistic earthquake demand analysis, the methods used to obtain the fragility curves and the details about the structural damage limit levels, and the analysis results are presented in Chapter 5. Chapter 6 contains the comparative results of the fragility curves of pristine and aged buildings. In Chapter 7, the findings are summarized, areas for improvement are mentioned, and suggestions for future research are made.

2. AGEING OF STRUCTURES

2.1. Terminology

Structures age with chemical or physical effects that they are exposed to over the years depending on different factors and this ageing can be interpreted as a reduction in strength, and a decrease in displacement capacity. Although these ageing effects involve a great deal of epistemic uncertainty, experimental and numerical approaches are used to understand them. In reinforced concrete structures, the principal of these factors is corrosion.

According to the Oxford Dictionary, corrosion is described as "the process of destroying something slowly, especially by chemical action; the condition that results from this process". But why does this corrosion occur? What is the cause of corrosion in reinforced concrete structures? Understanding the answers to these questions is correlated with understanding the ageing of structures. To figure out this, it is necessary to mention the chemical process leading to this issue. According to fib [3], there are two major factors that led to corrosion which are carbonation-, and chloride-induced corrosion.

Carbonation-induced corrosion is the increase of carbon dioxide in the air as a result of the rise in air pollution and its chemical interaction with the concrete, resulting in the moistening of the concrete, and this moisture reacts with the reinforcement and causes corrosion [31]. This situation depends on whether the structural element is an indoor or outdoor element that is related to interaction with the air, the carbon dioxide ratio in the atmosphere, and changes depending on the geometric properties of the cover concrete [3].

Chloride-induced corrosion, on the other hand, is an issue for reinforced concrete structures located in a water environment [32]. When concrete interacts with chlorides,

the ions of chloride can pass through the voids of the concrete and react chemically with reinforcement ending up with corrosion [31]. The ingress of chloride generally depends on the cover concrete depth, concrete age, and environmental factors [3].

Reinforced structural members contain three parts: cover concrete at the outer side, core concrete at the inner side, and reinforcement steel. One of the most important functions of cover concrete is to prevent corrosion of the structural steel. But concrete also contains voids and moisture, and it causes corrosion also. However, the pH value of the concrete leads to a passive layer forming on the steel surface; thus, it reduces the rate of corrosion over the years [33].

Structural steel, which is the most significant factor of corrosion in reinforced concrete elements, affects all these three conditions causing capacity and displacement reduction, and that is, ageing of the structures. However, whether carbonation-induced or chloride–induced, the chemical processes are the same for reinforcing steel. When corrosion starts, steel gives up its electrons first [33].

$$Fe = Fe^{2+} + 2e^{-} \tag{2.1}$$

This expression is an example of an anodic reaction meaning a metal element gives up its electrons and becomes positively charged metal ions. However, according to chemical principles, these electrons must react again, in other words, they should be consumed.

$$2e^{-} + H_2O + \frac{1}{2}O_2 = 2OH^{-} \tag{2.2}$$

Total reaction paths to the rust produced by corrosion.

$$Fe^{2+} + 2OH^{-} = Fe(OH)_2 \tag{2.3}$$

When rust occurs, it leads to volume expansion in steel compared to virgin material state, thus; breaks cover concrete, reduces its strength and ductility of concrete material, and decreases its material properties with respect to pristine stage [2]. It

also causes to deterioration in the confined concrete, especially in terms of ductility. This situation is examined at certain stages which are the initiation stage, propagation stage, and deterioration stage [1].

Corrosion initiation stage depends on the types of corrosion which are classified as carbonation-induced and chloride-induced corrosion. It must be stressed that poor laboring in the construction process, external factors such as the use of sea sand in the concrete mixture or oxidation of steel waited outside as in undeveloped areas is a situation known for deterioration where the theoretical and experimental equations still cannot explain the long-term response of the structures.

On the other hand, the corrosion propagation phase depends the type of corrosion developing in reinforcement bars. Past studies on this phase show that there are two main forms of corrosion in reinforcement that are pitting corrosion and uniform corrosion [7]. Uniform corrosion is a general rebar loss over the perimeter of reinforcement bars. Unlike uniform corrosion, pitting corrosion results in a reduction of the reinforcement area at certain locations (Figure 2.1, after [7]).

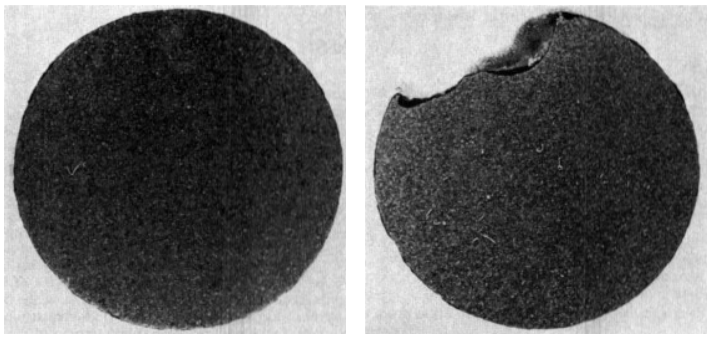

(a) (b)

Figure 2.1. Forms of corrosion in reinforcing bars (a) uniform corrosion, (b) pitting corrosion [7].

The deterioration phase is a stage entailing mechanical changes in the structural elements and deterioration in material properties in unconfined and confined concrete

material models. However, although the literature can explain the effect of reinforcement corrosion on unconfined concrete, its effect on confined concrete is still a subject of research.

2.2. Degradation Mechanism of Reinforcement Steel

The degradation of reinforcement steel is a result of corrosion causing significant strength and ductility loss in the mechanical property of the material [4,5], [36]. The quantification of corrosion ratio in reinforcement steel either can be detected by weight loss or diameter loss. Diameter loss is expressed as

$$Q_{corr} = 1 - (d_s/d)^2 \tag{2.4}$$

where Q_{corr} is the corrosion percentage of reinforcement, d_s is the diameter of non-virgin corroded rebar, and d is the pristine cross-sectional radius of rebar. Once the corrosion ratio is known, ductility and strength calculations can be done with Equations 2.5 and 2.6.

Du et. al. [4] investigated the reduction of the strength of reinforcement steel due to corrosion experimentally. According to his experimental study, corroded reinforcing bars may lose significant strength with respect to the pristine stage. Du et. al. [5] also examined the effect of corrosion on the ductility of rebars in concrete. Reduced strength and ductility post-corrosion expressed as

$$f_y{}^* = 1 - 0.005Q_{corr} \tag{2.5}$$

$$\epsilon_{u^*} = (1 - 0.05Q_{corr})\epsilon_u \tag{2.6}$$

where $f_y{}^*$ is the strength of corroded reinforcing bars, ϵ_{u^*} is the ultimate strain of corroded reinforcing bars, and ϵ_u is the ultimate strain of virgin reinforcing bars.

2.3. Degradation Mechanism of Unconfined Concrete

The explanation of the degradation of a concrete structure by corrosion is a complex phenomenon involving multiple reasons. As described, corrosion leads to the loss of the rebar cross–section transformed into rust. Generally, the volume of rust and steel is greater than the volume of virgin steel which causes dilatation in the bar, and a cracking in the concrete as a result (Figure 2.2, after [2]) [2,37].

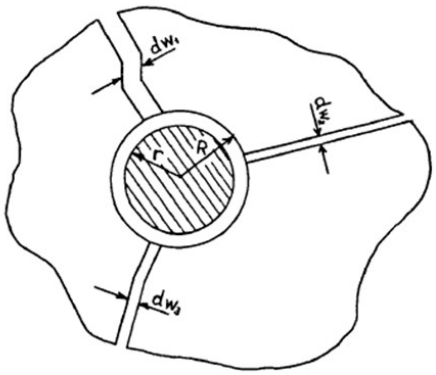

Figure 2.2. Cracking of concrete due to dilatation of reinforcing steel [2].

According to Coronelli and Gambarova [6], this mechanism can be described with a numerical solution given as

$$w_{cr} = \Sigma_i u_{icorr} = 2\pi(v_{rs} - 1)X \tag{2.7}$$

$$b_f - b_o = n_{bars} - w_{cr} \tag{2.8}$$

$$\epsilon_1 = (b_f - b_o)/b_o \tag{2.9}$$

$$f_c* = \frac{f_c}{1 + (\kappa\epsilon_1/\epsilon_{co})} \tag{2.10}$$

where v_{rs} is volumetric expansion rate of the oxides with respect to the pristine material taken as 2 as in [2], X is corrosion attack depth, u_{icorr} is the opening of each corrosion attack. On the other hand, n_{bars} represents the number of compression bars, b_o and b_f section width in the pristine state, and width increased by corrosion cracking (Figure 2.3, after [6]), respectively, ϵ_1 is average tensile strength, and ϵ_{co} is the strain

corresponds to the peak compressive stress.

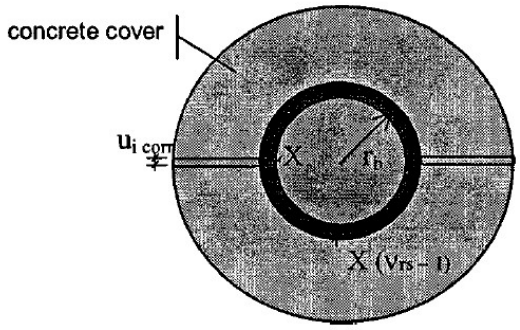

Figure 2.3. Corrosion build-up and total corrosion cracking around a bar [6].

The post-corrosion strength of unconfined concrete is decreased significantly compared to the virgin state. This problem causes an uncertainty in the stress-strain curve, and it is treated by Equation 2.11

$$\epsilon_{co}^{*} = 0.001(f_c^{*})^{0.25} \tag{2.11}$$

where ϵ_{co^*} and f_{c^*} is the strain at peak post-corrosion compressive stress and post-corrosion compressive strength [38].

2.4. Degradation Mechanism of Confined Concrete

The stress-strain model of confined concrete is influenced by the volumetric ratio of transverse reinforcement, and mechanical properties of reinforcing steel and concrete effectively. In the deterioration process, before longitudinal bars, confinement bars are ruptured due to the close distance to the concrete surface in a corroded environment, and this situation increases uncertainties [39]. Yet there are few experimental studies related to this issue [40-44], and there is a lack of data about corroded confined concrete results for reinforced concrete structural members; therefore, there is no complete solution. I approach this problem by changing the confined concrete stress-strain model by altering the mechanical properties of steel, and it paths to decreased ductility on the confined concrete model significantly.

2.5. Ageing and Corrosion: A Numerical Study

Reinforced concrete moment-resisting frame type buildings constitute 82.5% of the Istanbul building inventory consisting of approximately 1.2 million buildings of which 66% low-rise and 32% mid-rise structures. Construction year-wise classification of the inventory yields that 22%, 46%, and 32% of the buildings fall in pre-1980, 1980-2000, and post-2000 year bands respectively. For the consideration of ageing effects on the structural behavior and response, I evaluate the data including 1216 samples taken from 175 existing buildings in Istanbul. The construction year of these buildings varies between 1962 and 2004, and the sample data come from buildings with different heights and different plan configurations. Figure 2.4 illustrates the number of buildings studied and the years between which they were built.

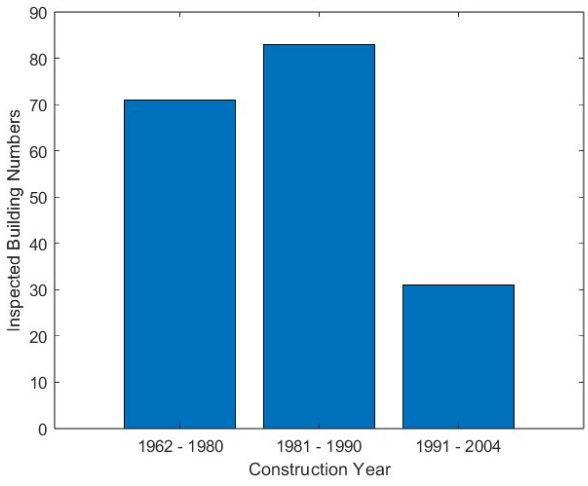

Figure 2.4. Distribution of the number of buildings with respect to their construction years.

Once the values of the amount of corrosion obtained from the 1216 samples are grouped based on the construction years of the examined buildings, the average corrosion rate is found to be 10%, and the average age of the buildings examined is deduced to be 40-year-old approximately. Figure 2.5 shows the variation of corrosion ratios as an amount of loss in the reinforcing bar diameter with the construction years

of the examined buildings. These data are presented as the mean of the data in the same group.

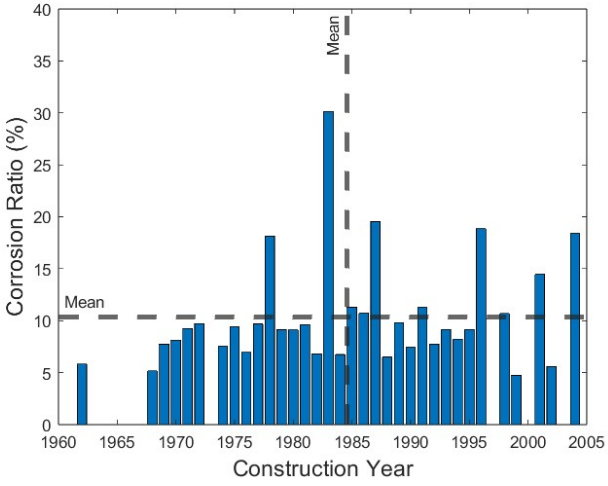

(a)

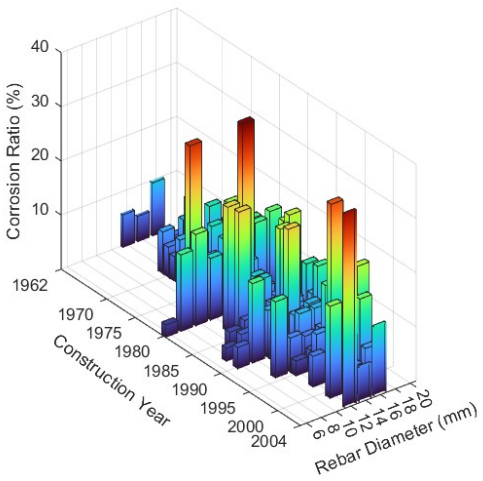

(b)

Figure 2.5. Variation of the corrosion ratios (a) with mean ratio from each construction year of buildings, (b) with construction year of buildings and reinforcing bar diameters.

3. DESCRIPTION OF STUDY BUILDINGS

3.1. Structural Plan and Configurations

In order to represent the low- and mid-rise building classes in Istanbul inventory, 3-story and 6-story buildings which are designed based on the requirements of the 1975, 1997, and 2018 Turkish Building Earthquake Codes are considered. Structural plans and the size of cross-sectional dimensions of structural members are taken from actual buildings described in Senol and Onder [45,46]. Each building is located in Kadıköy, Istanbul, and every story height is 2.9 meters. The cross-sectional dimensions of each structural member are given in Table 3.1.

Table 3.1. Cross-sectional dimensions of structural members.

	3-Story Buildings	**6-Story Buildings**
Edge Columns	400x400 mm	700x700 mm
Interior Columns	500x500 mm	700x700 mm
Exterior Columns	300x300 mm-500x500 mm	600x600 mm-700x700 mm
Interior Beams	250x600 mm	400x600 mm
Exterior Beams	400x450 mm-500x450 mm	500x600 mm
Slab Thickness	150 mm	160 mm

Figures 3.1 and 3.2 illustrates the three-dimensional finite element models for 3-story and 6-story buildings respectively.

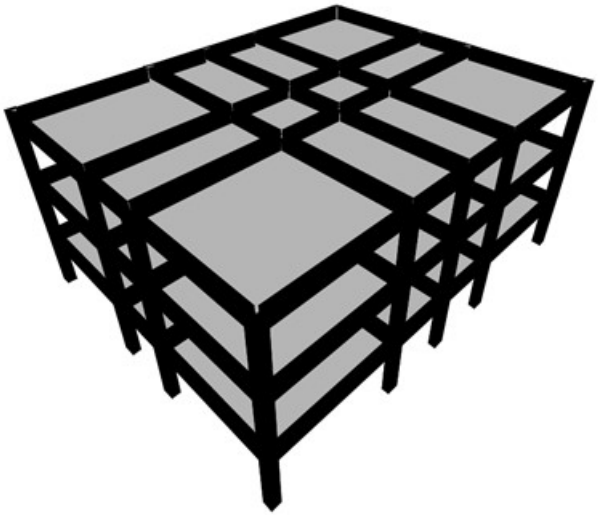

Figure 3.1. The 3D view of 3-story buildings.

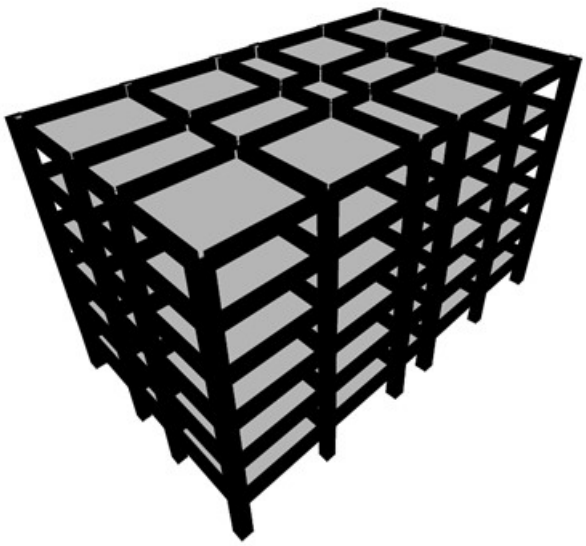

Figure 3.2. The 3D view of 6-story buildings.

3.2. Design and Nonlinear Modeling

Different provisions of Turkish Building Earthquake Code necessitate more articulated design approaches and higher performance criteria as time progresses. For each design process, ETABS [47] software is utilized with the guidance of TS500 [48,49] in accordance with the 1975, 1997, and 2018 provisions of Turkish Building Earthquake Code.

3.2.1. Materials

For each code, the minimum level of concrete classes is utilized. In all structures, as presented in Table 3.2, for TBEC-2018, C25 concrete class, for TBEC-1997, C20, and for TBEC-1975, C18 concrete classes are used with characteristic compressive strengths f_{ck}=25 MPa, f_{ck}=20 MPa, f_{ck}=18 MPa, respectively. The modulus of elasticity (E_c) and shear modulus (G_c) are calculated according to TS500 [47,48] and given in Equations 3.1, and 3.2 respectively. The Poisson's ratio of concrete (ν_c) is taken as 0.2, and the weight per unit volume of concrete (γ_c) is taken as 25 kN/m^3.

$$E_c = 3250(\sqrt{f_{ck}}) + 14000 \tag{3.1}$$

$$G_c = \frac{E_c}{2(1+\nu_c)} \tag{3.2}$$

Table 3.2. Minimum concrete and reinforcement classes considered in this study.

Code	f_{ck} **(MPa)**	f_{yk} **(MPa)**
TBEC-2018	25	420
TBEC-1997	20	420
TBEC-1975	18	220

3.2.2. Structural Members

To model structural elements, finite element model approach is utilized for each frame element (e.g., beams and columns) and shell element (e.g., slabs). In contrast to 1975 and 1997 codes, Turkish Building Earthquake Code-2018 requires cracked section analysis; therefore, stiffness modifiers are assigned to the members, and corresponding effective rigidity values are given in Table 3.3.

Table 3.3. Stiffness modifiers for reinforced concrete members [11].

Structural Wall-Slab (In-Plane)	**Axial**	**Shear**
Structural Walls	0.50	0.50
Basement Walls	0.80	0.50
Slab	0.25	0.25
Structural Wall-Slab (Out-of-Plane)	**Bending**	**Shear**
Structural Walls	0.25	1.00
Basement Walls	0.50	1.00
Slab	0.25	1.00
Frame Elements	**Bending**	**Shear**
Coupling Beams	0.15	1.00
Beams	0.35	1.00
Columns	0.70	1.00
Structural Walls (Equivalent Frame)	0.50	0.50

3.2.3. Gravitational Loads and Seismic Masses

Gravity loads which are dead and live loads are distributed uniformly to the slab elements, and non-structural wall loads are computed to beam elements. Dead loads are considered to be permanent at the buildings, while live load contribution is reduced while calculating the seismic masses, and contribution factors are taken as 1.00, and 0.30 respectively. Each building is designed with the same dead and live loads. Defined

loads are given in Table 3.4.

Table 3.4. Design loads.

Load Type	**Uniform Load** (kN/m^2)
Super-Imposed Dead Load	2.00
Peripheral Wall Load	4.325
Interior Wall Load	2.50
Live Load	2.00
Super-Imposed Dead Load (Roof)	4.00
Live Load (Roof)	1.50

3.2.4. Structural Models

Linear elastic models of the structures are computed based on the procedures described above and Turkish Building Earthquake Code guidance for 1975, 1997, and 2018 provisions. Buildings are named according to story number, and design codes, and Table 3.5 gives the fundamental natural periods of structures from free vibration analysis. Figures 3.3, 3.4, and 3.5 illustrate the first three mode shapes of each building with respect to 1975, 1997, and 2018 provisions of the earthquake code, respectively.

Table 3.5. Natural periods of buildings.

Building Name	**Mode 1 (s)**	**Mode 2 (s)**	**Mode 3 (s)**
3-story-2018 Code	0.5209	0.4907	0.4416
3-story-1997 Code	0.3859	0.3657	0.3384
3-story-1975 Code	0.3917	0.3711	0.3432
6-story-2018 Code	0.8093	0.7980	0.7396
6-story-1997 Code	0.5602	0.5523	0.5278
6-story-1975 Code	0.5687	0.5606	0.5356

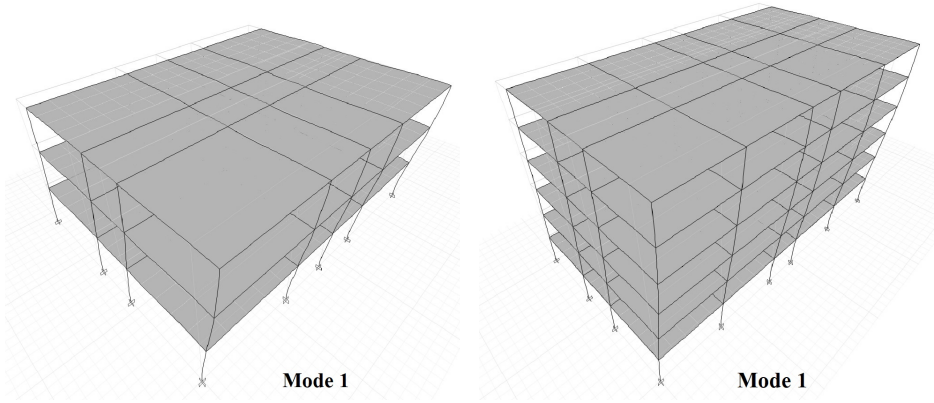

(a)

(b)

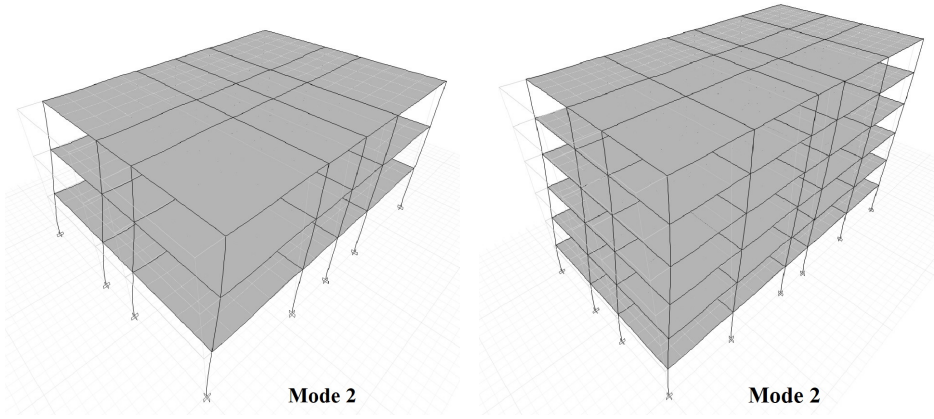

(c)

(d)

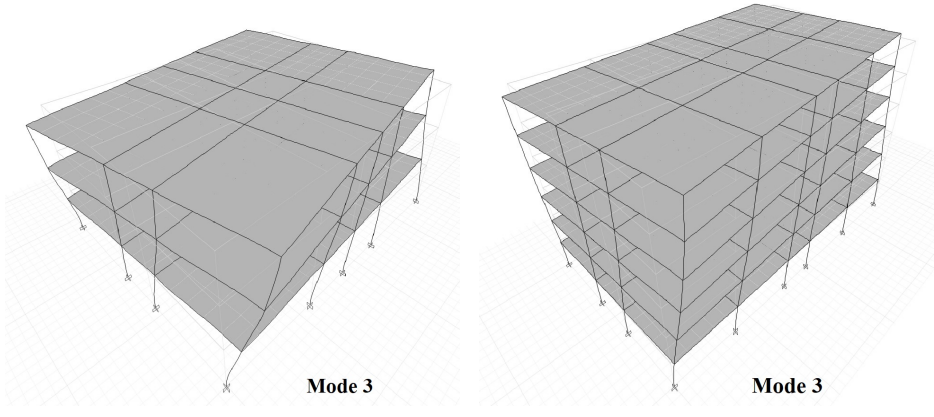

(e)

(f)

Figure 3.3. First three mode shapes of the buildings design in accordance with the 2018 code (a), (c), (e): 3-story buildings, (b), (d), (f): 6-story buildings.

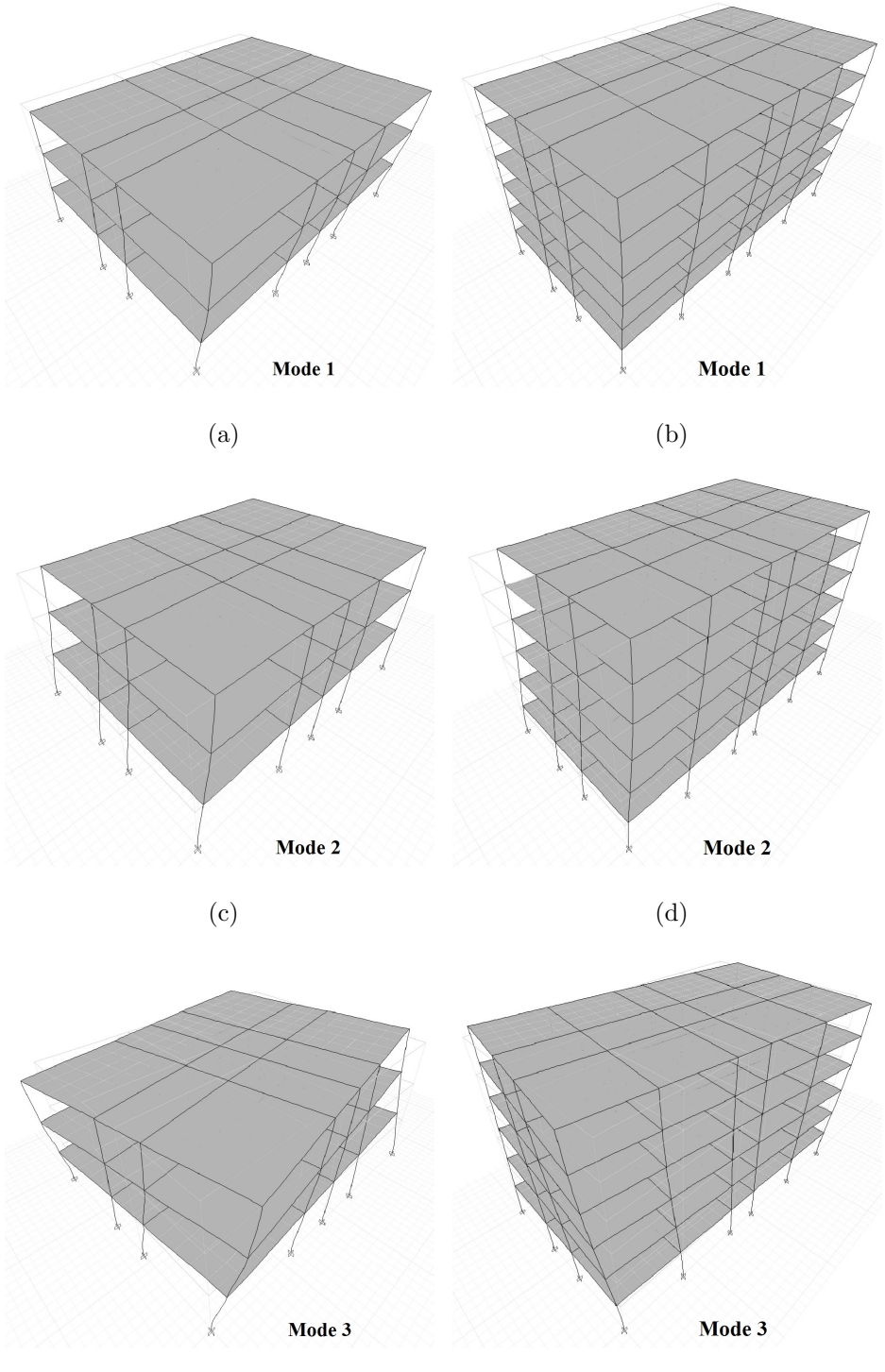

Figure 3.4. First three mode shapes of the buildings design in accordance with the 1997 code (a), (c), (e): 3-story buildings, (b), (d), (f): 6-story buildings.

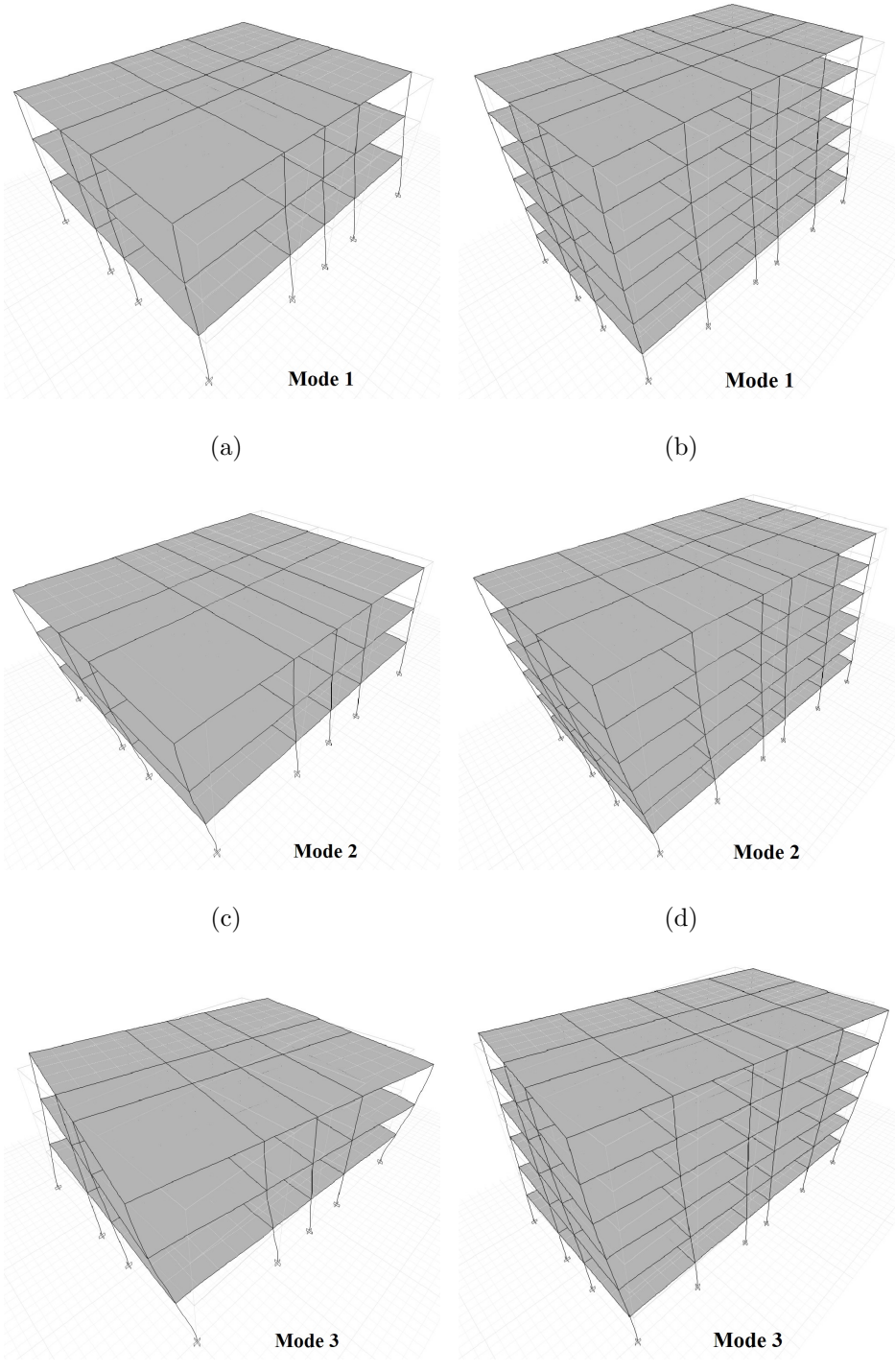

Figure 3.5. First three mode shapes of the buildings design in accordance with the 1975 code (a), (c), (e): 3-story buildings, (b), (d), (f): 6-story buildings.

3.2.5. Analysis Methodology for Preliminary Design

Structures are located in 40.990N, 29.050E, (Figure 3.6) and according to [45], shear-wave velocity to a depth of 30 meters (V_{s30}) is 666 m/s. 1997 and 1975 earthquake codes consider the location as 1^{st} and 2^{nd} degree earthquake-prone area respectively.

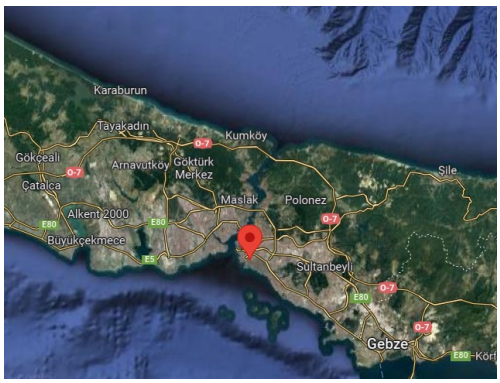

Figure 3.6. The location of buildings.

On the other hand, the 2018 earthquake code necessitates spectral coefficients which are acquired from the seismic hazard map when creating the 5% damped elastic design spectrum rather than zoning seismic areas. In line with this information and within the framework of code rules, design spectra are created and shown in Figure 3.7.

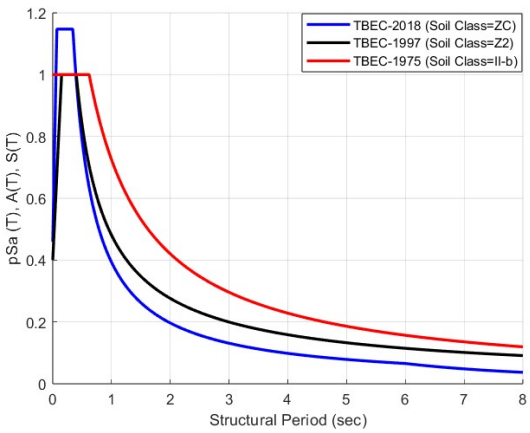

Figure 3.7. 5%-damped elastic design spectra for each code.

For the preliminary design of structural members, equivalent lateral force methodology is implemented considering accidental eccentricity. Additionally, slabs are modeled as rigid diaphragms, and each lateral load is applied to the diaphragms at the center of mass.

3.2.6. Nonlinear Modeling

Three-dimensional finite element models of the study buildings are elaborated in OpenSees [50] environment for nonlinear dynamic analysis. The inelastic behavior of the structural components is modeled with fibre sections which represent an idealization of nonlinear behavior along the element by numerical integration from uni-axial stress-strain relationships of individual fibres in the section [51]. Plane sections remain plane assumption is enforced. Geometric nonlinearities are taken into account for column elements, and fixed supports are defined to joints at the base level.

Buildings are modeled with beam and column elements only. Rigid diaphragms are assigned to each floor at the center of mass. Each slab element load is distributed to the beam elements, and the nodal loads are computed in accordance with the combination of dead and live loads. For material modeling, the uni-axial hysteretic constitutive model for reinforcing steel proposed by Menegetto and Pinto is used [52]. Popovic's concrete model is implemented for confined and unconfined concrete models [53]. An average of 10% uniform corrosion rate is taken into account in material constitutive models for aged buildings. The first two natural periods of 12 buildings designed with "nonlinearBeamColumn" elements are given in Table 3.6.

Figure 3.8 illustrates a section from 3-story building designed per TBEC-2018 consisting of reinforcing steel (black), unconfined (red), and confined (blue) concrete parts. Figure 3.9 on the other hand shows the stress-strain comparisons of pristine and aged materials for this given section to demonstrate the relationship better.

Table 3.6. Natural periods of pristine and aged buildings.

Building Name	**First Mode (s)**	**Second Mode (s)**
Pristine-3-2018	0.318	0.287
Pristine-3-1997	0.343	0.310
Pristine-3-1975	0.331	0.301
Pristine-6-2018	0.479	0.469
Pristine-6-1997	0.487	0.477
Pristine-6-1975	0.450	0.441
Aged-3-2018	0.338	0.313
Aged-3-1997	0.373	0.336
Aged-3-1975	0.360	0.327
Aged-6-2018	0.509	0.498
Aged-6-1997	0.517	0.507
Aged-6-1975	0.479	0.469

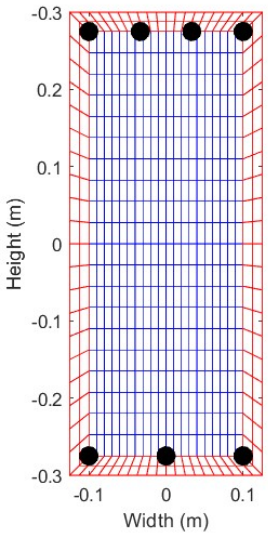

Figure 3.8. The pristine fibre model of the example section.

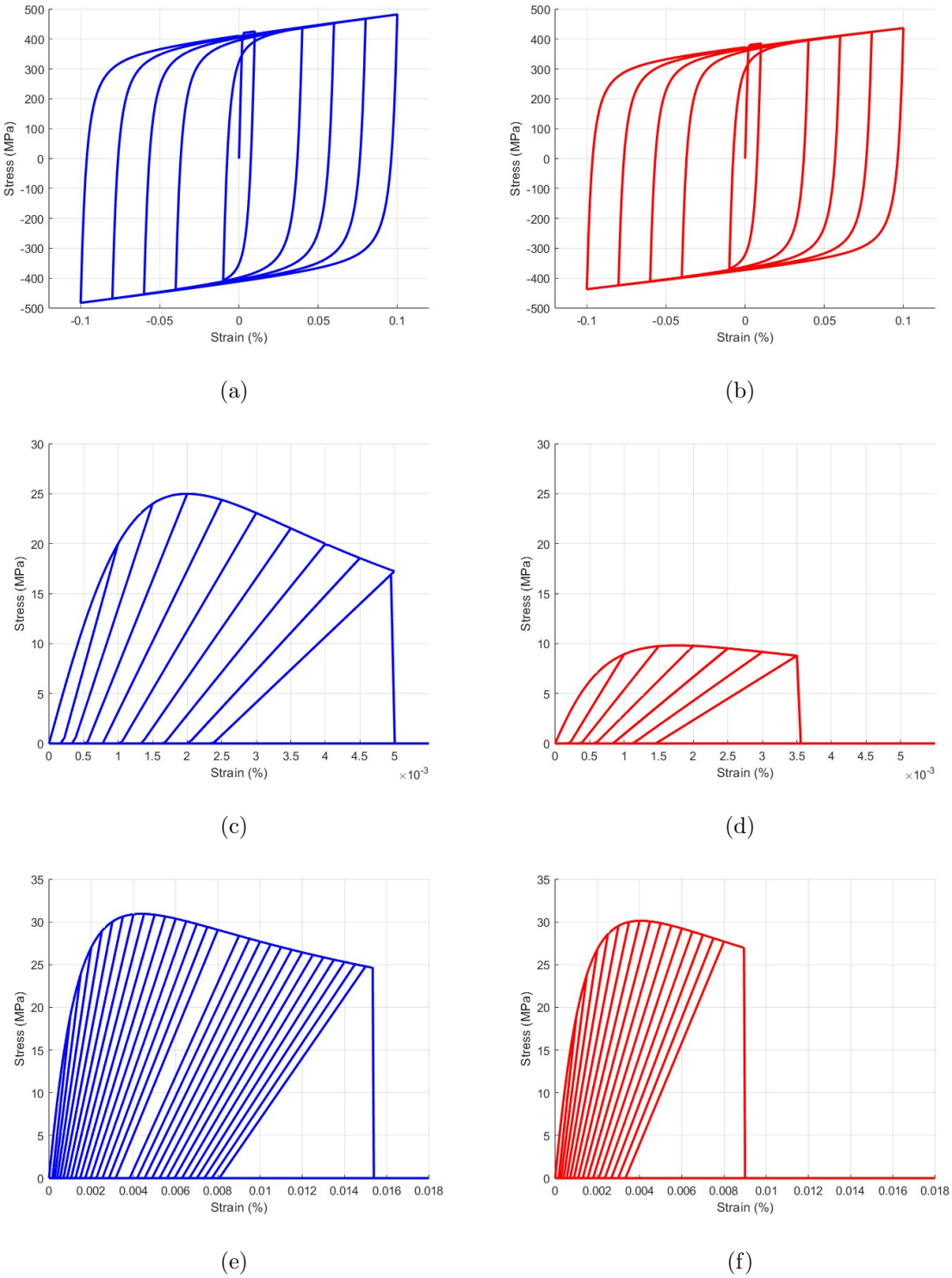

Figure 3.9. Stress-strain relationship for pristine and aged material models for given example (a) pristine reinforcing bar, (b) aged reinforcing bar, (c) pristine unconfined concrete, (d) aged unconfined concrete, (e) pristine confined concrete, (f) aged confined concrete.

3.2.7. Damping Modeling

Dynamic analyses are performed assuming modal damping ratio $\xi = 5\%$ and, Rayleigh damping is derived considering natural vibration modes of the building as

$$c = a_0 m + a_1 k \tag{3.3}$$

where a_0 and a_1 constants having units of sec^{-1}, and m and k represent mass and stiffness matrices respectively. The damping ratio for the n^{th} mode can be expressed as in Equation 4.5

$$\xi_n = \frac{a_0}{2}\frac{1}{w_n} + \frac{a_1}{2} w_n \tag{3.4}$$

where w_n is n^{th} mode's natural angular frequency.

Figure 3.10 illustrates the variation of modal damping ratio with respect to natural frequencies for a pristine 3-story building designed per TBEC-18 as an example.

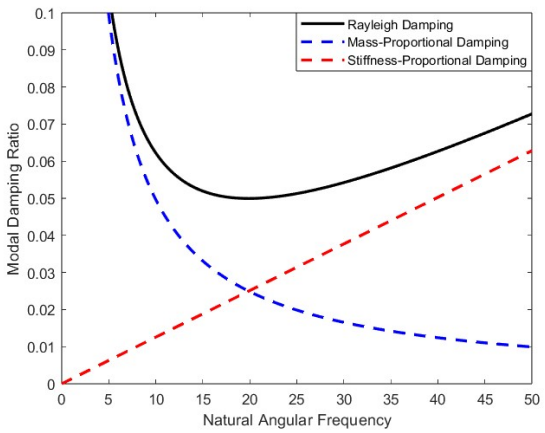

Figure 3.10. Rayleigh, mass proportional and stiffness proportional damping distribution with natural angular frequency for example building (pristine-3-2018).

4. GROUND MOTION SELECTION AND SCALING

Ground motion records for nonlinear analysis are selected from NGAWest2 Ground Motion Database [54] considering the seismicity of the site (e.g., distance from the epicenter, fault mechanism, etc.). The location of buildings and the shortest distance from the site to fault surface (R_{JB}) is illustrated in Figure 4.1, and ground motion selection parameters are presented in Table 4.1.

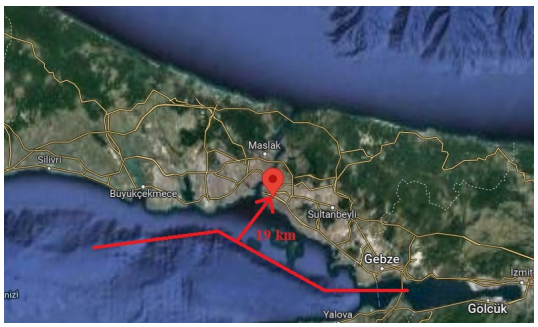

Figure 4.1. The location of buildings and the shortest distance from the site to fault surface (R_{JB}).

Table 4.1. Ground motion selection parameters.

Fault Type	Strike Slip
Magnitude (M_w)	6.2-8.2
R_{JB} (km)	15-60
V_{s30} (m/s)	300-820

The nonlinear time history analyses are conducted using eleven ground motion records selected from eight earthquakes considering the seismic hazard in this area. Eleven stripes are defined to represent the ground motion intensity measure levels in terms of spectral displacement and acceleration at the first period of the buildings.

To provide ground motion records for each stripe, first, a target response spectrum preserving code-based spectral shape is developed for each IM level (Figure 4.2) and then the acceleration time series are scaled up or down to match their response spectra with the target spectrum.

Spectral acceleration-based IM levels are defined between 0.10g and 2.90g (0.10, 0.25, 0.5, 0.8, 1.1, 1.4, 1.7, 2.0, 2.3, 2.6, 2.9). Pseudo-spectral acceleration values are considered using the same levels from spectral acceleration IM levels and converted to spectral displacement values as

$$pSa = w^2 S_d \tag{4.1}$$

where pSa, S_d, and w means pseudo-spectral acceleration, spectral displacement, and natural angular frequency respectively.

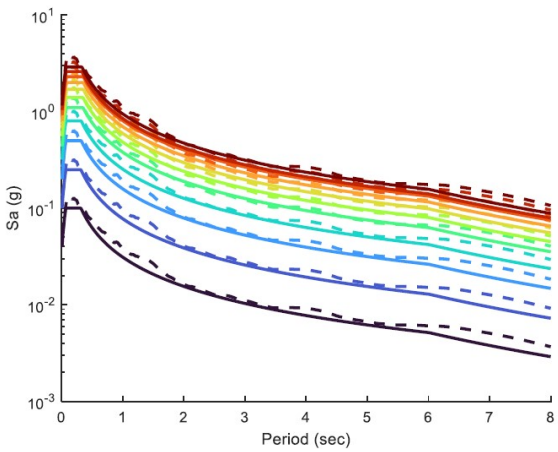

Figure 4.2. Mean spectral acceleration spectra for selected and scaled ground motions (dashed lines) and design spectra for each IM level (solid lines).

Examples of the scaled ground motions' spectra for a pristine 3-story building designed based on TBEC-18 rules (pristine-3-2018) are presented in Figures 4.3 and 4.4. It must be stressed that the same process is utilized for every building.

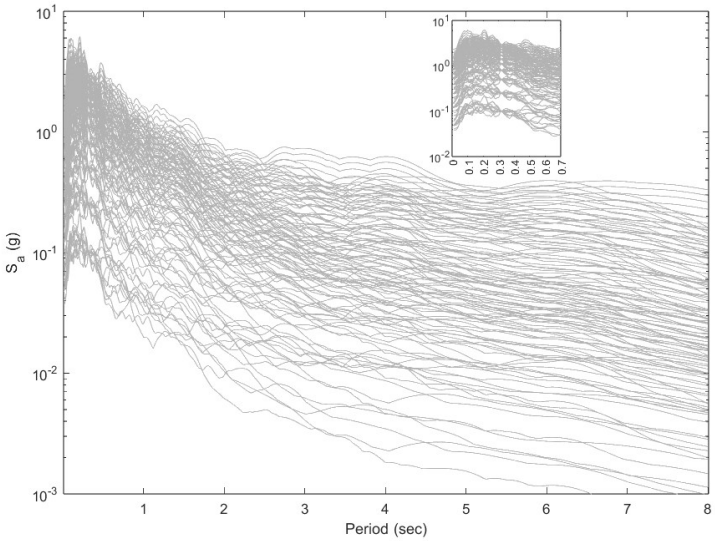

Figure 4.3. Scaled ground motions to define IM levels by multiple-stripes in terms of spectral acceleration ($S_a(T_1,5\%)$, pristine-3-2018).

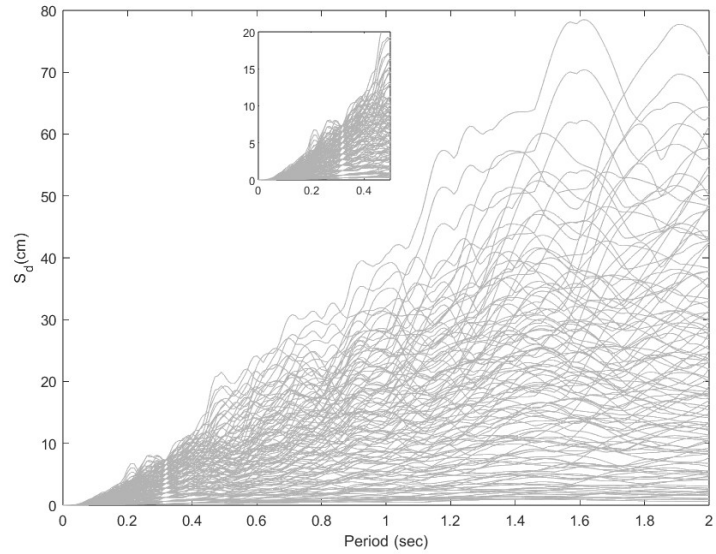

Figure 4.4. Scaled ground motions to define IM levels by multiple-stripes in terms of spectral displacement ($S_d(T_1,5\%)$, pristine-3-2018).

Selected and scaled ground motions and their parameters are given in Table 4.2.

Table 4.2. Properties of selected and scaled ground motions.

Record Number	**Earthquake Name**	**Year**	R_{JB} **(km)**	V_{s30} **(m/s)**
880	Landers	1992	26.96	355.42
1170	Kocaeli	1999	51.17	384.86
1836	Hector Mine	1999	42.06	635.01
2107	Denali, Alaska	2002	49.94	399.35
2935	Chi-Chi	1999	37.54	665.2
3854	Chi-Chi	1999	31.60	538.69
4092	Parkfield	2004	53.87	351.43
4106	Parkfield	2004	15.49	359.03
6874	Joshua Tree	1992	17.15	333.89
6878	Joshua Tree	1992	21.40	367.84
6933	Darfield	2010	33.54	342.70

5. MULTIPLE-STRIPE ANALYSIS AND DERIVATION OF FRAGILITY FUNCTIONS

5.1. Methodology

Multiple-stripe analysis is a wide-range nonlinear dynamic structural analysis procedure referring to stripes for suitable ground motions that are scaled up or down to desired multiple IM levels (e.g., spectral acceleration) considering the seismic threat at the site [55].

In this chapter, multiple-stripe analysis results are illustrated in terms of maximum-inter-story drift ratio and structures' roof displacement. Displacement time histories are recorded throughout the nonlinear dynamic analyses process at the mass center of structures at each story. To derive analytical fragility functions, each engineering demand parameter (roof displacement, maximum-inter-story drift ratio) is considered in different ways. Based on pushover analysis results, fragility functions are derived considering EDP as top displacement.

To assess and understand the global nonlinear response characteristics of structures, nonlinear static analysis procedure is conducted. Each building is exposed to lateral loads increasing incrementally defined based on their first-mode corresponding shape vector.

However, uncertainties to define structural threshold levels from pushover analysis results are significantly known. The definition of yield and ultimate displacement values and the definition of damage threshold levels based on those values can be given as examples. Yet, there are different methodologies to define threshold values in literature as some examples are mentioned in Section 1.3.

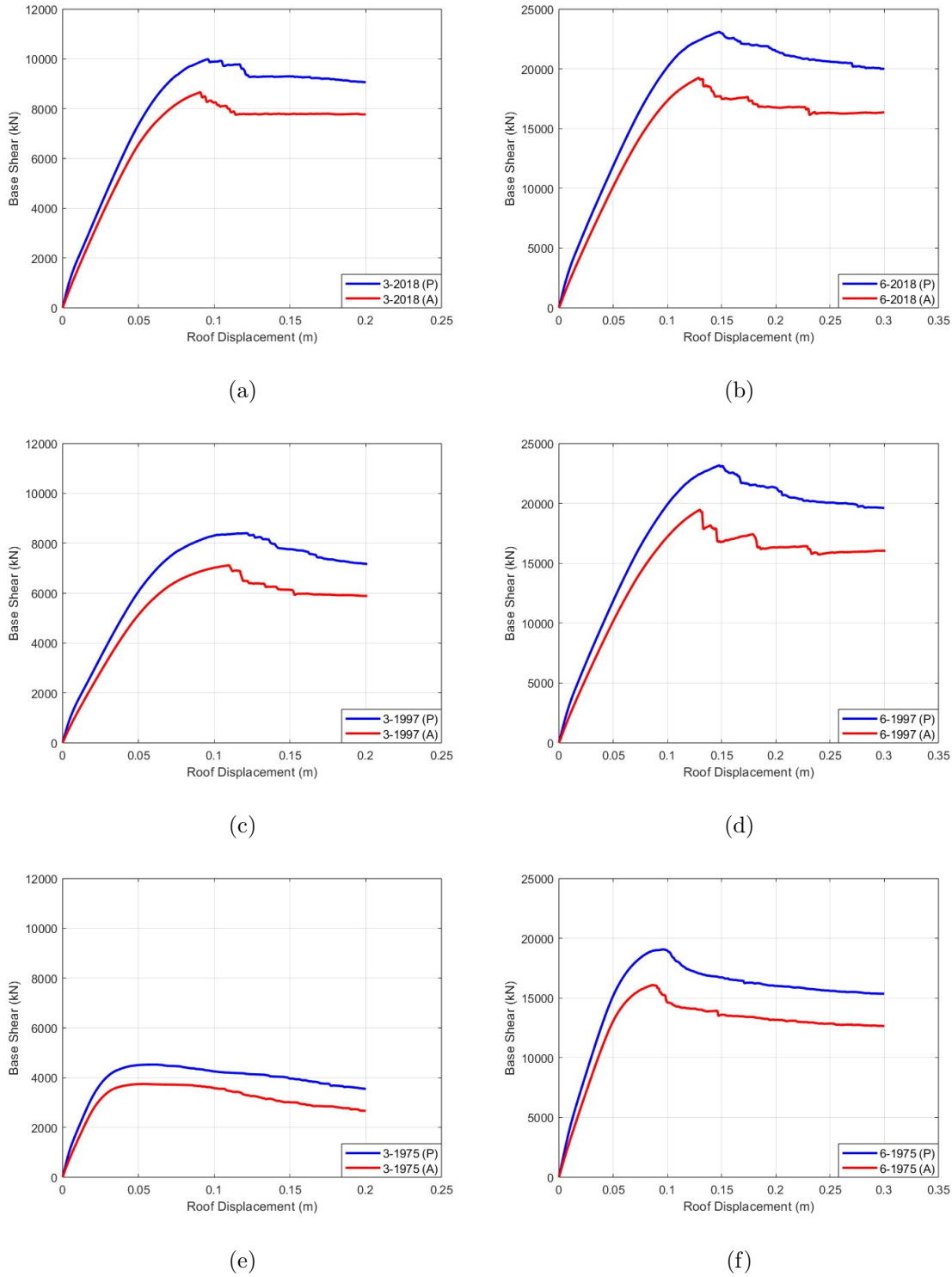

Figure 5.1. Comparison of pushover curves for pristine (P) and aged (A) buildings (a) 3-2018, (b) 6-2018, (c) 3-1997, (d) 6-1997, (e) 3-1975, (f) 6-1975.

Figure 5.1 illustrates pushover analysis results and comparisons for each pristine and aged building. To derive nonlinear curves, displacement-controlled pushover analysis methodology is utilized, and displacement responses are recorded at the center of mass at the roof via OpenSees [50].

As mentioned, some examples to define structural limit states are mentioned in Section 1.3. In this study, a global structural damage definition method suggested by Silva et. al. [30] is implemented. Silva et. al. defines 4 damage levels, based on yield and ultimate displacement values, and converts the nonlinear curve to bilinear approximation. To do that, the ultimate response of buildings must be defined, rather than selected, or pushed displacement points. For this purpose, the methodology suggested by Park is implemented (Figure 5.2, after [56]) [56]. For each characteristic curve, a suitable process is selected.

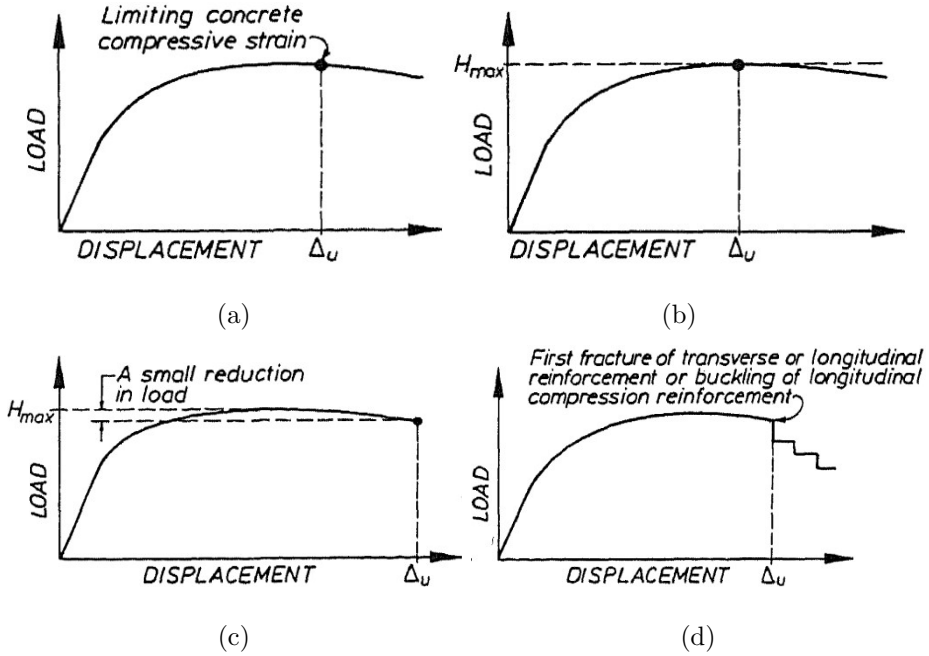

Figure 5.2. Different definitions for ultimate displacement (a) based on element strain, (b) based on maximum load, (c) based on load capacity after peak load, (d) based on fracture or buckling in reinforcement [56].

While implementing this methodology, piecewise bilinear fitting (Figure 5.3, 5.4) is conducted using De Luca et. al. [57], and software proposed by Vamvatsikos [58].

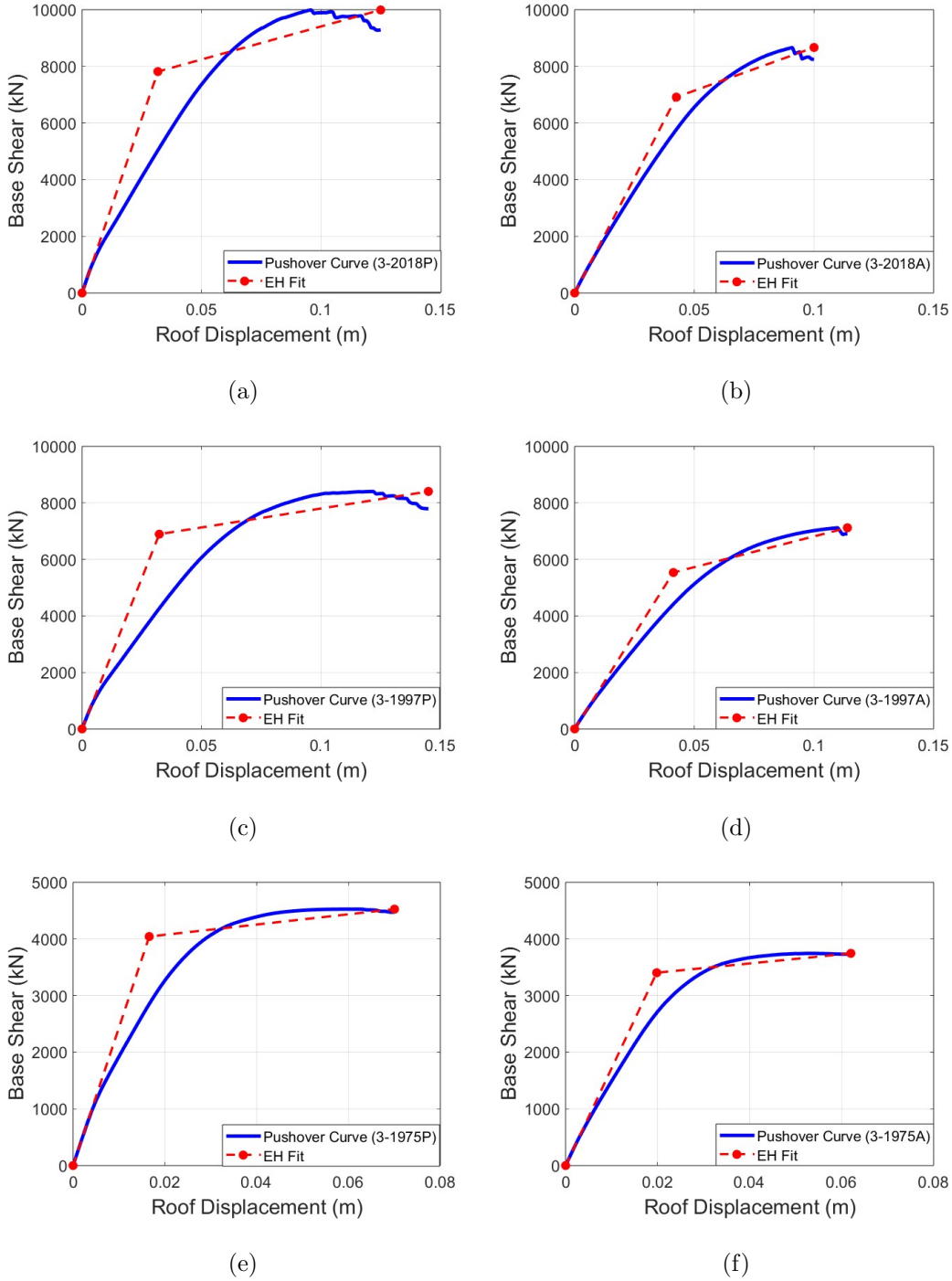

Figure 5.3. Ultimate displacement point definition and bilinear curve fitting for buildings (a) pristine 3-2018, (b) aged 3-2018, (c) pristine 3-1997, (d) aged 3-1997, (e) pristine 3-1975, (f) aged 3-1975.

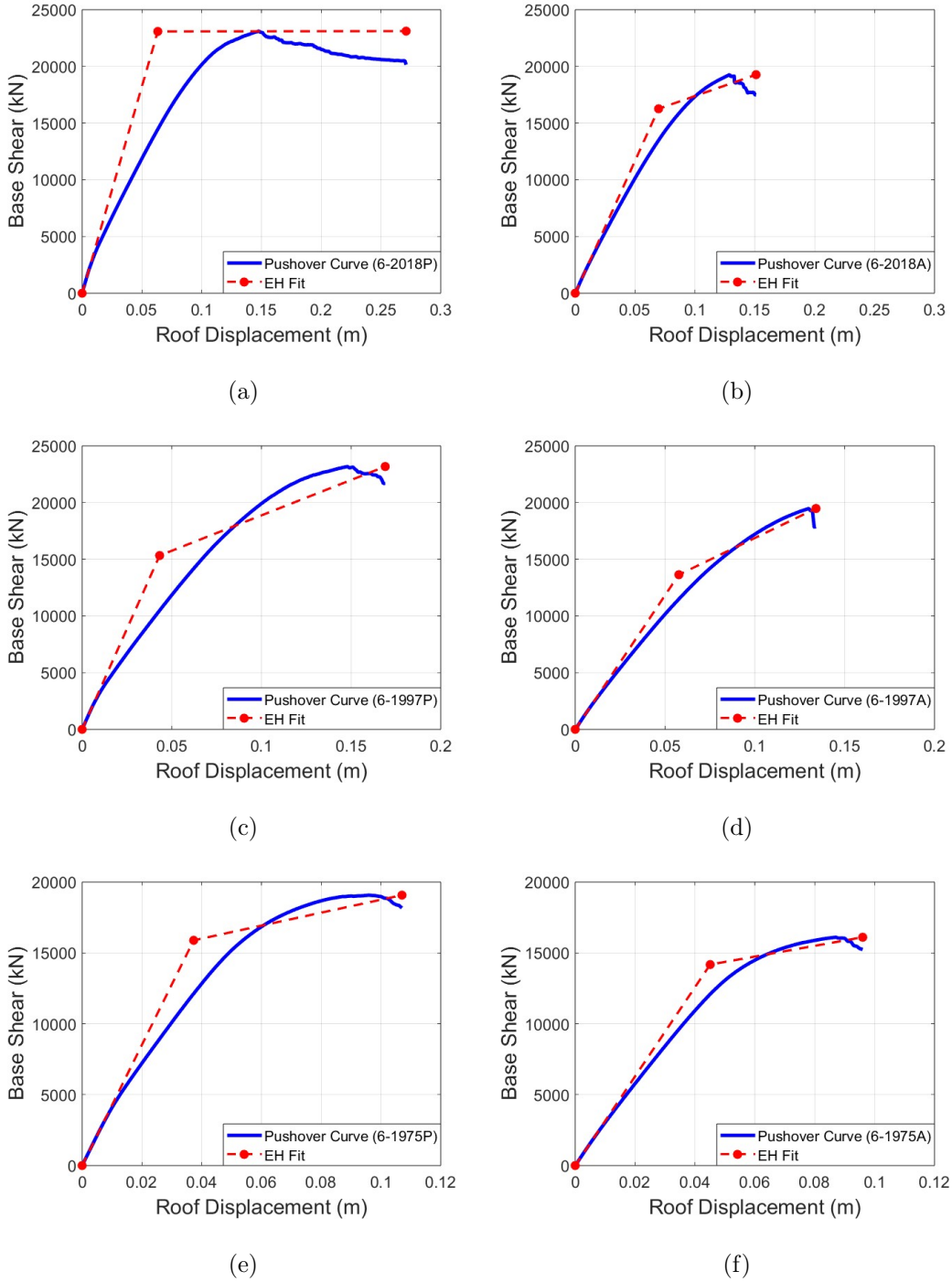

Figure 5.4. Ultimate displacement point definition and bilinear curve fitting for buildings (a) pristine 6-2018, (b) aged 6-2018, (c) pristine 6-1997, (d) aged 6-1997, (e) pristine 6-1975, (f) aged 6-1975.

Yield and ultimate displacement points are considered based on piecewise bilinear fitting, and the first point is selected as the yield, whereas the second is selected as the ultimate point, and limit states are determined by values given in Table 5.1 [30]. Defined threshold levels are given in Table 5.2 for each building.

Table 5.1. Pushover based damage levels.

Damage State	**Damage Threshold**
Slight	$0.7D_y$
Moderate	$0.75D_y$+$0.25D_u$
Extensive	$0.5(D_y + D_u)$
Complete	D_u

Table 5.2. Defined pushover-based roof displacement limit states (in terms of meters).

Building Name	**Slight**	**Moderate**	**Extensive**	**Complete**
Pristine-3-2018	0.022	0.055	0.078	0.125
Pristine-3-1997	0.022	0.060	0.088	0.144
Pristine-3-1975	0.011	0.029	0.043	0.070
Pristine-6-2018	0.044	0.115	0.167	0.271
Pristine-6-1997	0.030	0.074	0.106	0.168
Pristine-6-1975	0.026	0.054	0.072	0.107
Aged-3-2018	0.029	0.056	0.072	0.1
Aged-3-1997	0.028	0.059	0.077	0.113
Aged-3-1975	0.013	0.030	0.040	0.062
Aged-6-2018	0.048	0.089	0.110	0.150
Aged-6-1997	0.040	0.076	0.095	0.133
Aged-6-1975	0.031	0.057	0.070	0.096

In addition, maximum-inter-story drift ratio is considered while defining limit states as EDP. In this study, I use a numerical study based on experimental data, field observations and measurements, and theoretical analysis proposed by Ghobarah [29].

Ghobarah's work focuses on 3,6,9, and 12-story moment-resisting frames, and used buildings in that research clearly fit this study as well in terms of story number and building heights. Proposed drift ratio threshold levels by Ghobarah for different damage states defined for moment resisting frames (e.g., ductile, non-ductile) are given in Table 5.3.

Table 5.3. MIDR (%) threshold values for damage states.

Damage State	**Ductile MRF**	**Non-ductile MRF**
Slight	0.40	0.20
Moderate	1.00	0.50
Extensive	1.80	0.80
Complete	3.00	1.00

Section 5.2 illustrate multiple-stripe analysis results in terms of unconverged and converged situations with blue and red circles respectively. Collapse situations are considered when dynamic instability occurs in the analysis procedure (i.e., non-convergence) in high stripe levels where maximum inter-story drift ratios significantly increase or give no result at all as suggested in [55]. An example from a building is given in Table 5.4.

Table 5.4 illustrates the procedure for a 3-story building (aged-3-2018) where dynamic instability occurred analyses' last step at the highest IM level. It is evident that at 2.90g IM level, the building must collapse since damage measure result is significantly lower compared to smaller measures, and the former result exceeds the complete damage limit state. Due to non-convergence problems, similar cases that occurred in post-processing are taken as collapse situations.

Table 5.4. Analyses results for 3-story building (aged-3-2018).

MIDR (%)	IM (g) ($S_a(T_1$,5%))
1.27	1.40
1.58	1.70
2.43	2.00
3.35	2.30
4.05	2.60
1.48	2.90

5.2. Multiple-Stripe Analyses Results

This section illustrates multiple-stripe analysis results in terms of spectral acceleration and spectral displacement.

Figures 5.5, 5.8, 5.11, and 5.14 illustrate peak inter-story drift ratio (%) results which are recorded throughout the nonlinear dynamic analyses procedure from the center of mass for each building. Figures 5.6, 5.7, 5.9, 5.10, 5.12, and 5.13 illustrate multiple-stripe analysis results that are scattered for each intensity measure level in terms of maximum inter-story drift ratio (%) and roof displacement.

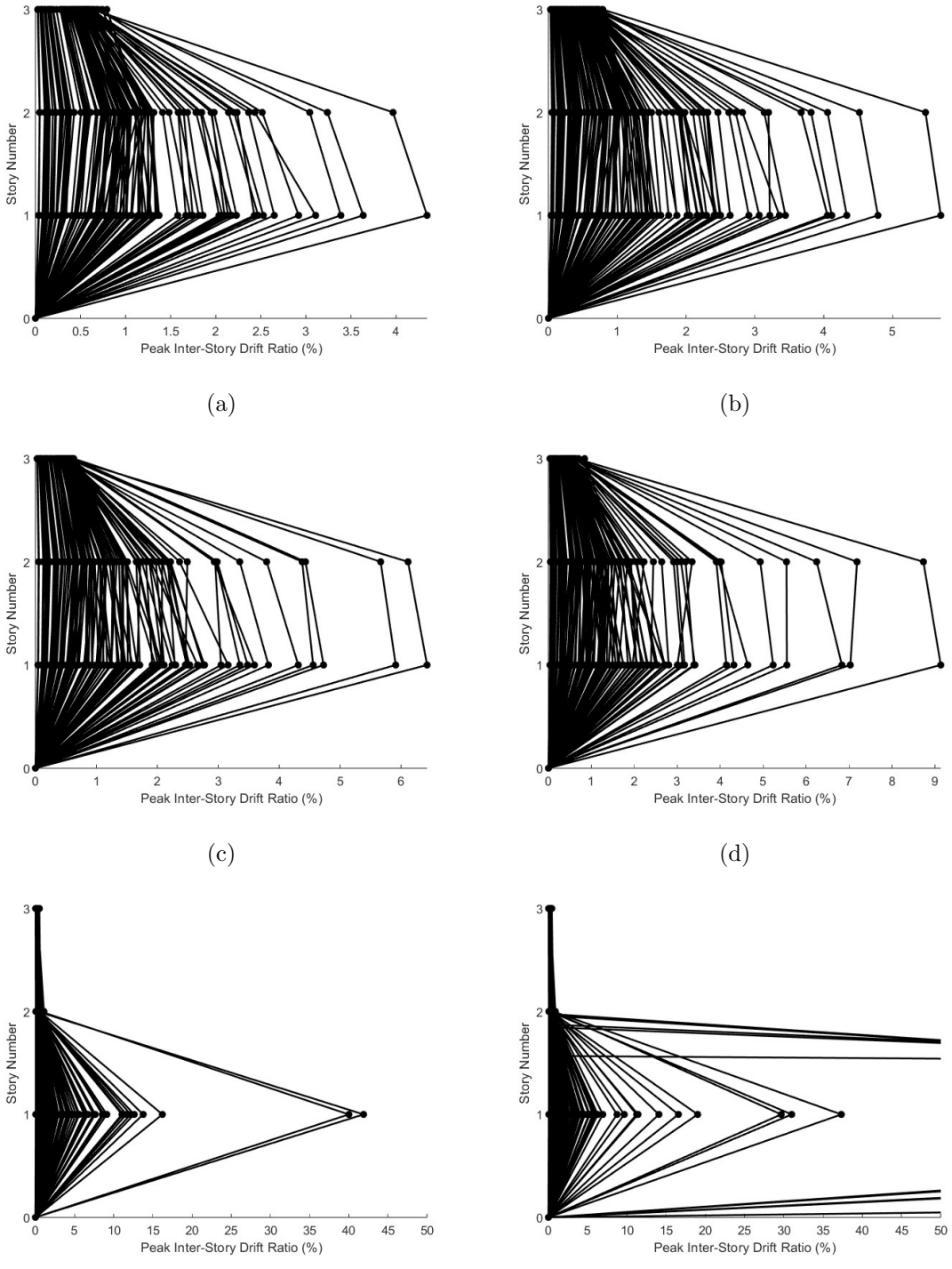

Figure 5.5. Peak inter-story drift ratio results (IM $S_a(T_1,5\%)$) (a) pristine 3-2018, (b) aged 3-2018, (c) pristine 3-1997, (d) aged 3-1997, (e) pristine 3-1975, (f) aged 3-1975.

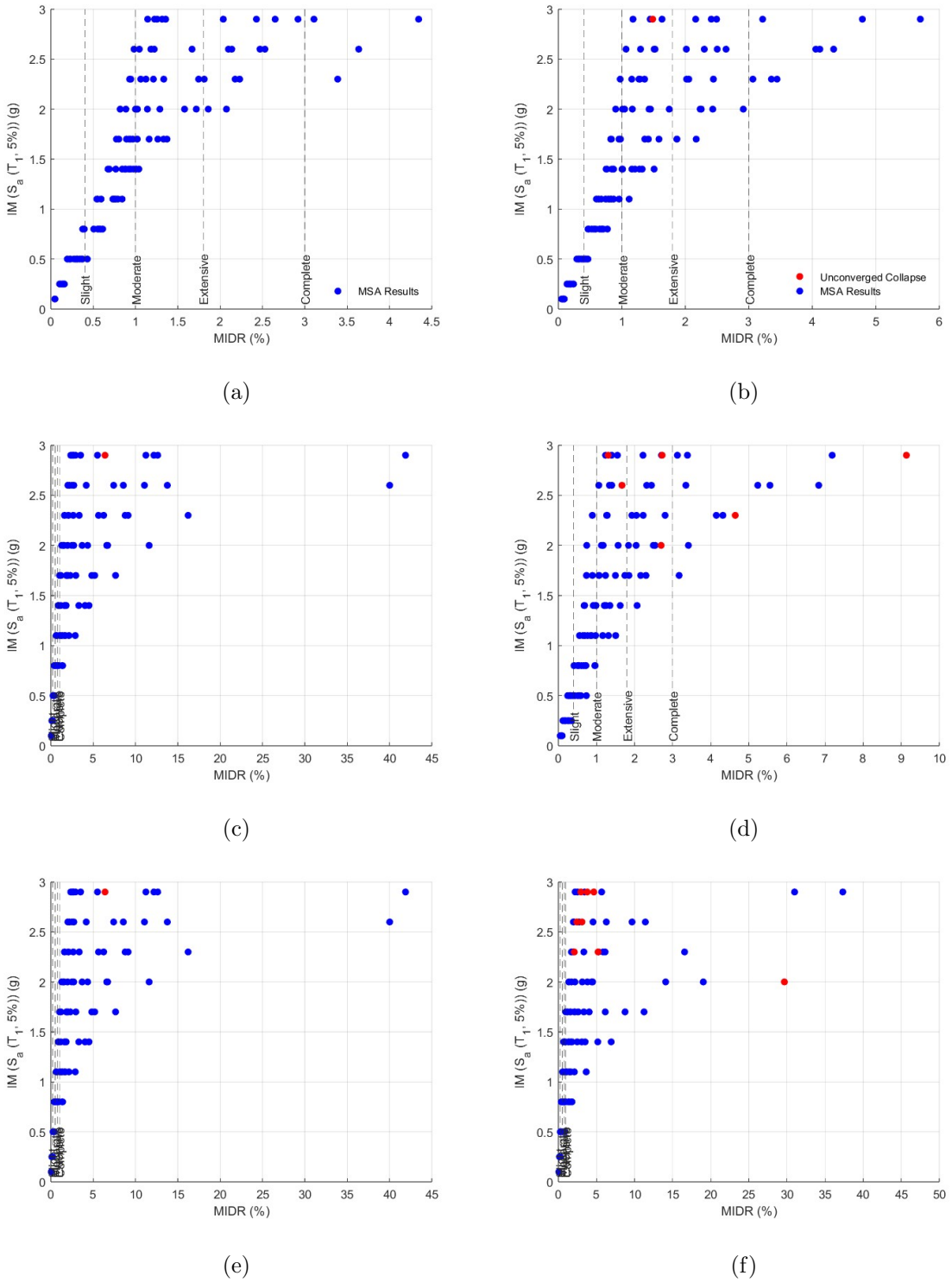

Figure 5.6. Multiple-stripe analyses results for (IM $S_a(T_1$,5%), EDP=MIDR%) (a) pristine 3-2018, (b) aged 3-2018, (c) pristine 3-1997, (d) aged 3-1997, (e) pristine 3-1975, (f) aged 3-1975.

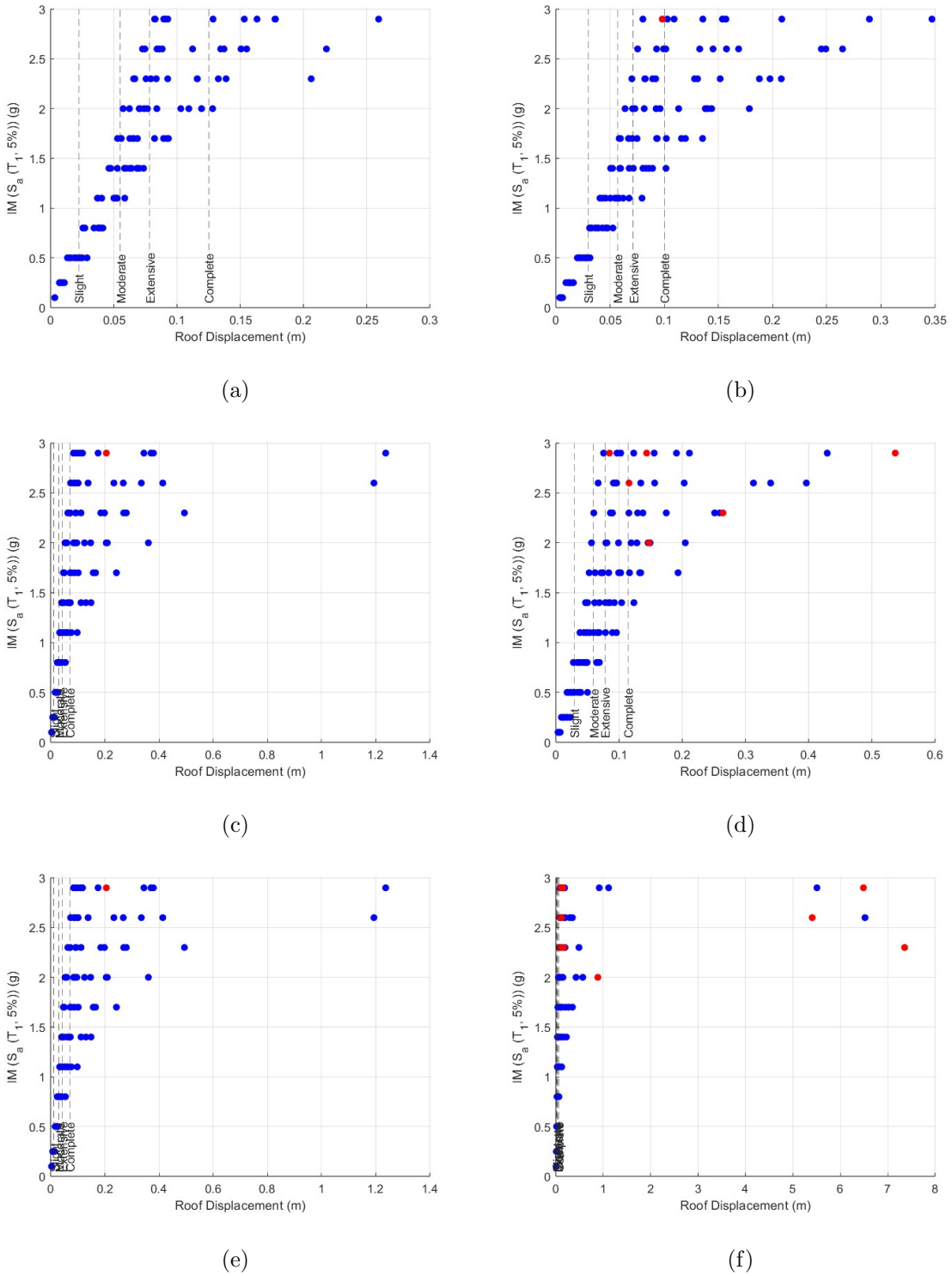

Figure 5.7. Multiple-stripe analyses results for (IM $S_a(T_1$,5%), EDP=D_{Top}) (a) pristine 3-2018, (b) aged 3-2018, (c) pristine 3-1997, (d) aged 3-1997, (e) pristine 3-1975, (f) aged 3-1975.

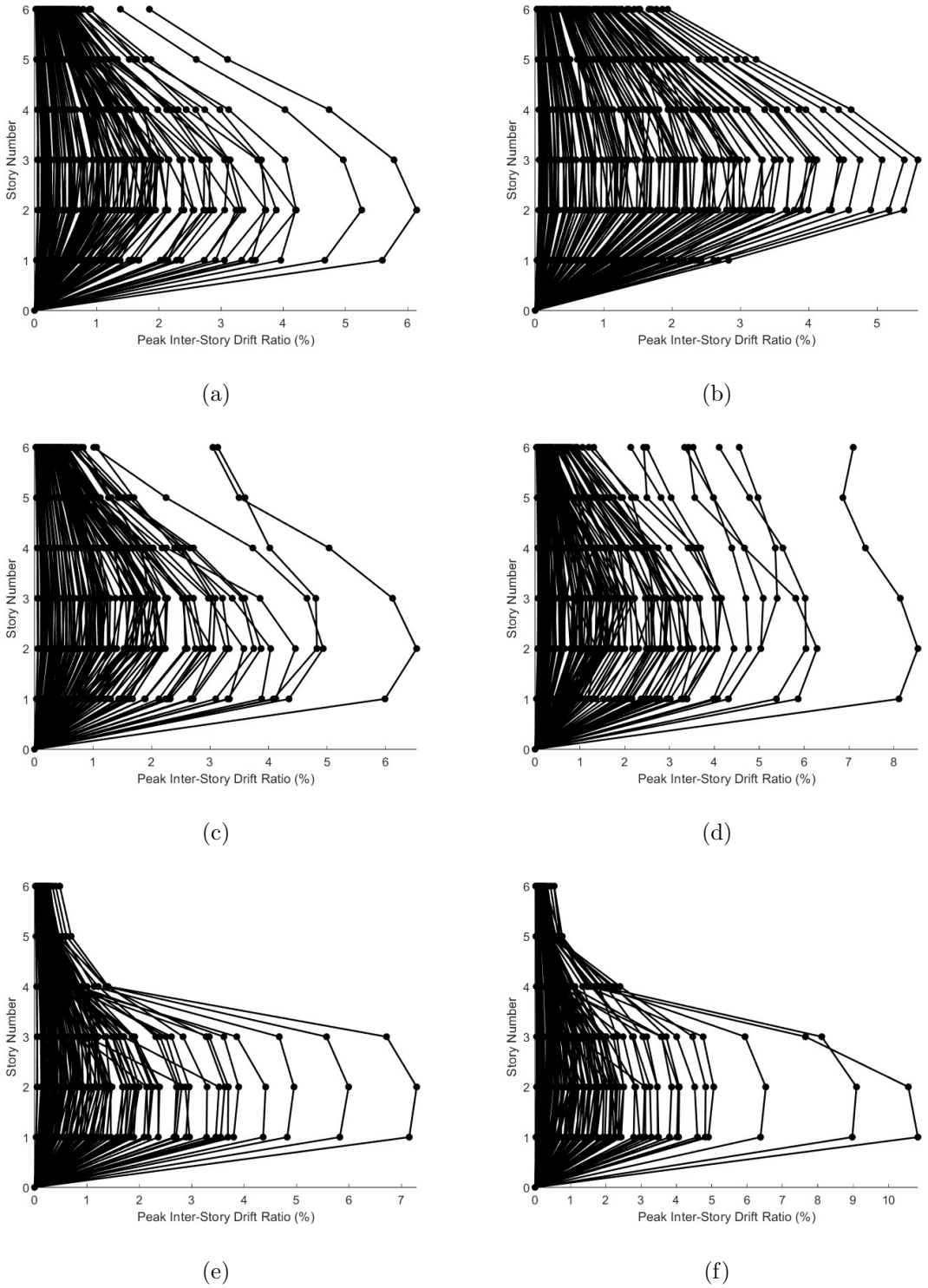

Figure 5.8. Peak inter-story drift ratio results (IM $S_a(T_1,5\%)$) (a) pristine 6-2018, (b) aged 6-2018, (c) pristine 6-1997, (d) aged 6-1997, (e) pristine 6-1975, (f) aged 6-1975.

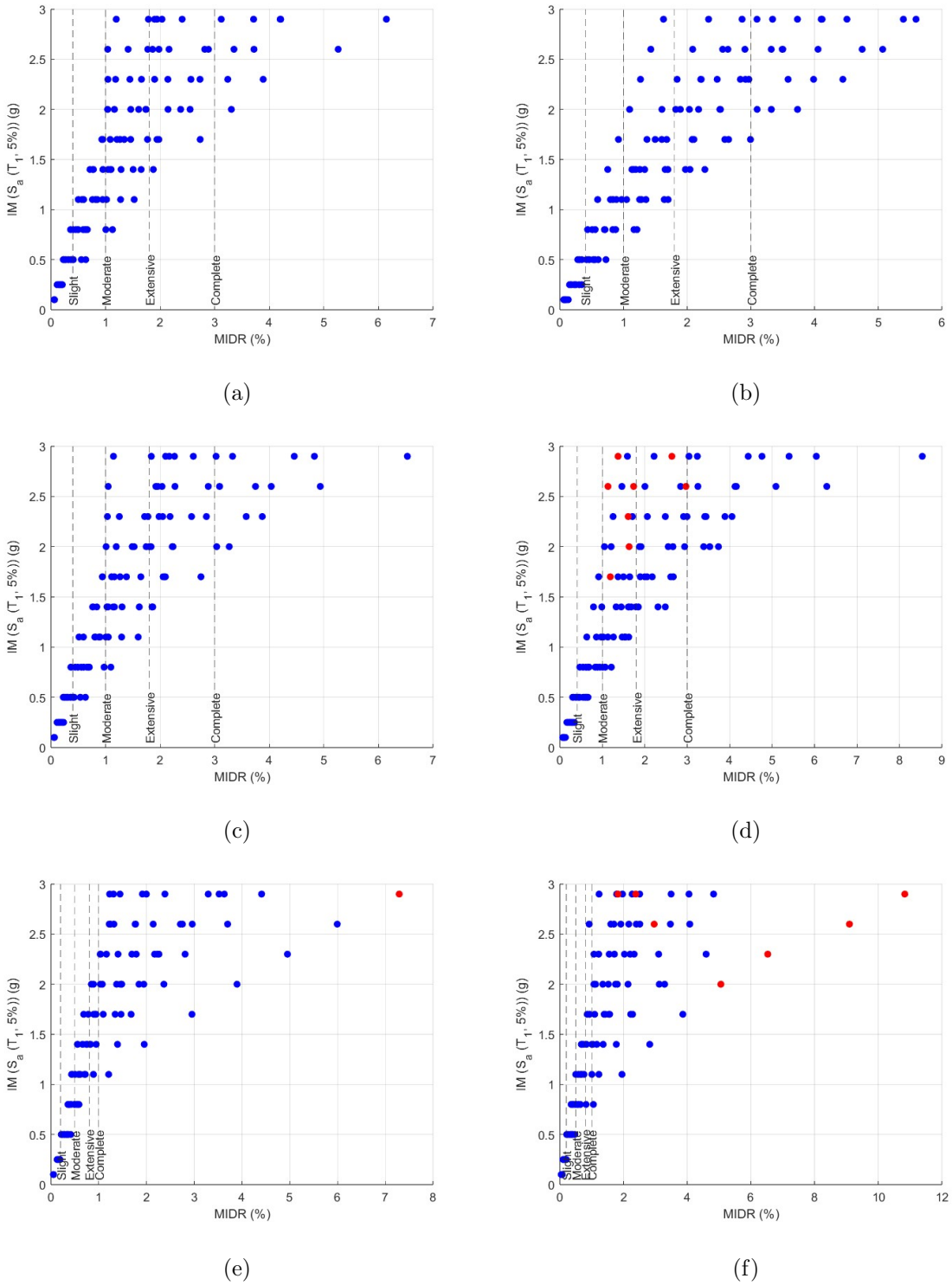

Figure 5.9. Multiple-stripe analyses results for (IM $S_a(T_1$,5%), EDP=MIDR%) (a) pristine 6-2018, (b) aged 6-2018, (c) pristine 6-1997, (d) aged 6-1997, (e) pristine 6-1975, (f) aged 6-1975.

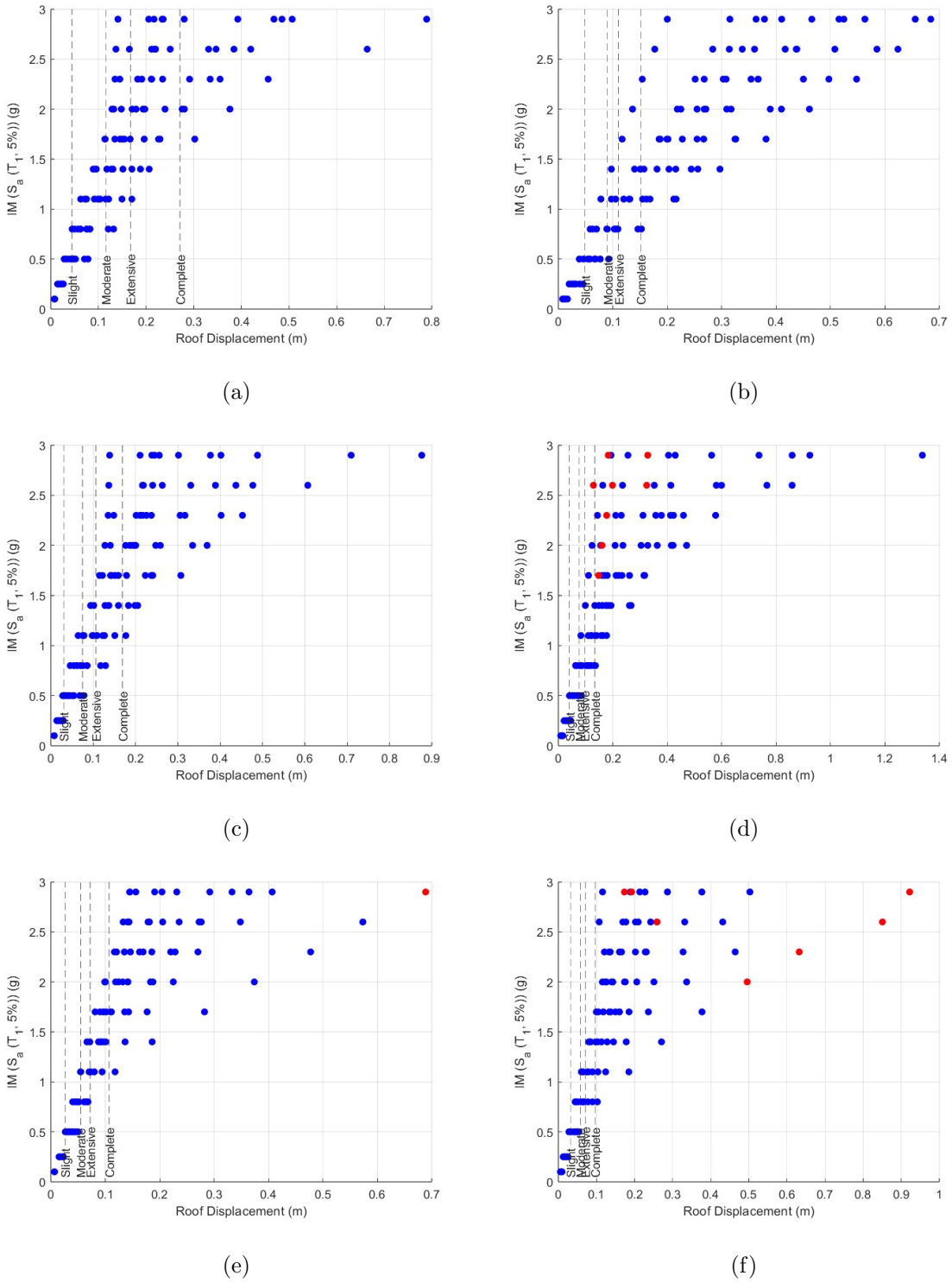

(a) (b)

(c) (d)

(e) (f)

Figure 5.10. Multiple-stripe analyses results for (IM $S_a(T_1$,5%), EDP=D_{Top}) (a) pristine 6-2018, (b) aged 6-2018, (c) pristine 6-1997, (d) aged 6-1997, (e) pristine 6-1975, (f) aged 6-1975.

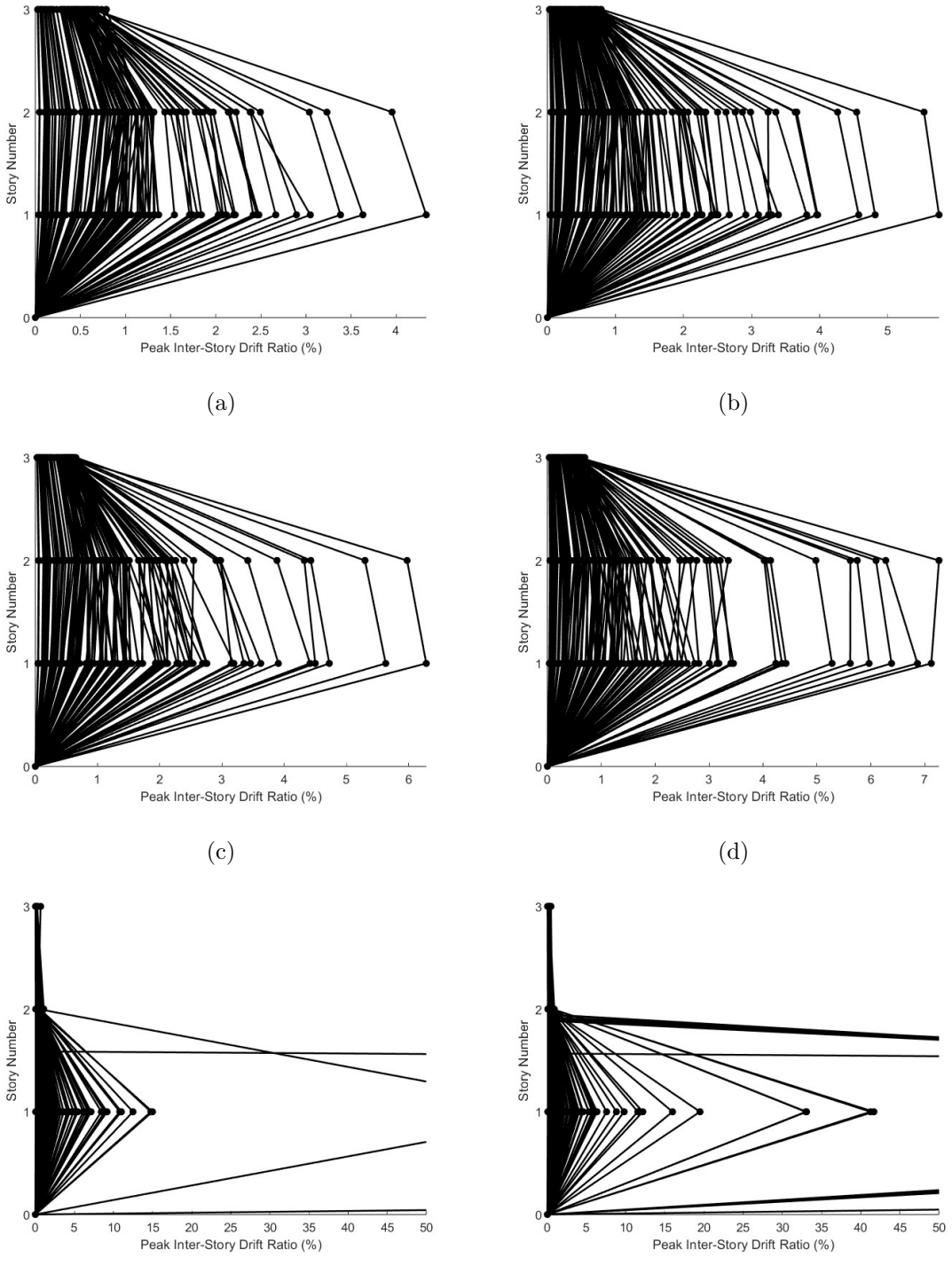

Figure 5.11. Peak inter-story drift ratio results (IM $S_d(T_1,5\%)$) (a) pristine 3-2018, (b) aged 3-2018, (c) pristine 3-1997, (d) aged 3-1997, (e) pristine 3-1975, (f) aged 3-1975.

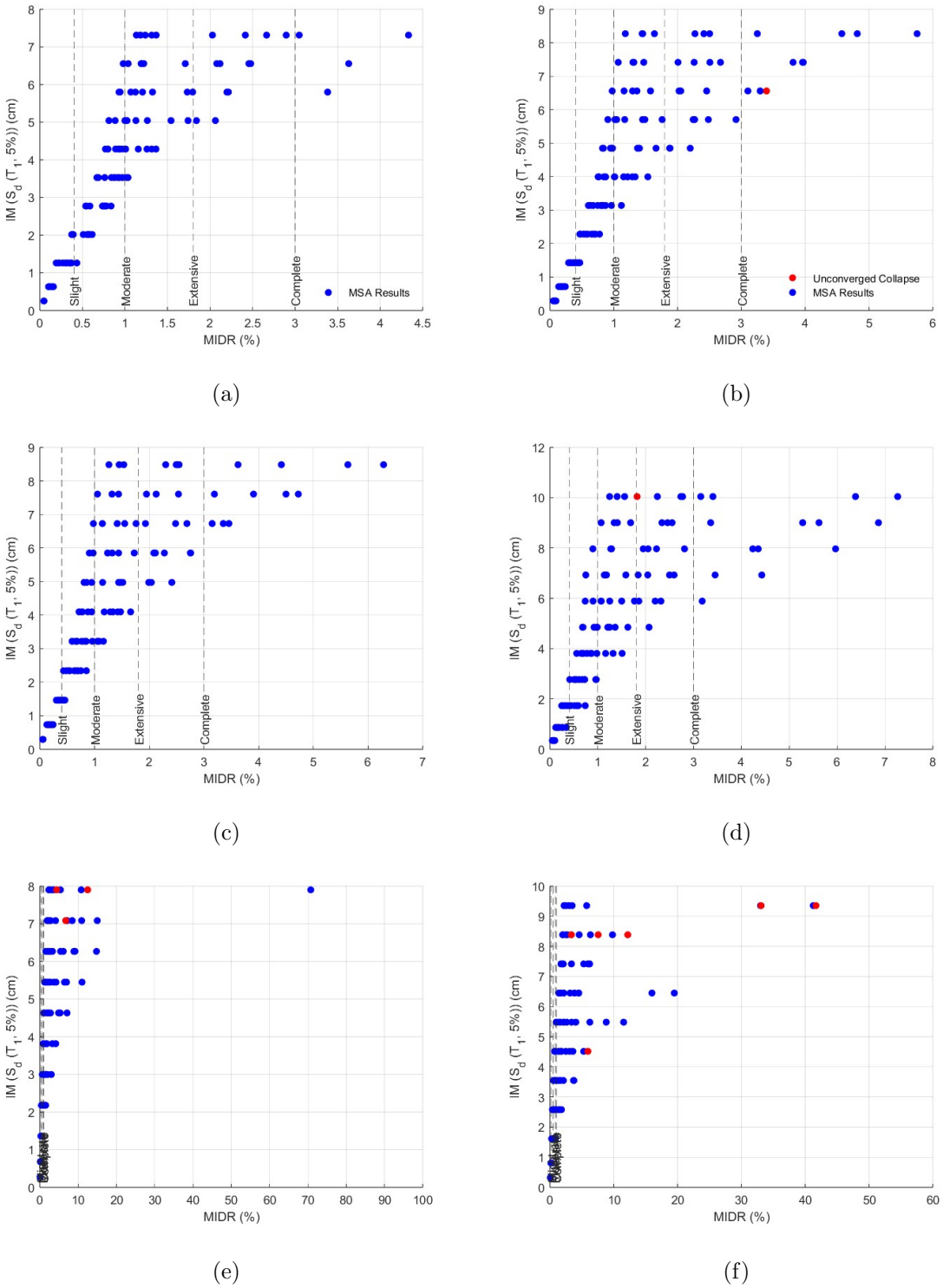

Figure 5.12. Multiple-stripe analyses results for (IM $S_d(T_1$,5%), EDP=MIDR%) (a) pristine 3-2018, (b) aged 3-2018, (c) pristine 3-1997, (d) aged 3-1997, (e) pristine 3-1975, (f) aged 3-1975.

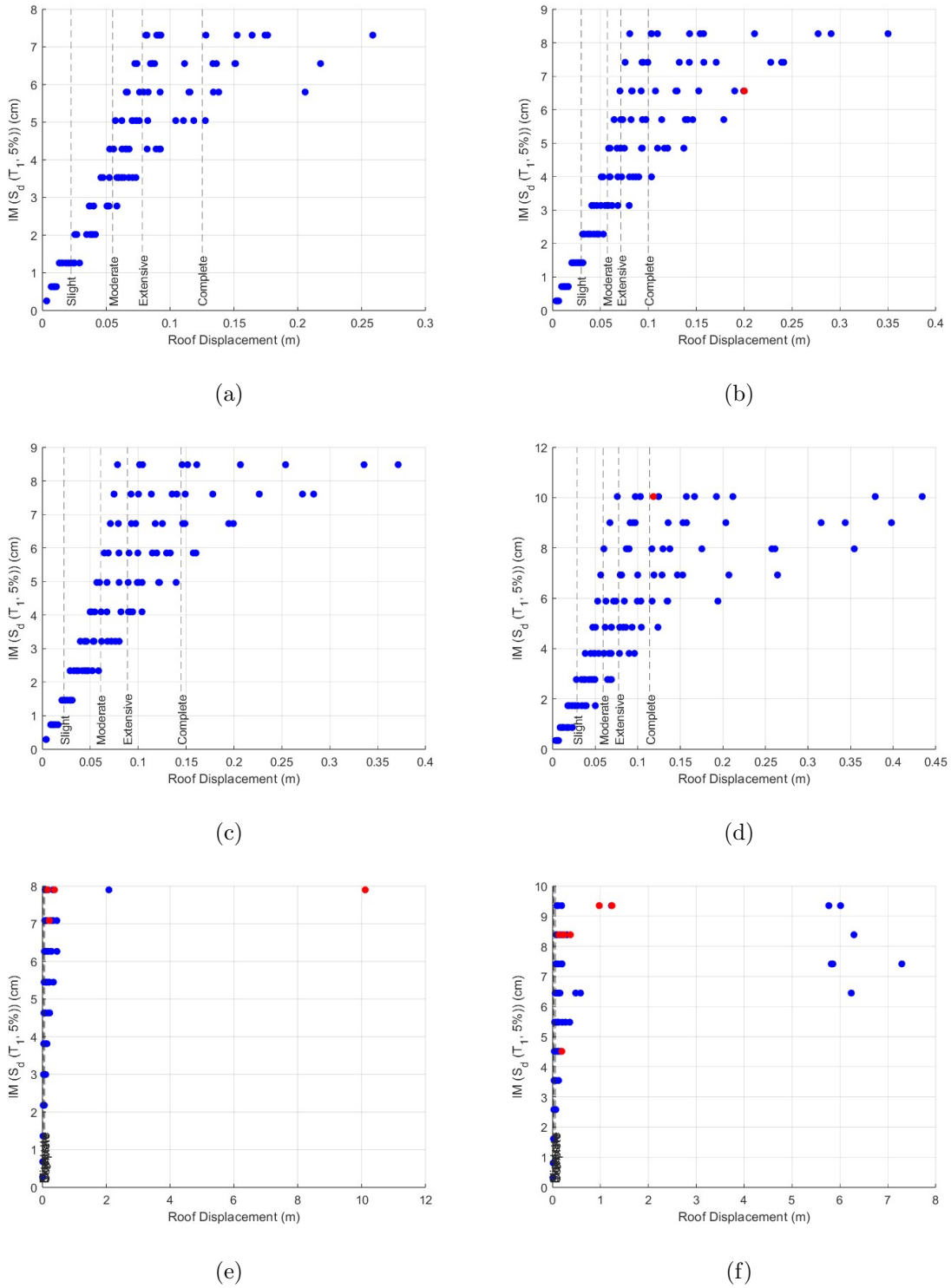

Figure 5.13. Multiple-stripe analyses results for (IM $S_d(T_1,5\%)$, D_{Top}) (a) pristine 3-2018, (b) aged 3-2018, (c) pristine 3-1997, (d) aged 3-1997, (e) pristine 3-1975, (f) aged 3-1975.

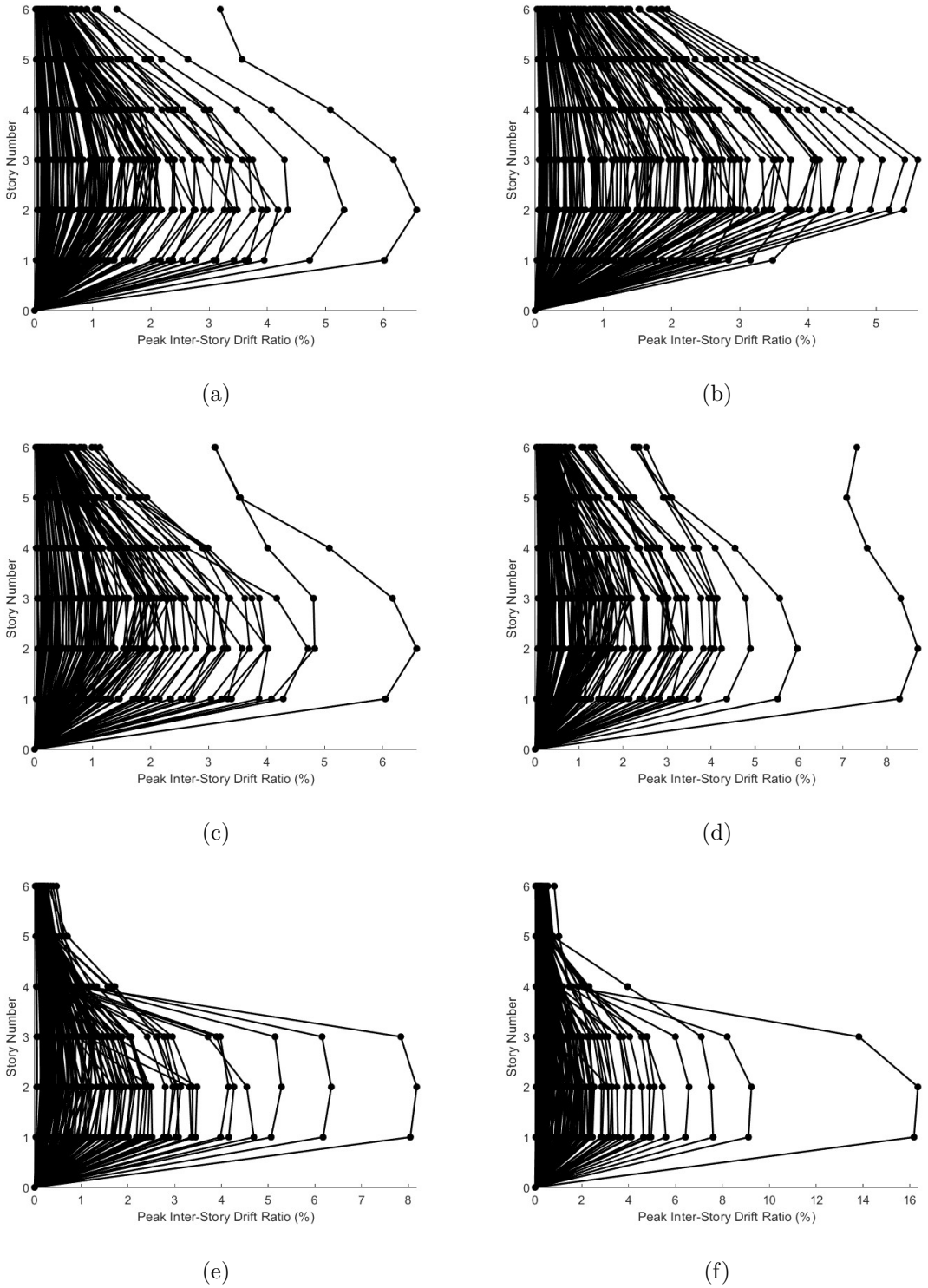

Figure 5.14. Peak inter-story drift ratio results (IM $S_d(T_1,5\%)$) (a) pristine 6-2018, (b) aged 6-2018, (c) pristine 6-1997, (d) aged 6-1997, (e) pristine 6-1975, (f) aged 6-1975.

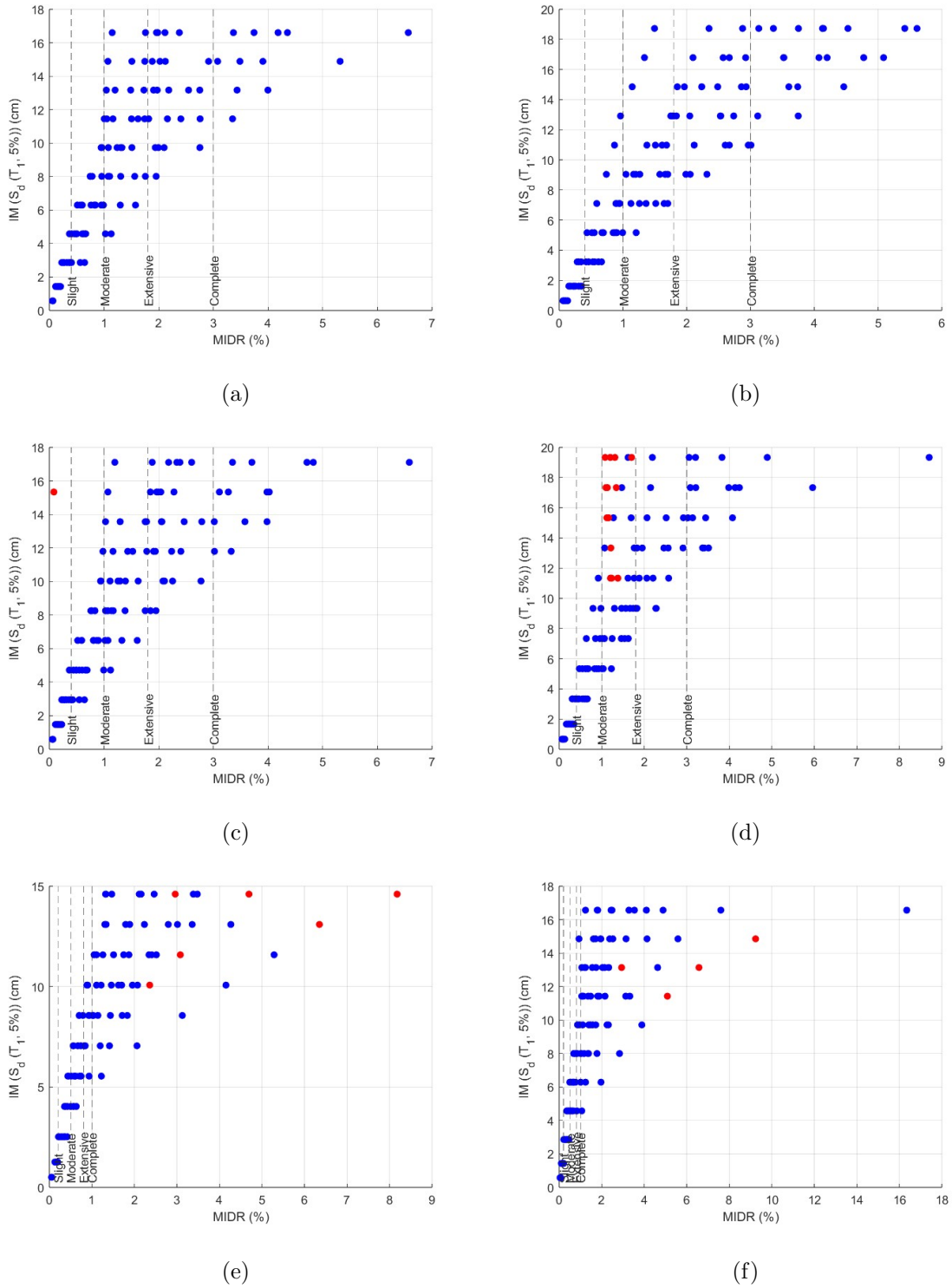

(a) (b)

(c) (d)

(e) (f)

Figure 5.15. Multiple-stripe analyses results for (IM $S_d(T_1$,5%), EDP=MIDR%) (a) pristine 6-2018, (b) aged 6-2018, (c) pristine 6-1997, (d) aged 6-1997, (e) pristine 6-1975, (f) aged 6-1975.

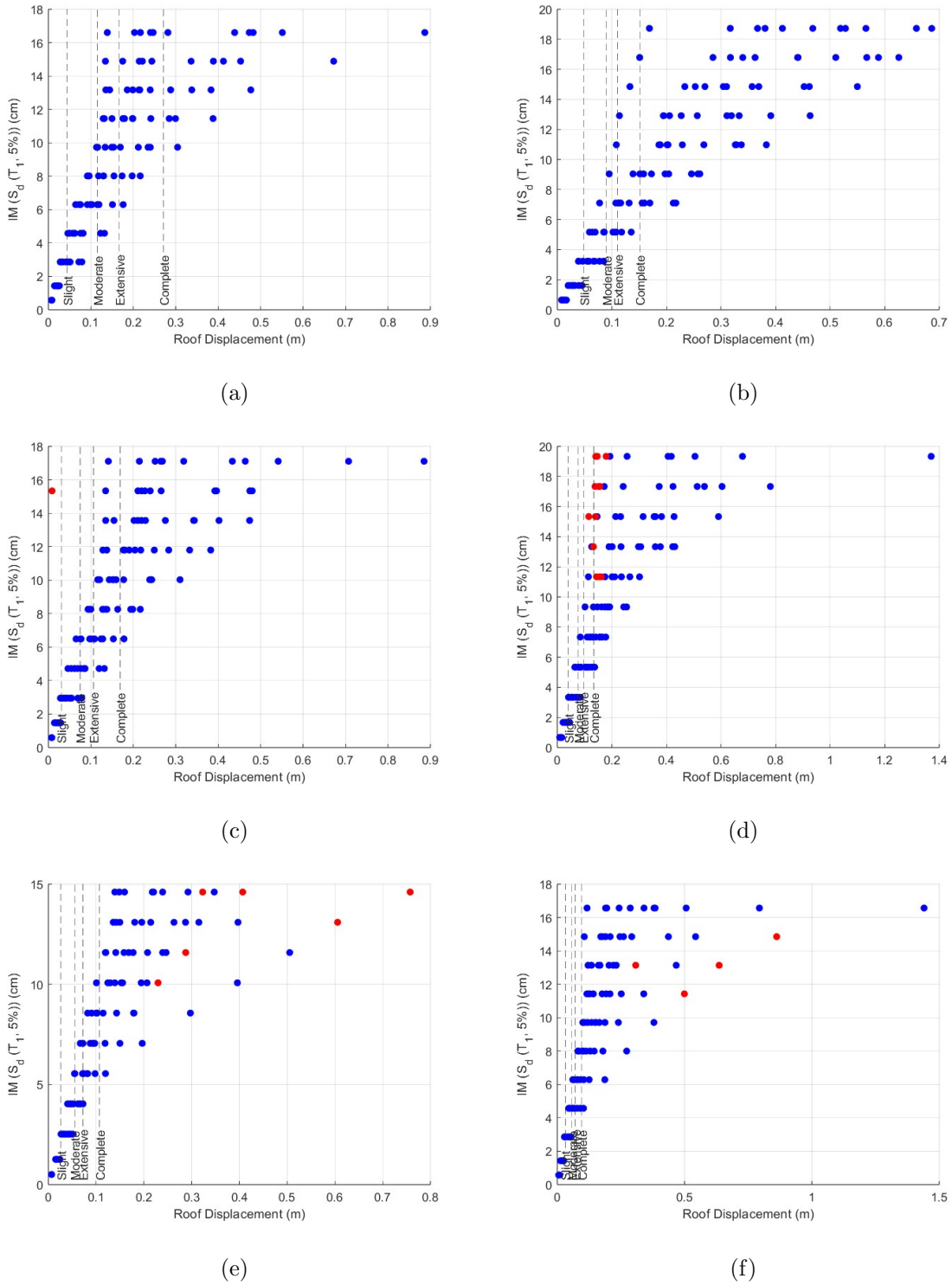

Figure 5.16. Multiple-stripe analyses results for (IM $S_d(T_1,5\%)$, EDP=D_{Top}) (a) pristine 6-2018, (b) aged 6-2018, (c) pristine 6-1997, (d) aged 6-1997, (e) pristine 6-1975, (f) aged 6-1975.

5.3. Derivation of Analytical Fragility Functions

The engineering demand parameters for the definition of fragility functions are considered as maximum inter-story drift ratio and roof displacement. Damage states (i.e. slight, moderate, extensive, and complete) for maximum inter-story drift ratio are defined on the basis of the threshold values on maximum inter-story drift ratios for each building obtained from Ghobarah as: 0.4% for slight damage, 1.0% for moderate damage, 1.8% for extensive damage, and 3.0% for complete damage for moment-resisting ductile frames for buildings designed per TBEC-2018, and TBEC-1997, and 0.2% for slight damage, 0.5% for moderate damage, 0.8% for extensive damage, and 1.0% for complete damage for moment-resisting non-ductile frames for buildings designed per TBEC-1975. In terms of roof displacement, damage threshold levels presented in Table 5.2 are utilized.

For each damage state, a best-fit log-normal cumulative probability distribution function is computed. The probability of reaching or exceeding a damage state for a given level of ground motion intensity is presented with the following standard normal cumulative distribution function expressed as

$$P(DS \geq ds_i | IM = x) = \Phi(\frac{ln(x/\theta_i)}{\beta_i}) \tag{5.1}$$

where $P(DS \geq ds_i | IM = x)$ is the probability that a ground motion with IM = x will cause the building reaching or exceeding the pre-defined damage state ds_i, $\Phi()$ is the standard normal cumulative distribution function, θ is the median of the fragility function, and β is the standard deviation of ln IM [10].

In order to find the optimum values of the median and standard deviation representing the best-fit fragility curve, the maximum likelihood estimation method is implemented [10]. Fragility curves are illustrated in Figures 5.17 to 5.24, and parameters of fragility functions are presented in Tables 5.5 to 5.12.

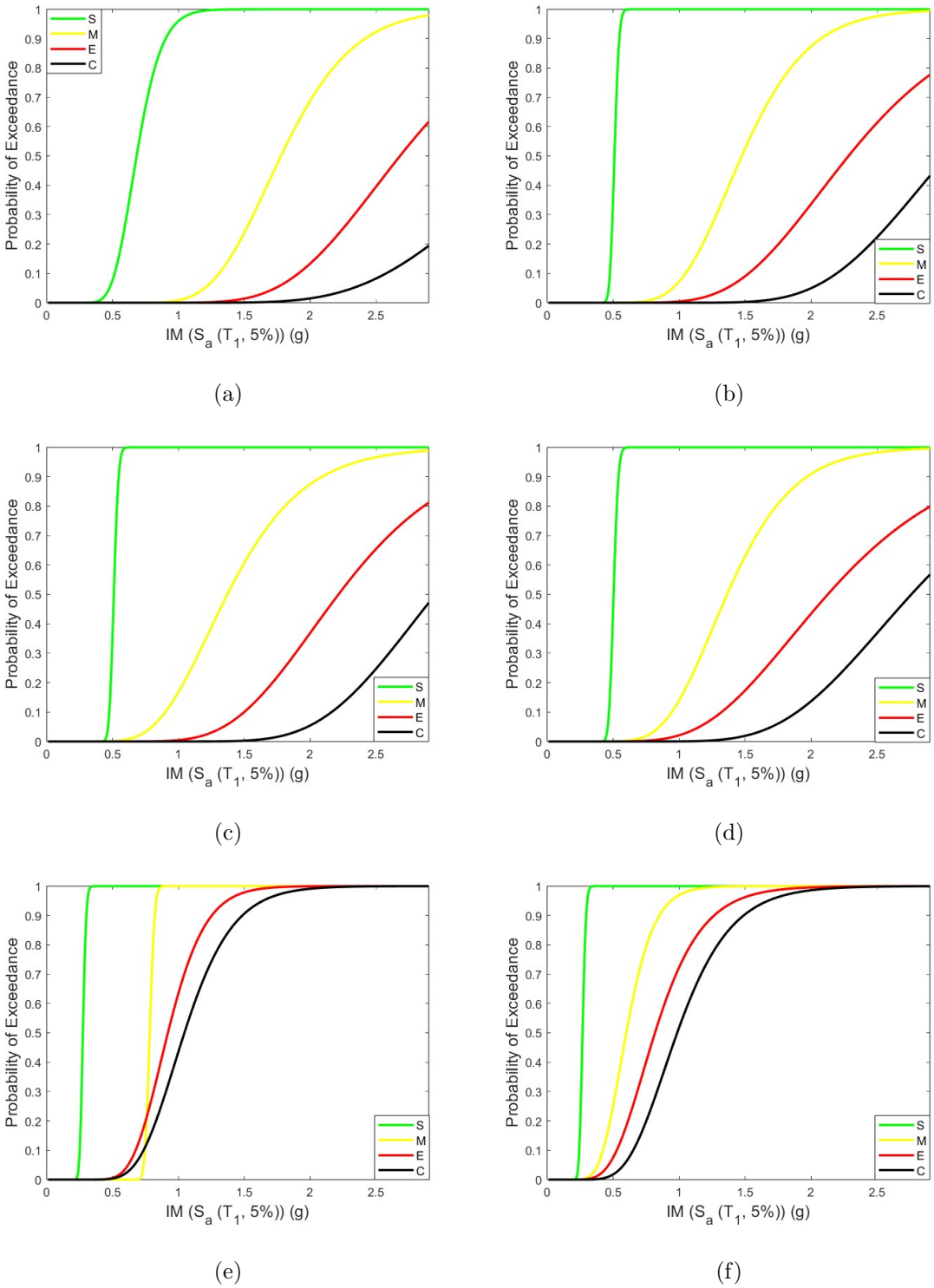

Figure 5.17. Fragility curves in terms of spectral acceleration for 3-story buildings (EDP=MIDR%) (S=Slight, M=Moderate, E=Extensive, C=Complete) (a) pristine 3-2018, (b) aged 3-2018, (c) pristine 3-1997, (d) aged 3-1997, (e) pristine 3-1975, (f) aged 3-1975.

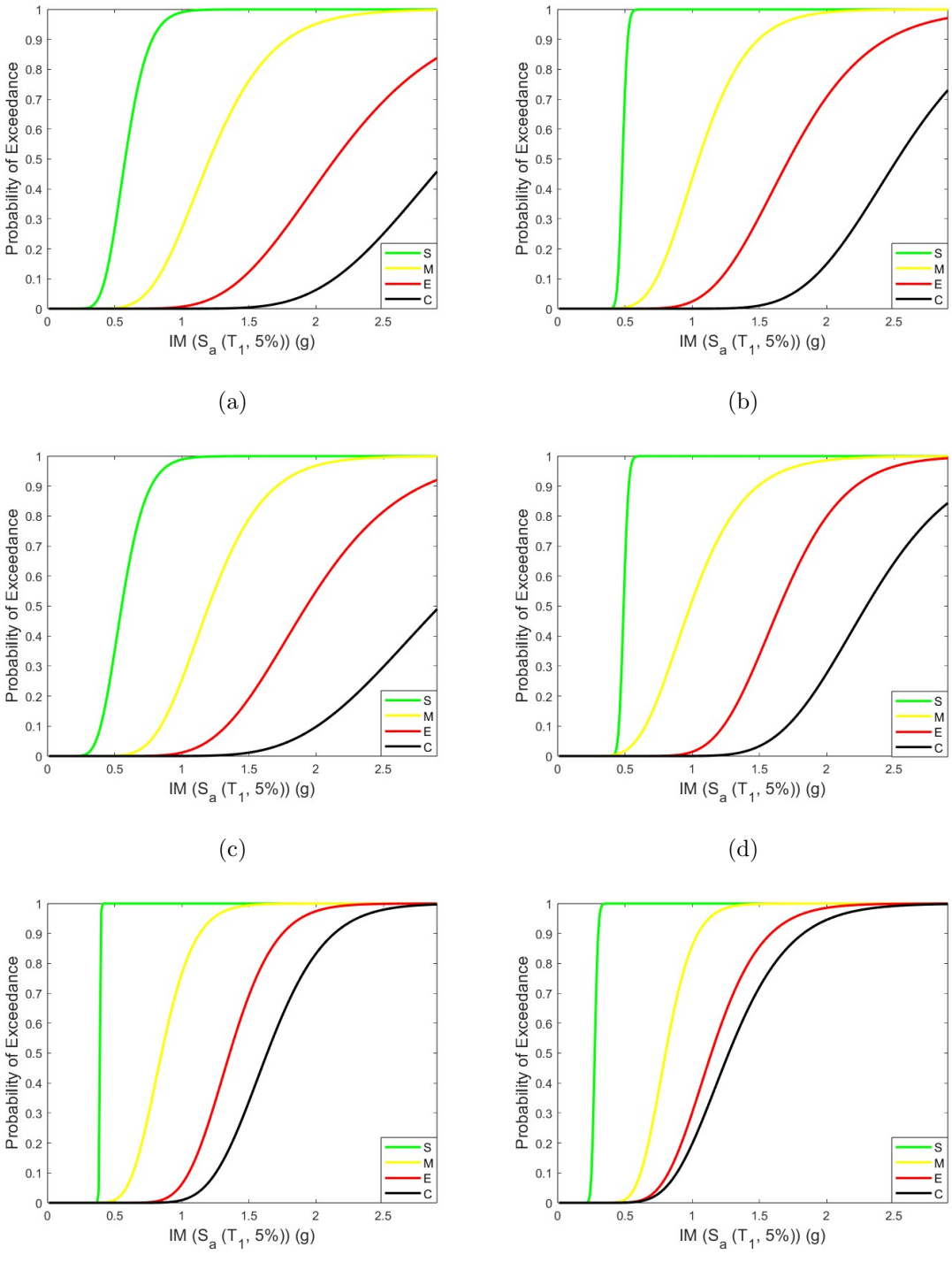

Figure 5.18. Fragility curves in terms of spectral acceleration for 6-story buildings (EDP=MIDR%) (S=Slight, M=Moderate, E=Extensive, C=Complete) (a) pristine 6-2018, (b) aged 6-2018, (c) pristine 6-1997, (d) aged 6-1997, (e) pristine 6-1975, (f) aged 6-1975.

Table 5.5. Parameters of the spectral acceleration-based fragility functions for 3-story buildings (EDP=MIDR%).

Building Name	Slight		Moderate		Extensive		Complete	
	θ (g)	β	θ (g)	β	θ (g)	β	θ (g)	β
Pristine 3-2018	0.682	0.218	1.778	0.239	2.681	0.264	3.699	0.282
Pristine 3-1997	0.509	0.054	1.371	0.328	2.214	0.304	2.950	0.242
Pristine 3-1975	0.274	0.070	0.782	0.036	0.919	0.241	1.045	0.274
Aged 3-2018	0.509	0.054	1.474	0.266	2.283	0.314	3.026	0.251
Aged 3-1997	0.503	0.055	1.363	0.286	2.125	0.371	2.758	0.294
Aged 3-1975	0.267	0.075	0.599	0.272	0.816	0.341	0.984	0.322

Table 5.6. Parameters of the spectral acceleration-based fragility functions for 6-story buildings (EDP=MIDR%).

Building Name	Slight		Moderate		Extensive		Complete	
	θ (g)	β	θ (g)	β	θ (g)	β	θ (g)	β
Pristine 6-2018	0.322	0.234	1.207	0.304	2.142	0.307	2.979	0.260
Pristine 6-1997	0.551	0.260	1.199	0.275	1.928	0.289	2.921	0.293
Pristine 6-1975	0.389	0.013	0.848	0.225	1.356	0.198	1.635	0.208
Aged 6-2018	0.482	0.059	1.046	0.278	1.720	0.274	2.525	0.225
Aged 6-1997	0.489	0.058	0.984	0.322	1.650	0.228	2.294	0.231
Aged 6-1975	0.274	0.070	0.801	0.205	1.141	0.256	1.271	0.282

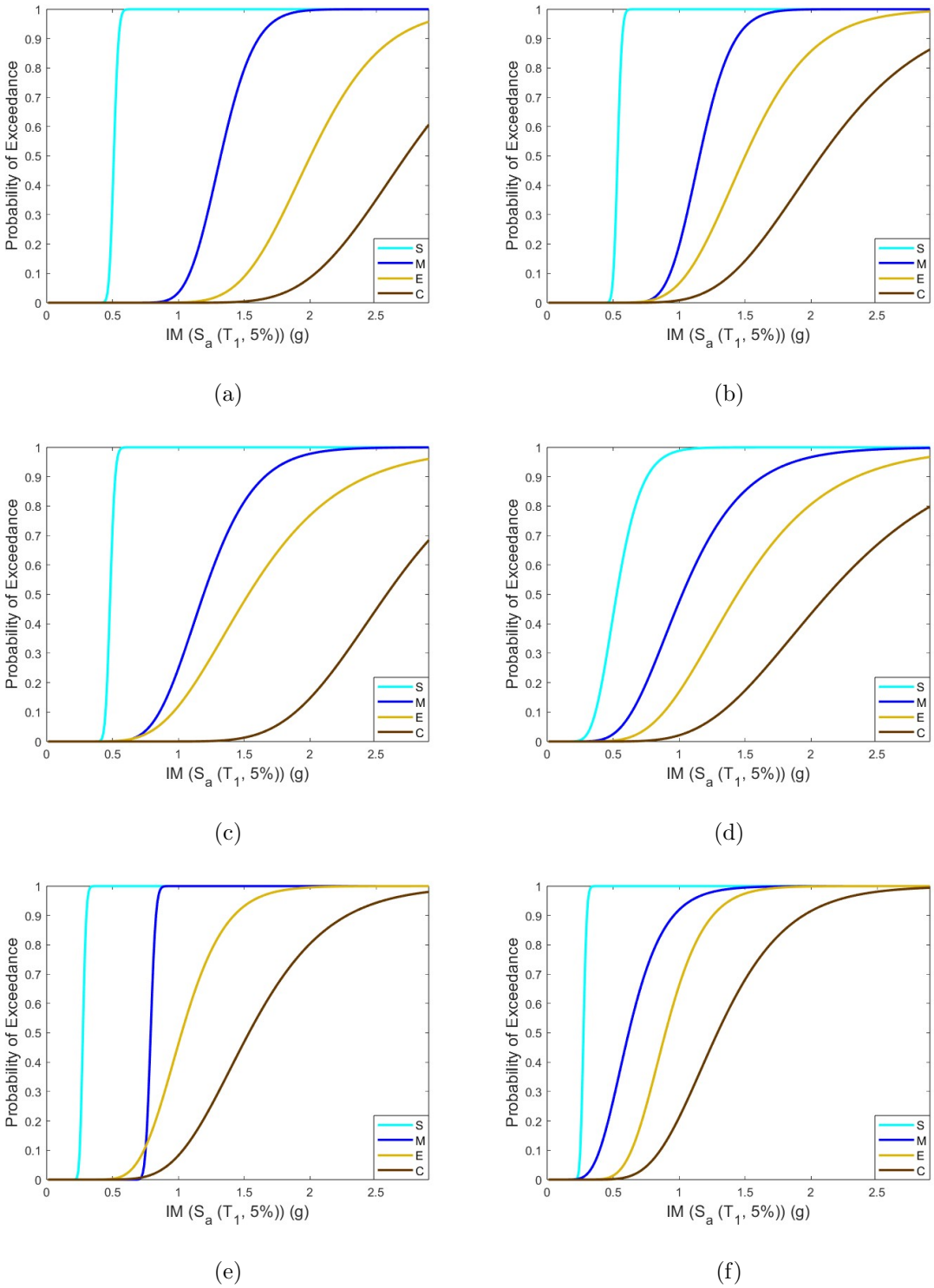

Figure 5.19. Fragility curves in terms of spectral acceleration for 3-story buildings (EDP=D_{Top}) (S=Slight, M=Moderate, E=Extensive, C=Complete) (a) pristine 3-2018, (b) aged 3-2018, (c) pristine 3-1997, (d) aged 3-1997, (e) pristine 3-1975, (f) aged 3-1975.

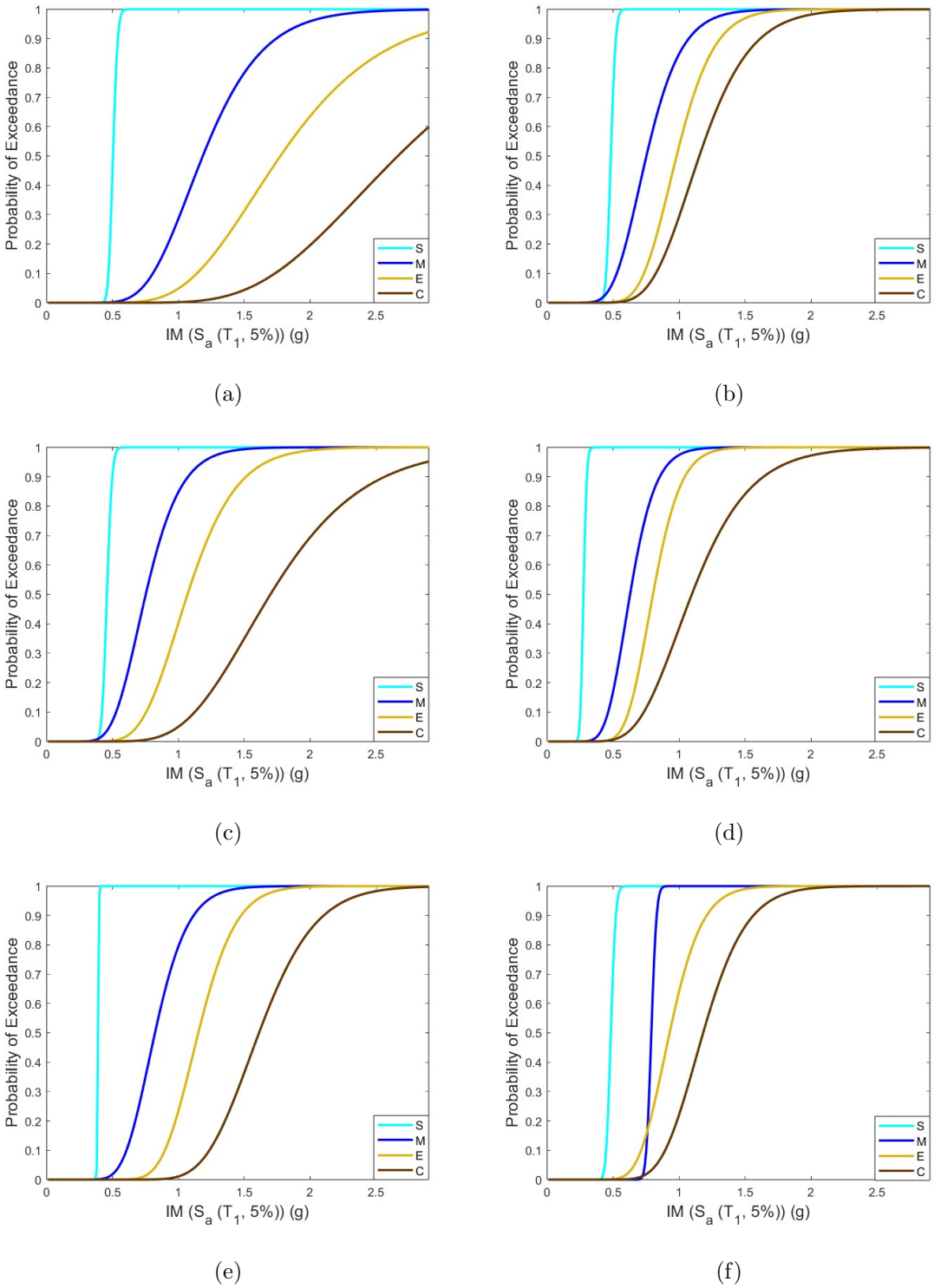

Figure 5.20. Fragility curves in terms of spectral acceleration for 6-story buildings (EDP=D_{Top}) (S=Slight, M=Moderate, E=Extensive, C=Complete) (a) pristine 6-2018, (b) aged 6-2018, (c) pristine 6-1997, (d) aged 6-1997, (e) pristine 6-1975, (f) aged 6-1975.

Table 5.7. Parameters of the spectral acceleration-based fragility functions for 3-story buildings (EDP=D_{Top}).

Building Name	Slight		Moderate		Extensive		Complete	
	θ (g)	β	θ (g)	β	θ (g)	β	θ (g)	β
Pristine 3-2018	0.509	0.054	1.320	0.153	2.002	0.214	2.727	0.226
Pristine 3-1997	0.482	0.059	1.190	0.257	1.530	0.363	2.580	0.243
Pristine 3-1975	0.274	0.070	0.789	0.039	1.024	0.255	1.535	0.308
Aged 3-2018	0.533	0.048	1.155	0.167	1.499	0.269	2.076	0.305
Aged 3-1997	0.526	0.283	1.022	0.365	1.439	0.380	2.125	0.371
Aged 3-1975	0.274	0.070	0.617	0.343	0.895	0.263	1.290	0.319

Table 5.8. Parameters of the spectral acceleration-based fragility functions for 6-story buildings (EDP=D_{Top}).

Building Name	Slight		Moderate		Extensive		Complete	
	θ (g)	β	θ (g)	β	θ (g)	β	θ (g)	β
Pristine 6-2018	0.503	0.055	1.185	0.300	1.774	0.344	2.665	0.335
Pristine 6-1997	0.457	0.067	0.751	0.277	1.069	0.271	1.698	0.322
Pristine 6-1975	0.389	0.013	0.822	0.238	1.150	0.194	1.611	0.207
Aged 6-2018	0.482	0.059	0.751	0.277	0.980	0.226	1.152	0.263
Aged 6-1997	0.274	0.070	0.627	0.239	0.801	0.205	1.095	0.314
Aged 6-1975	0.482	0.059	0.789	0.039	0.927	0.206	1.181	0.218

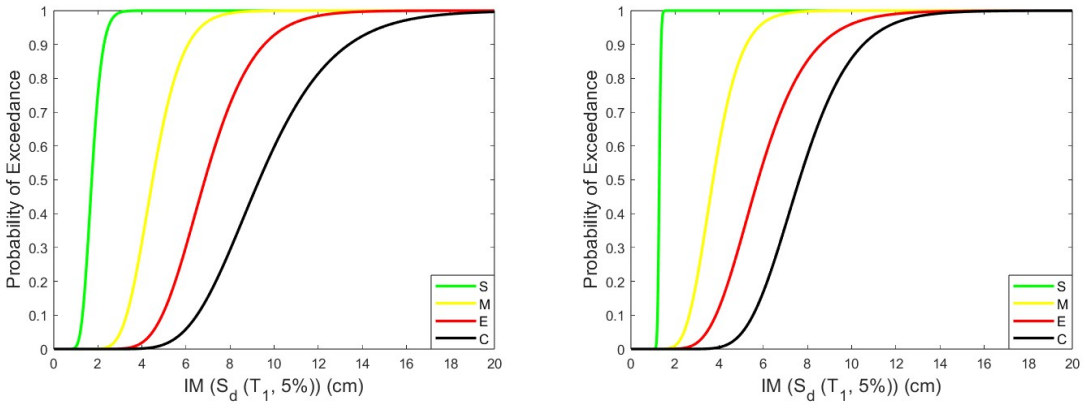

(a)

(b)

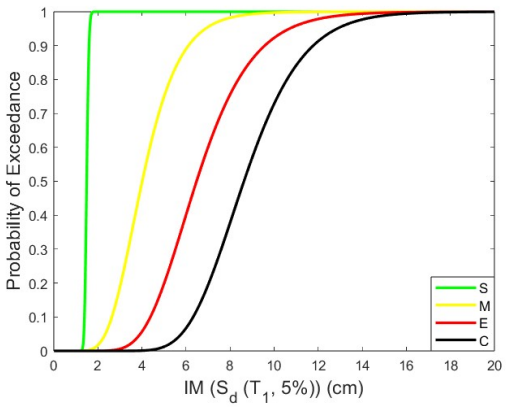

(c)

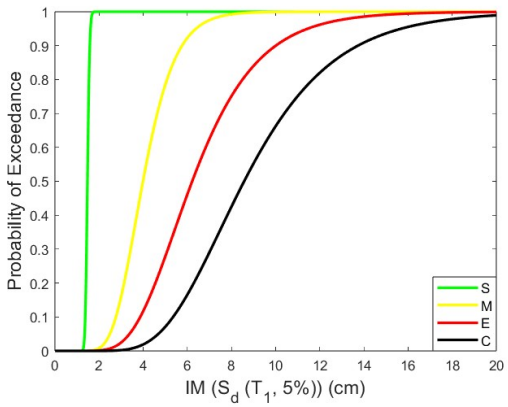

(d)

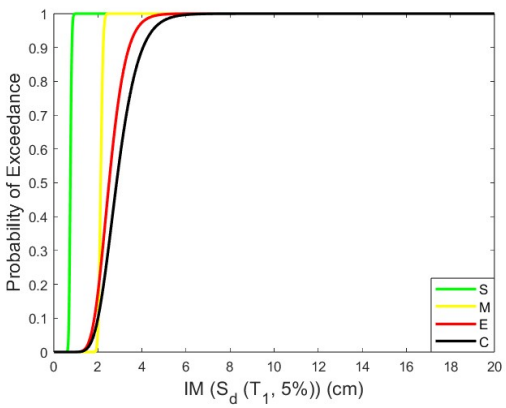

(e)

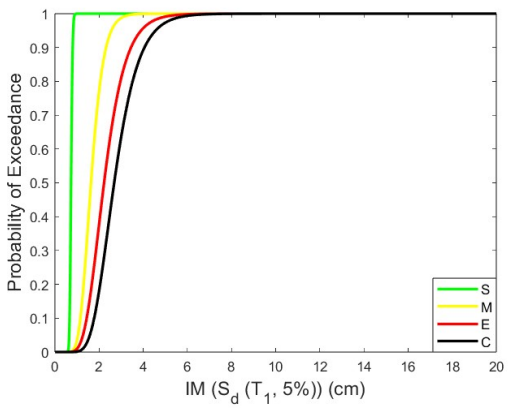

(f)

Figure 5.21. Fragility curves in terms of spectral displacement for 3-story buildings (EDP=MIDR%) (S=Slight, M=Moderate, E=Extensive, C=Complete) (a) pristine 3-2018, (b) aged 3-2018, (c) pristine 3-1997, (d) aged 3-1997, (e) pristine 3-1975, (f) aged 3-1975.

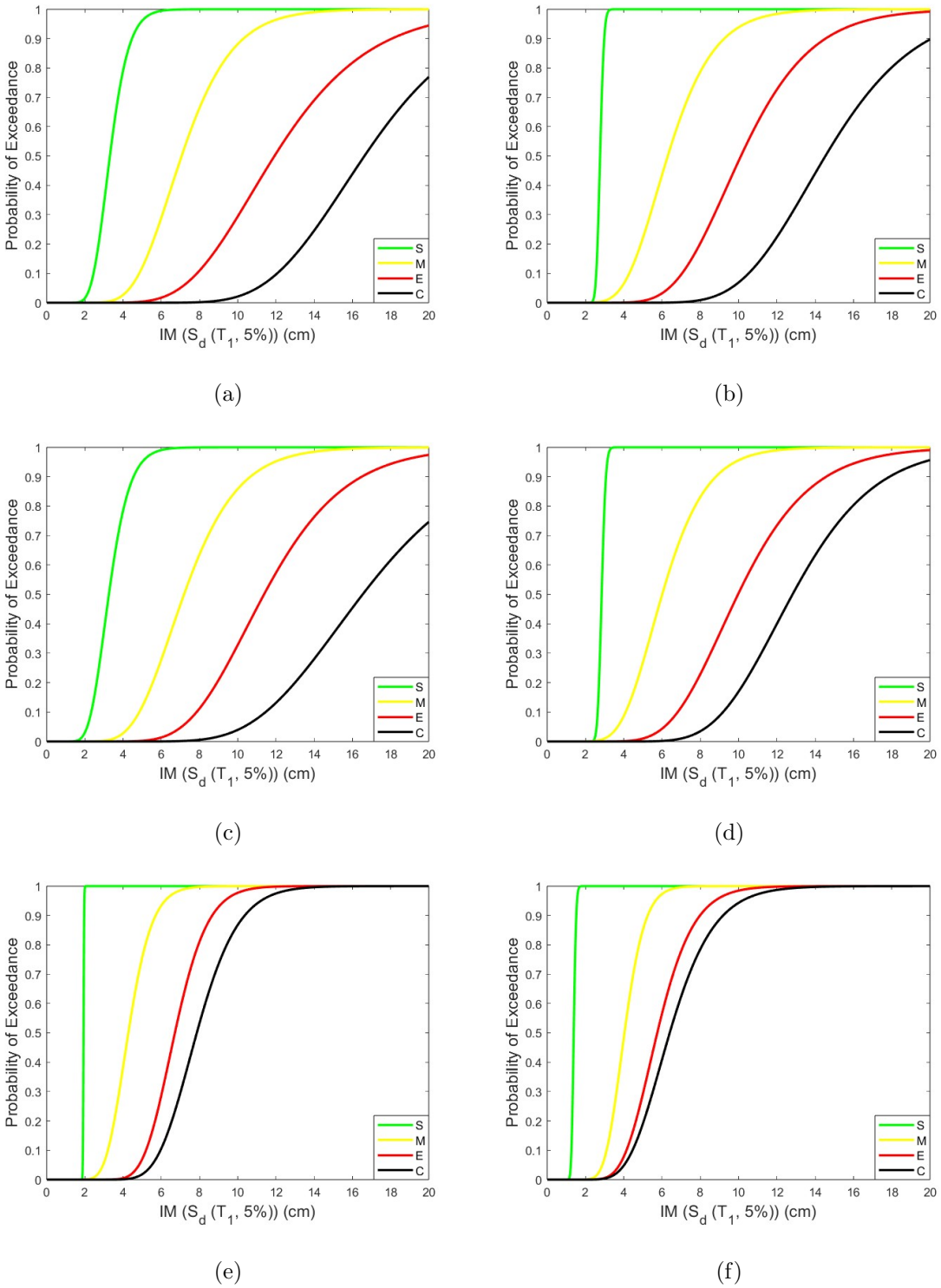

Figure 5.22. Fragility curves in terms of spectral displacement for 6-story buildings (EDP=MIDR%) (S=Slight, M=Moderate, E=Extensive, C=Complete) (a) pristine 6-2018, (b) aged 6-2018, (c) pristine 6-1997, (d) aged 6-1997, (e) pristine 6-1975, (f) aged 6-1975.

Table 5.9. Parameters of the spectral displacement-based fragility functions for 3-story buildings (EDP=MIDR%).

Building Name	Slight		Moderate		Extensive		Complete	
	θ (cm)	β	θ (cm)	β	θ (cm)	β	θ (cm)	β
Pristine 3-2018	1.720	0.218	4.484	0.239	6.855	0.258	9.329	0.282
Pristine 3-1997	1.490	0.054	4.012	0.328	6.477	0.304	8.629	0.242
Pristine 3-1975	0.748	0.070	2.126	0.040	2.506	0.241	2.847	0.274
Aged 3-2018	1.283	0.050	3.718	0.266	5.757	0.314	7.630	0.251
Aged 3-1997	1.471	0.055	3.988	0.286	6.217	0.371	8.571	0.367
Aged 3-1975	0.729	0.075	1.632	0.272	2.224	0.341	2.683	0.322

Table 5.10. Parameters of the spectral displacement-based fragility functions for 6-story buildings (EDP=MIDR%).

Building Name	Slight		Moderate		Extensive		Complete	
	θ (cm)	β	θ (cm)	β	θ (cm)	β	θ (cm)	β
Pristine 6-2018	3.309	0.234	7.063	0.294	11.922	0.324	16.631	0.250
Pristine 6-1997	3.255	0.260	7.188	0.307	11.375	0.289	16.537	0.286
Pristine 6-1975	1.928	0.013	4.274	0.225	6.710	0.199	7.856	0.216
Aged 6-2018	2.762	0.059	6.299	0.299	10.121	0.282	14.534	0.252
Aged 6-1997	2.844	0.059	6.008	0.298	9.968	0.296	12.817	0.259
Aged 6-1975	1.385	0.071	4.036	0.205	5.749	0.256	6.400	0.282

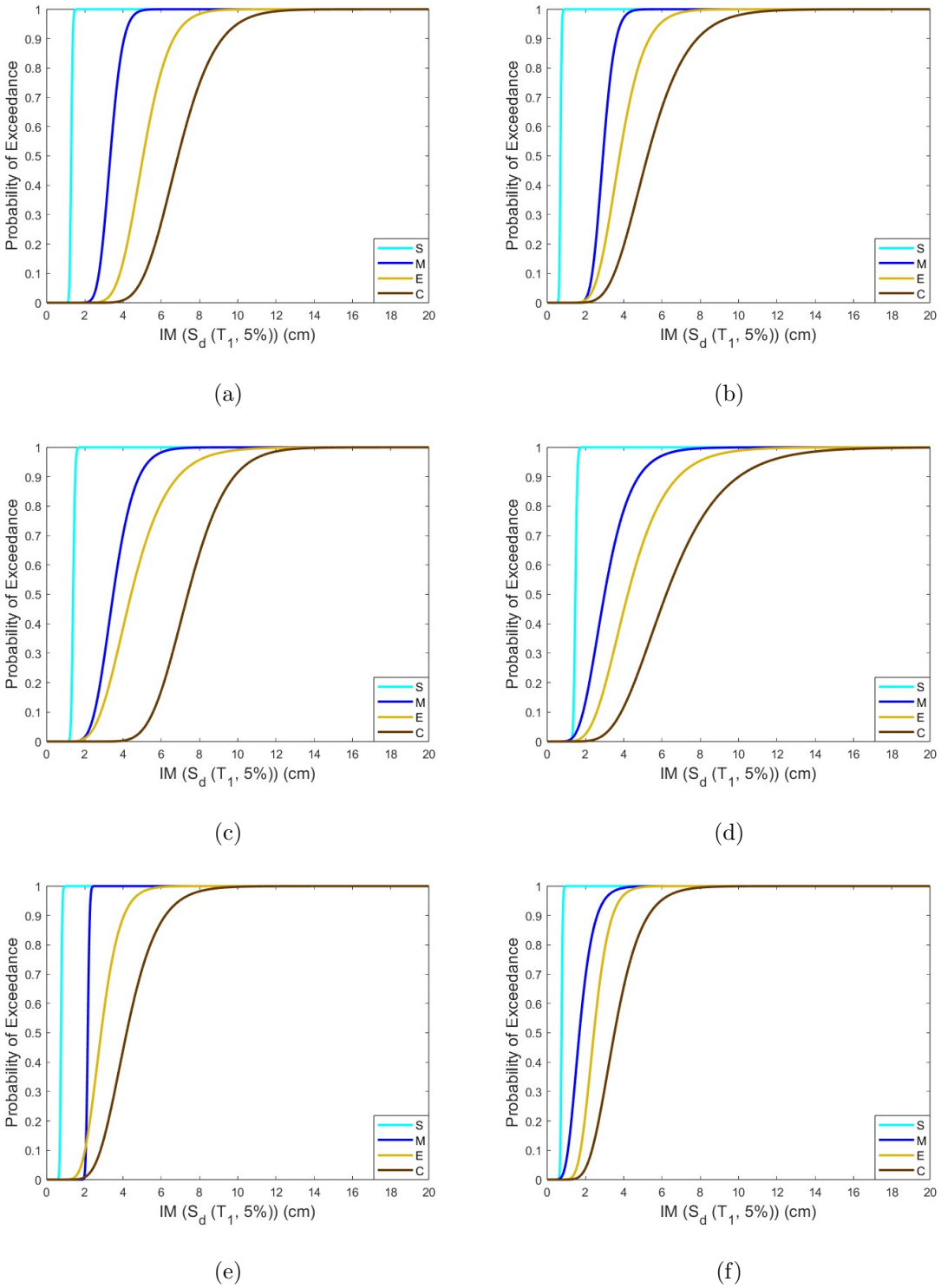

Figure 5.23. Fragility curves in terms of spectral displacement for 3-story buildings (EDP=D_{Top}) (S=Slight, M=Moderate, E=Extensive, C=Complete) (a) pristine 3-2018, (b) aged 3-2018, (c) pristine 3-1997, (d) aged 3-1997, (e) pristine 3-1975, (f) aged 3-1975.

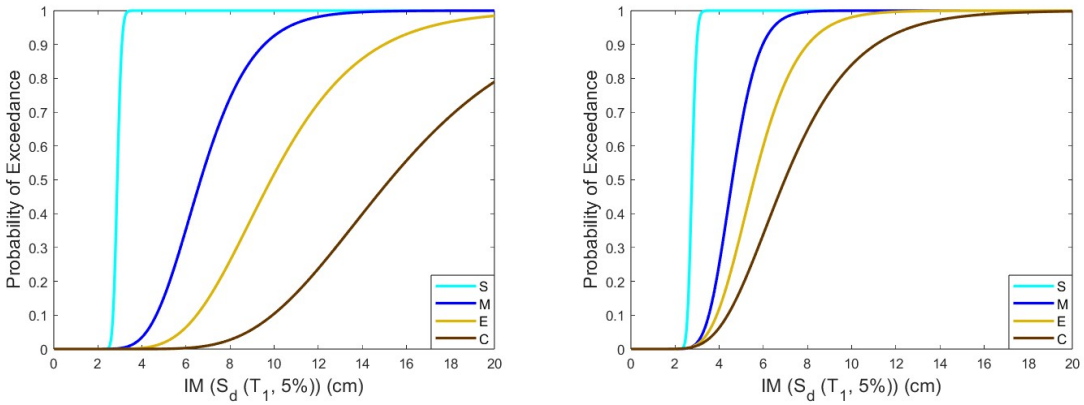

(a)

(b)

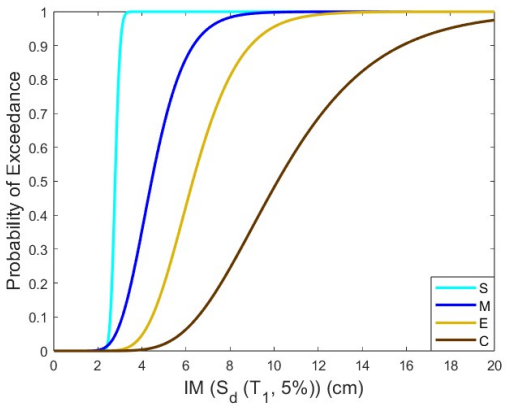

(c)

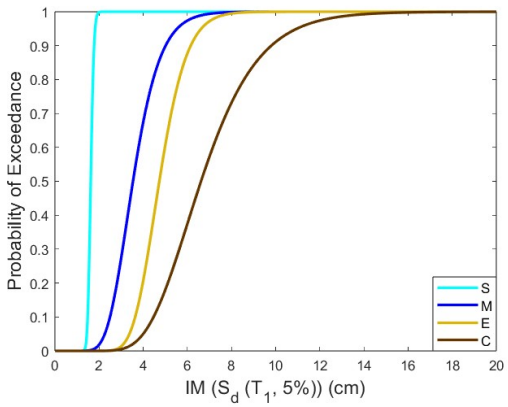

(d)

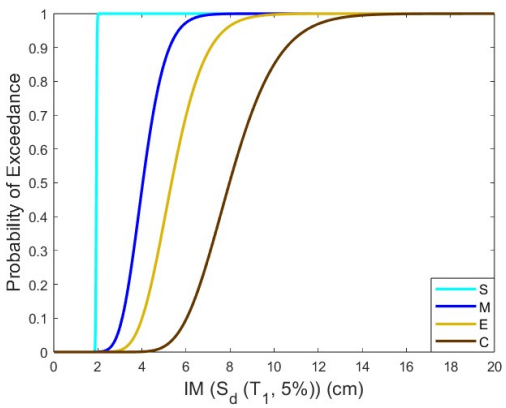

(e)

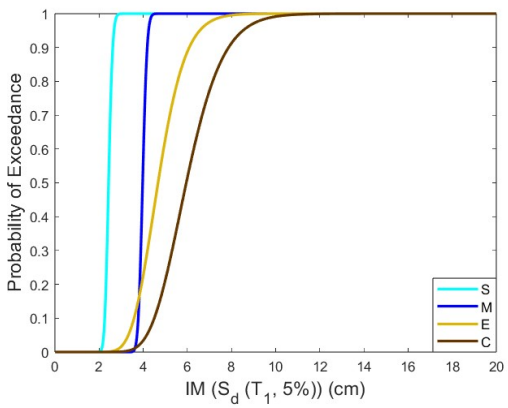

(f)

Figure 5.24. Fragility curves in terms of spectral displacement for 6-story buildings (EDP=D_{Top}) (S=Slight, M=Moderate, E=Extensive, C=Complete) (a) pristine 6-2018, (b) aged 6-2018, (c) pristine 6-1997, (d) aged 6-1997, (e) pristine 6-1975, (f) aged 6-1975.

Table 5.11. Parameters of the spectral displacement-based fragility functions for 3-story buildings (EDP=D_{Top}).

Building Name	Slight		Moderate		Extensive		Complete	
	θ (cm)	β	θ (cm)	β	θ (cm)	β	θ (cm)	β
Pristine 3-2018	1.283	0.050	3.330	0.153	5.049	0.214	6.876	0.226
Pristine 3-1997	1.384	0.060	3.482	0.257	4.417	0.345	7.388	0.221
Pristine 3-1975	0.748	0.070	2.151	0.038	2.847	0.274	4.182	0.308
Aged 3-2018	0.694	0.072	2.912	0.167	3.782	0.269	5.243	0.314
Aged 3-1997	1.471	0.055	2.991	0.365	4.210	0.380	6.218	0.371
Aged 3-1975	0.748	0.070	1.682	0.343	2.440	0.263	3.514	0.319

Table 5.12. Parameters of the spectral displacement-based fragility functions for 6-story buildings (EDP=D_{Top}).

Building Name	Slight		Moderate		Extensive		Complete	
	θ (cm)	β	θ (cm)	β	θ (cm)	β	θ (cm)	β
Pristine 6-2018	2.880	0.054	6.663	0.281	9.860	0.327	15.260	0.335
Pristine 6-1997	2.782	0.064	4.435	0.277	6.305	0.271	10.154	0.344
Pristine 6-1975	1.928	0.013	4.036	0.205	5.341	0.224	7.973	0.218
Aged 6-2018	2.762	0.059	4.590	0.205	5.580	0.282	6.972	0.362
Aged 6-1997	1.620	0.070	3.535	0.272	4.728	0.205	6.618	0.306
Aged 6-1975	2.429	0.058	3.972	0.039	4.670	0.206	5.950	0.217

6. RESULTS AND DISCUSSION

In this study, fragility functions are derived for pristine and aged cases of 3-story and 6-story, moment resisting frame-type reinforced concrete buildings. The buildings representing the low- and mid-rise classes in Istanbul are designed in accordance with the requirements of three seismic codes, namely TBEC-2018, TBEC-1997, and TBEC-1975. To age buildings, 10% corrosion ratio is taken into account based on the study mentioned in Section 2.5.

Nonlinear dynamic analyses are performed by using multiple-stripe analysis using 11 strong ground motion data with 11 IM levels in terms of spectral acceleration and spectral displacement at the fundamental period of the buildings. Fragility results are derived based on dynamic analysis results using structural limit states obtained from nonlinear static analysis as roof displacement, and maximum inter-story drift ratios proposed by Ghobarah [29]. Results are compared in Figures 6.1 to 6.8.

It is clear that a comparison of aged and pristine buildings' fragility curves shows there is a significant decrease in the aged buildings' lateral load-carrying systems resulting in higher damage exceeding probabilities. The relation of fragility curves also displays that there is drastic mitigation in the buildings' response designed per TBEC-75.

There is one thing it must be pointed out from Figure 6.5 (b) illustrating the comparison of fragility curves for a 3-story building designed according to TBEC-97. The figure shows that pristine building has a higher damage probability than aged building after an 8 cm IM value. However, it must be stressed that multiple-stripe analyses are conducted in a certain range, and in that range, result correlates with the expectancy that aged buildings must have lower capacity than pristine buildings.

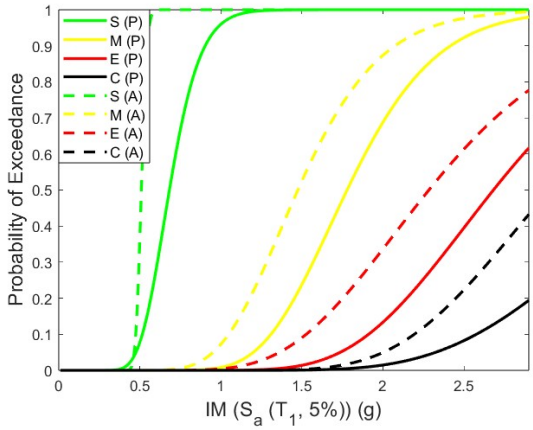

(a)

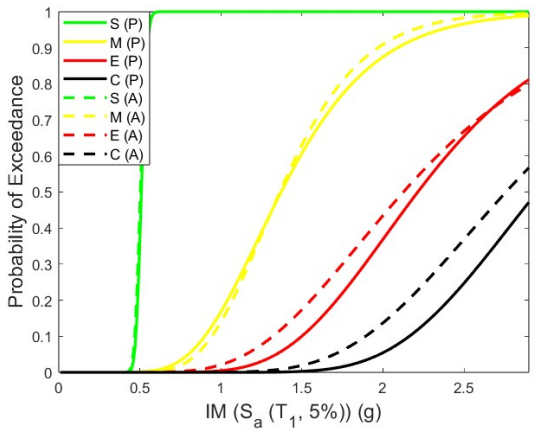

(b)

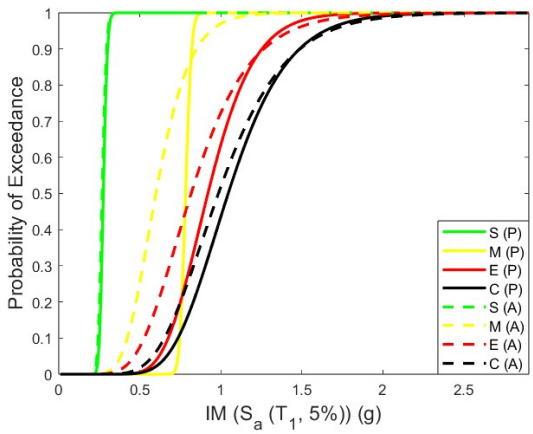

(c)

Figure 6.1. Comparison of fragility curves for pristine (P) (solid) and aged (A) (dashed) 3-story buildings (IM $S_a(T_1,5\%)$, EDP=MIDR%) (S=Slight, M=Moderate, E=Extensive, C=Complete) (a) 3-2018, (b) 3-1997, (c) 3-1975.

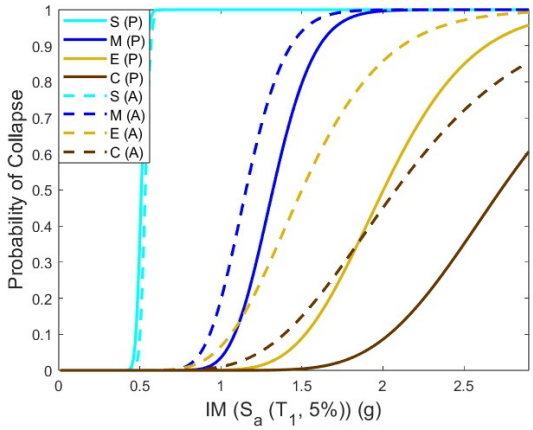

(a)

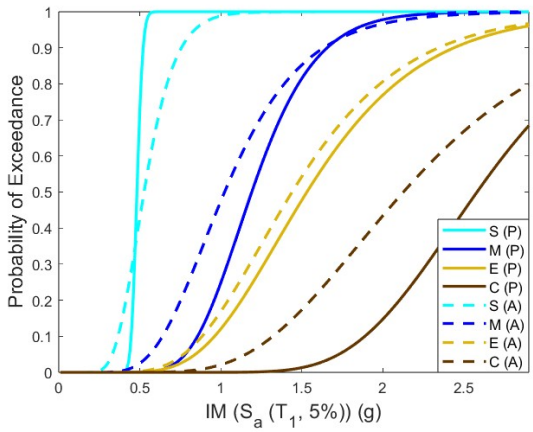

(b)

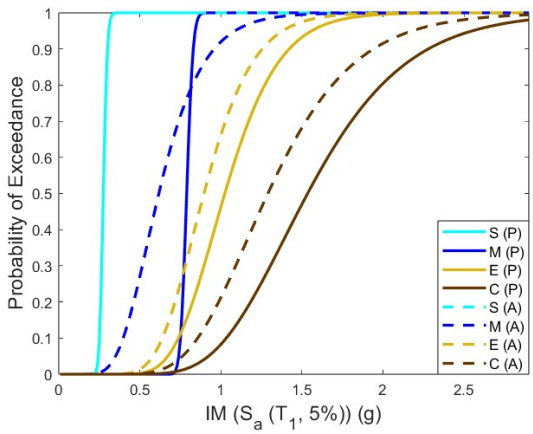

(c)

Figure 6.2. Comparison of fragility curves for pristine (P) (solid) and aged (A) (dashed) 3-story buildings (IM $S_a(T_1$,5%), EDP=D_{Top}) (S=Slight, M=Moderate, E=Extensive, C=Complete) (a) 3-2018, (b) 3-1997, (c) 3-1975.

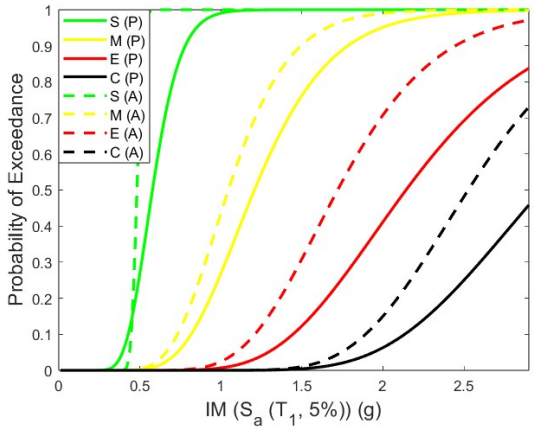

(a)

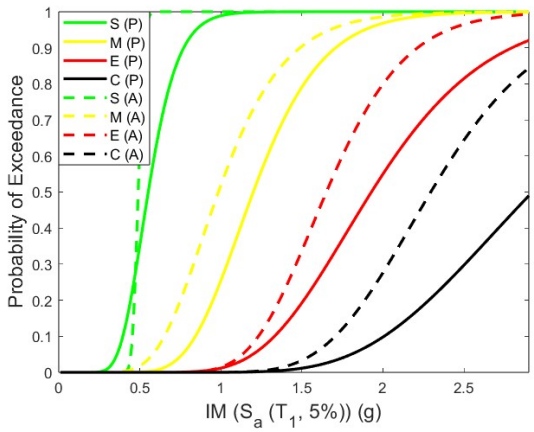

(b)

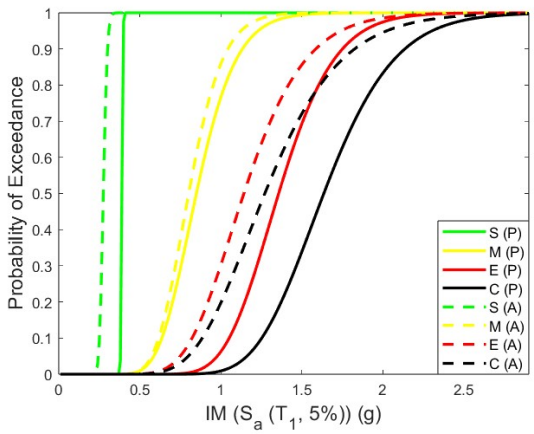

(c)

Figure 6.3. Comparison of fragility curves for pristine (P) (solid) and aged (A) (dashed) 6-story buildings (IM $S_a(T_1,5\%)$, EDP=MIDR%) (S=Slight, M=Moderate, E=Extensive, C=Complete) (a) 6-2018, (b) 6-1997, (c) 6-1975.

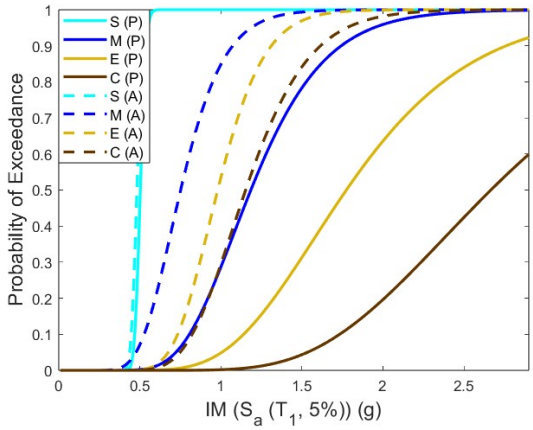

(a)

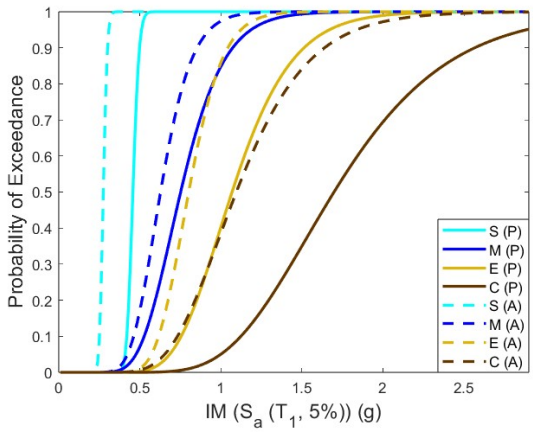

(b)

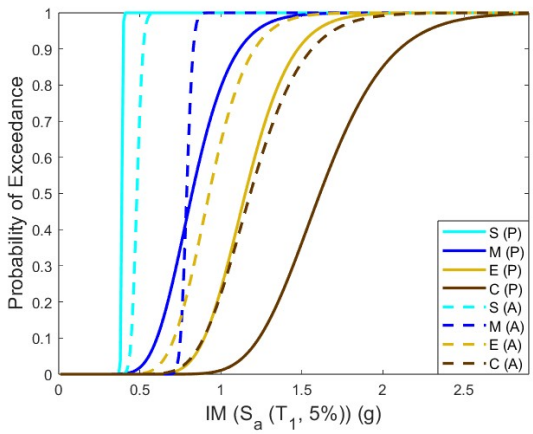

(c)

Figure 6.4. Comparison of fragility curves for pristine (P) (solid) and aged (A) (dashed) 6-story buildings (IM $S_a(T_1,5\%)$, EDP=D_{Top}) (S=Slight, M=Moderate, E=Extensive, C=Complete) (a) 6-2018, (b) 6-1997, (c) 6-1975.

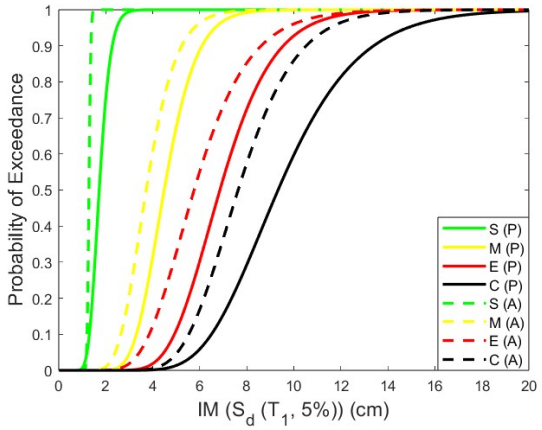

(a)

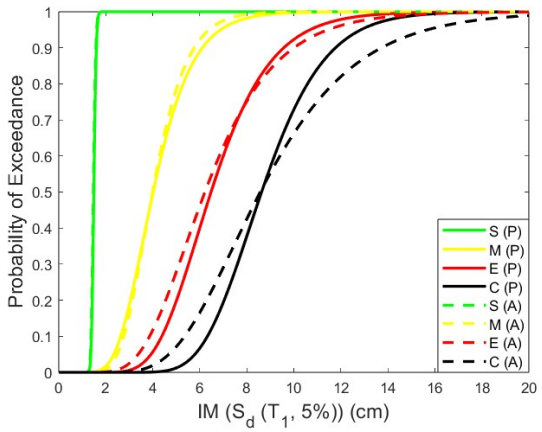

(b)

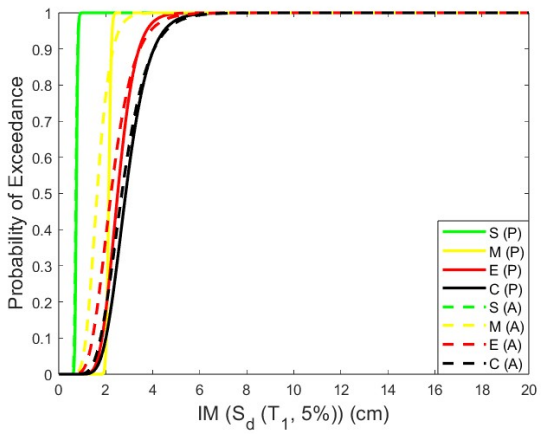

(c)

Figure 6.5. Comparison of fragility curves for pristine (P) (solid) and aged (A) (dashed) 3-story buildings (IM $S_d(T_1,5\%)$, EDP=MIDR%) (S=Slight, M=Moderate, E=Extensive, C=Complete) (a) 3-2018, (b) 3-1997, (c) 3-1975.

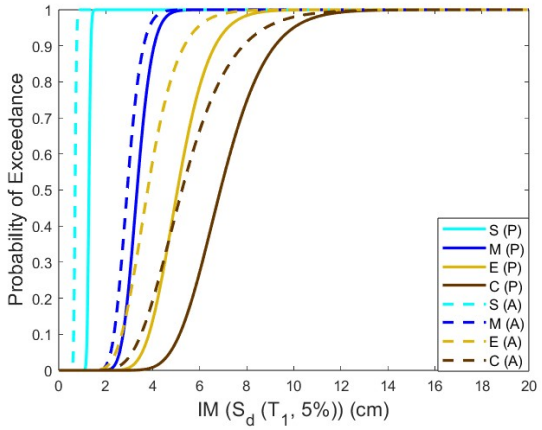

(a)

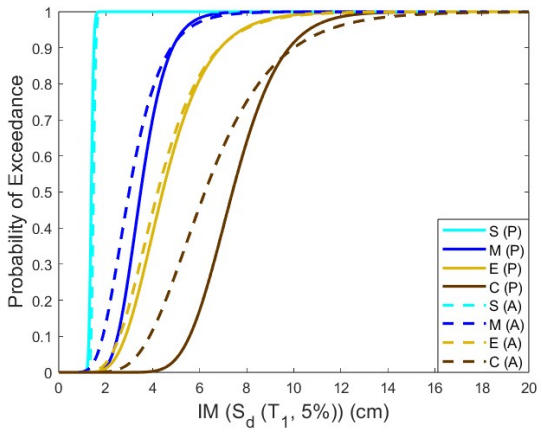

(b)

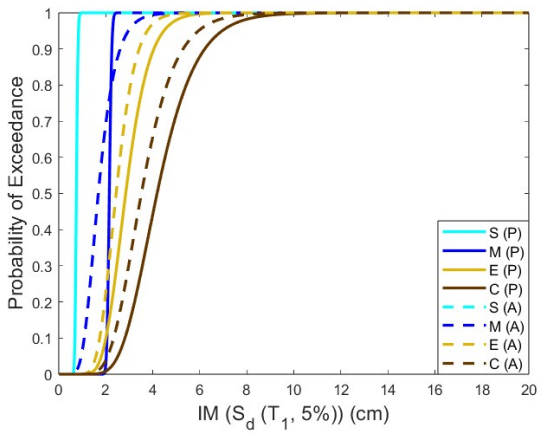

(c)

Figure 6.6. Comparison of fragility curves for pristine (P) (solid) and aged (A) (dashed) 3-story buildings (IM $S_d(T_1,5\%)$, EDP=D_{Top}) (S=Slight, M=Moderate, E=Extensive, C=Complete) (a) 3-2018, (b) 3-1997, (c) 3-1975.

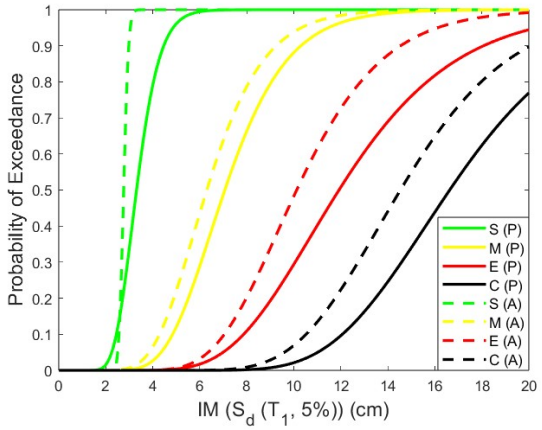

(a)

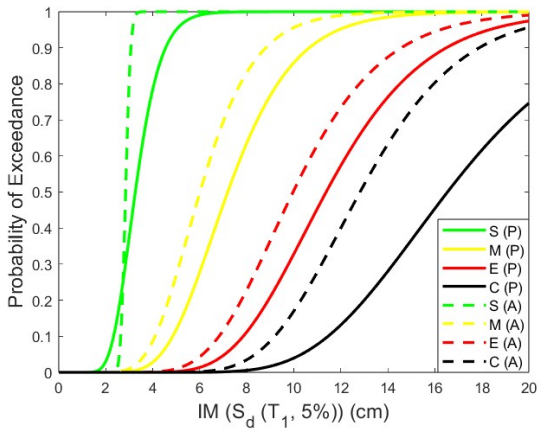

(b)

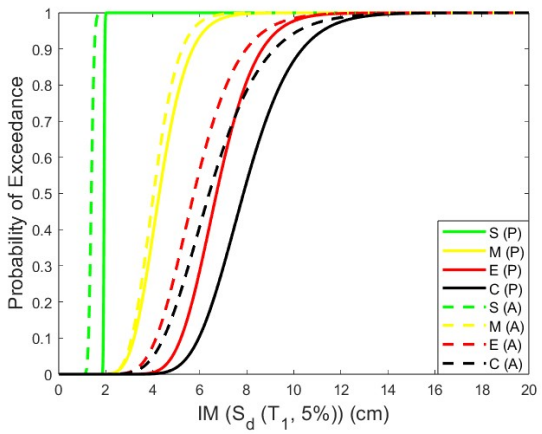

(c)

Figure 6.7. Comparison of fragility curves for pristine (P) (solid) and aged (A) (dashed) 6-story buildings (IM $S_d(T_1,5\%)$, EDP=MIDR%) (S=Slight, M=Moderate, E=Extensive, C=Complete) (a) 6-2018, (b) 6-1997, (c) 6-1975.

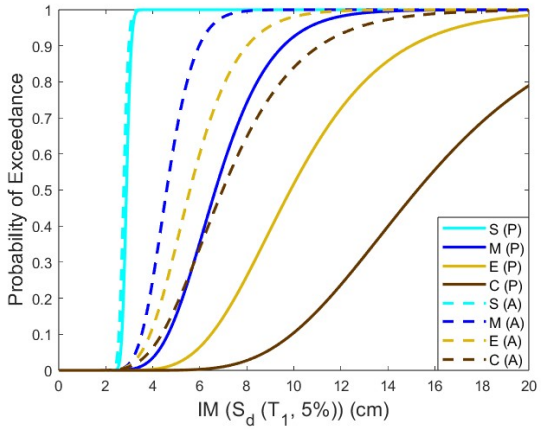

(a)

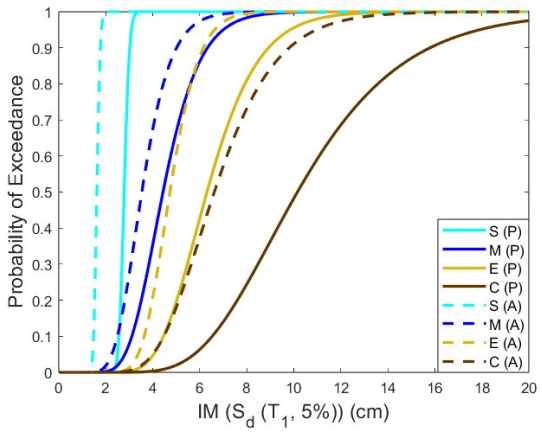

(b)

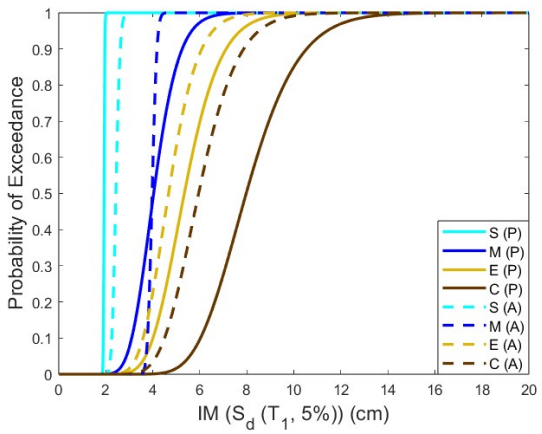

(c)

Figure 6.8. Comparison of fragility curves for pristine (P) (solid) and aged (A) (dashed) 6-story buildings (IM $S_d(T_1,5\%)$, EDP=D_{Top}) (S=Slight, M=Moderate, E=Extensive, C=Complete) (a) 6-2018, (b) 6-1997, (c) 6-1975.

Analytical fragility functions and fragility curves derived for this study are compared to the former study conducted for Istanbul. Probable earthquake loss estimations for Istanbul province [59] are investigated for low and mid-rise reinforced concrete frame structures. Building inventory classification and numeration of structure types are given in Table 6.1 according to [59].

Table 6.1. Building classes and numbers subjected to fragility analysis according to IMM-2019 [59].

Building Type (i)	Story Number (j)	Construction Year (k)	Building Index (B_{ijk})
RC Frame (i=5)	1-4 (j=1)	pre-1980 (k=1)	B511
		1980-2000 (k=2)	B512
		post-2000 (k=3)	B513
	5-8 (j=2)	pre-1980 (k=1)	B521
		1980-2000 (k=2)	B522
		post-2000 (k=3)	B523

In probable earthquake loss estimations for Istanbul province [59], low-rise and mid-rise building classification is considered by story number which is 1-4, and 5-8 respectively. In addition, this research investigates the damage assessment considering the construction years of structures.

The construction years used in this study are also related to earthquake regulations. It is assumed that the buildings built before 1980 were not designed according to any earthquake code, the 1975 regulation were used in the designs of those built between 1980-2000, and the 1997 code was used in the post-2000 ones. Fragility curves based on building index are given in Figure 6.9.

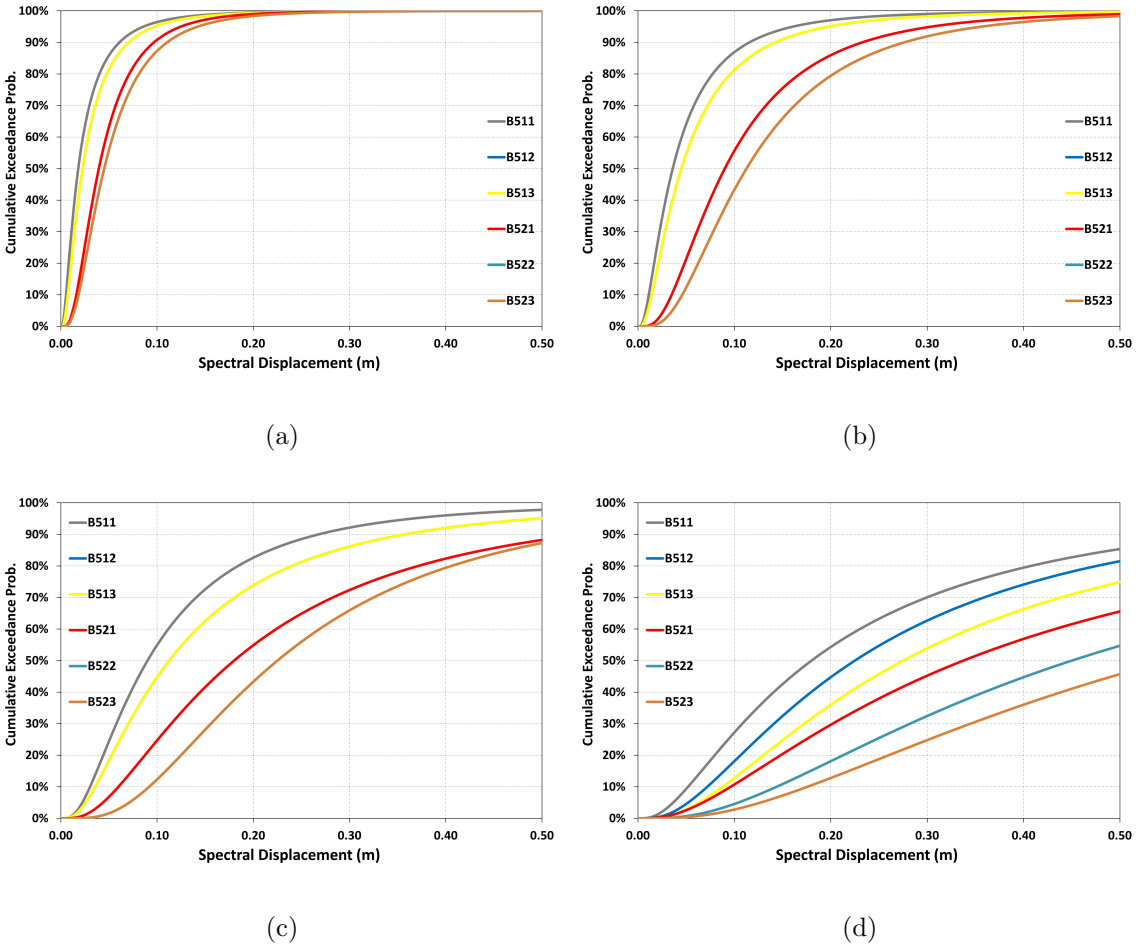

Figure 6.9. Fragility curves from probable earthquake loss estimations for Istanbul province (a) slight, (b) moderate, (c) extensive, (d) complete damage states.

Figure 6.9 illustrates fragility curves for different building index described in Table 6.1. To measure the results better, each damage states' results are presented from the probable earthquake loss estimations for Istanbul province in Figures 6.10 to 6.13, and compared with results that are obtained from this study.

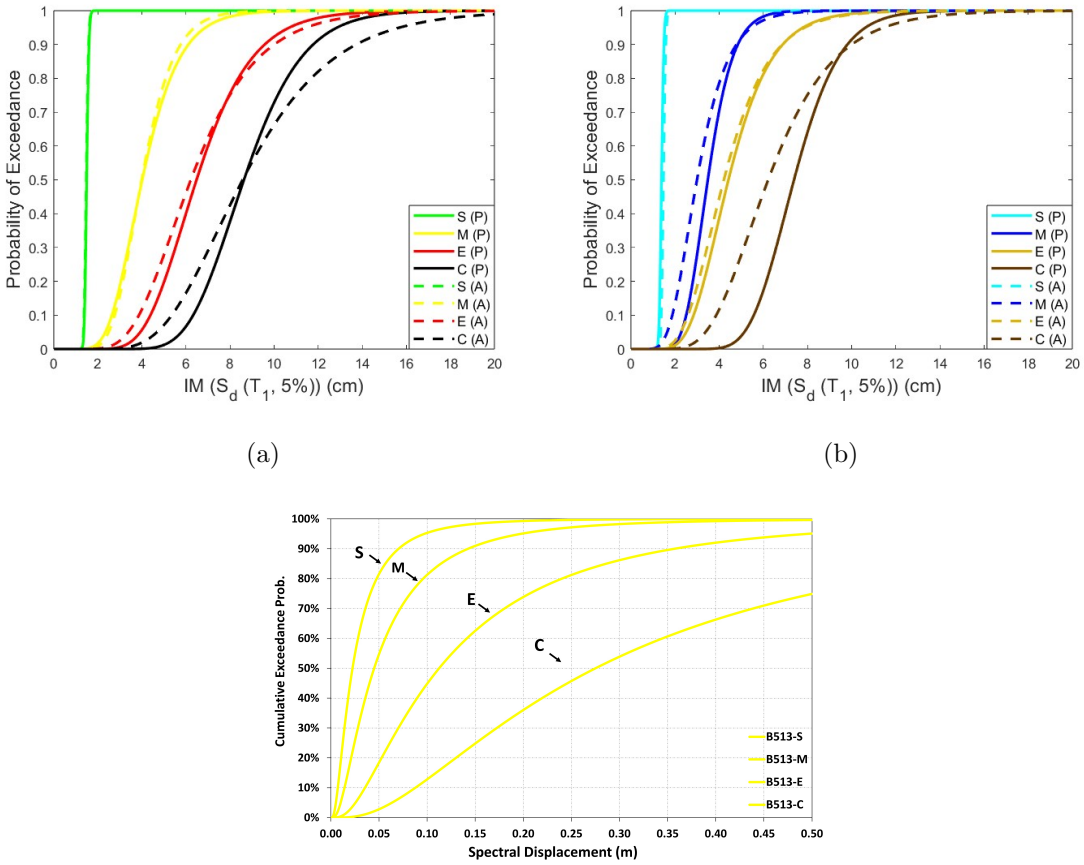

Figure 6.10. The comparison of spectral-displacement based fragility curves from this study, and probable earthquake loss estimations for Istanbul province (S=Slight, M=Moderate, E=Extensive, C=Complete) (a) 3-1997 pristine (solid) and aged (dashed) (EDP=MIDR%), (b) 3-1997 pristine (solid) and aged (dashed) (EDP=D_{Top}), (c) B513.

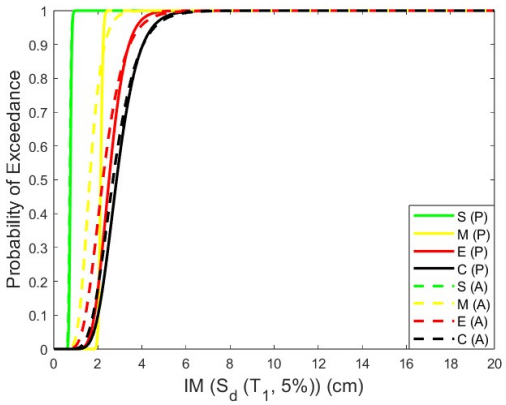

(a)

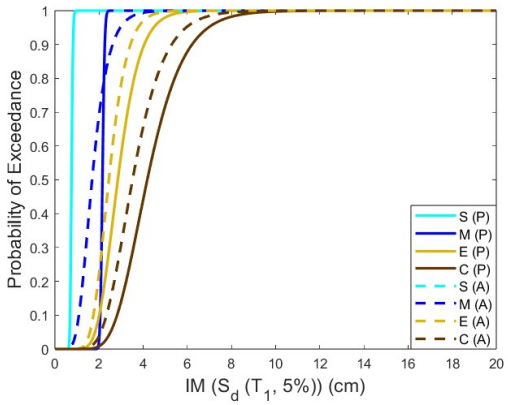

(b)

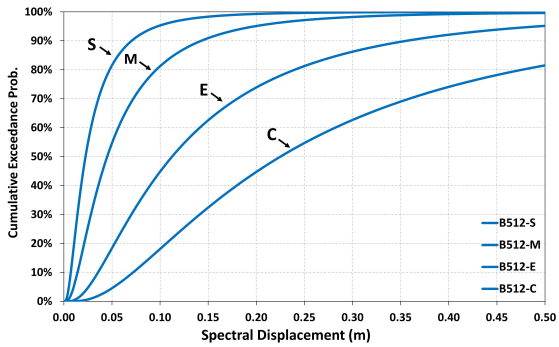

(c)

Figure 6.11. The comparison of spectral-displacement based fragility curves from this study, and probable earthquake loss estimations for Istanbul province (S=Slight, M=Moderate, E=Extensive, C=Complete) (a) 3-1975 pristine (solid) and aged (dashed) (EDP=MIDR%), (b) 3-1975 pristine (solid) and aged (dashed) (EDP=D_{Top}), (c) B512.

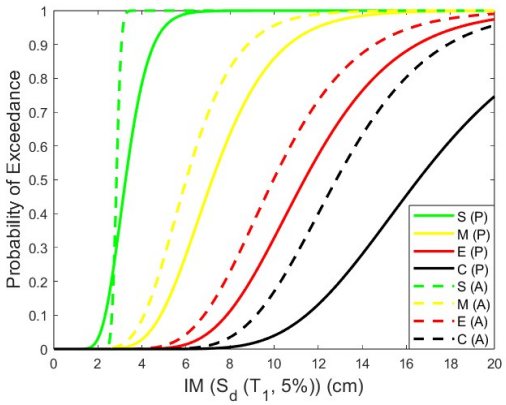

(a)

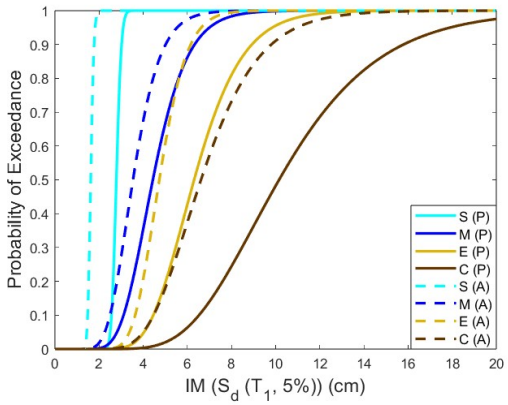

(b)

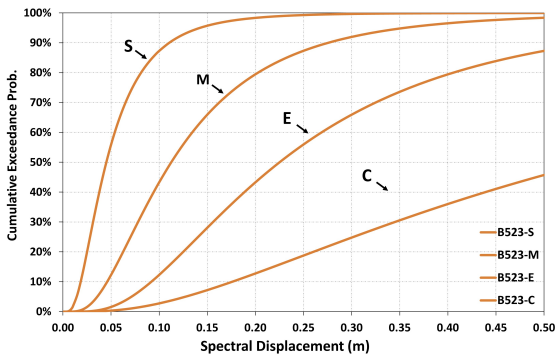

(c)

Figure 6.12. The comparison of spectral-displacement based fragility curves from this study, and probable earthquake loss estimations for Istanbul province (S=Slight, M=Moderate, E=Extensive, C=Complete) (a) 6-1997 pristine (solid) and aged (dashed) (EDP=MIDR%), (b) 6-1997 pristine (solid) and aged (dashed) (EDP=D_{Top}), (c) B523.

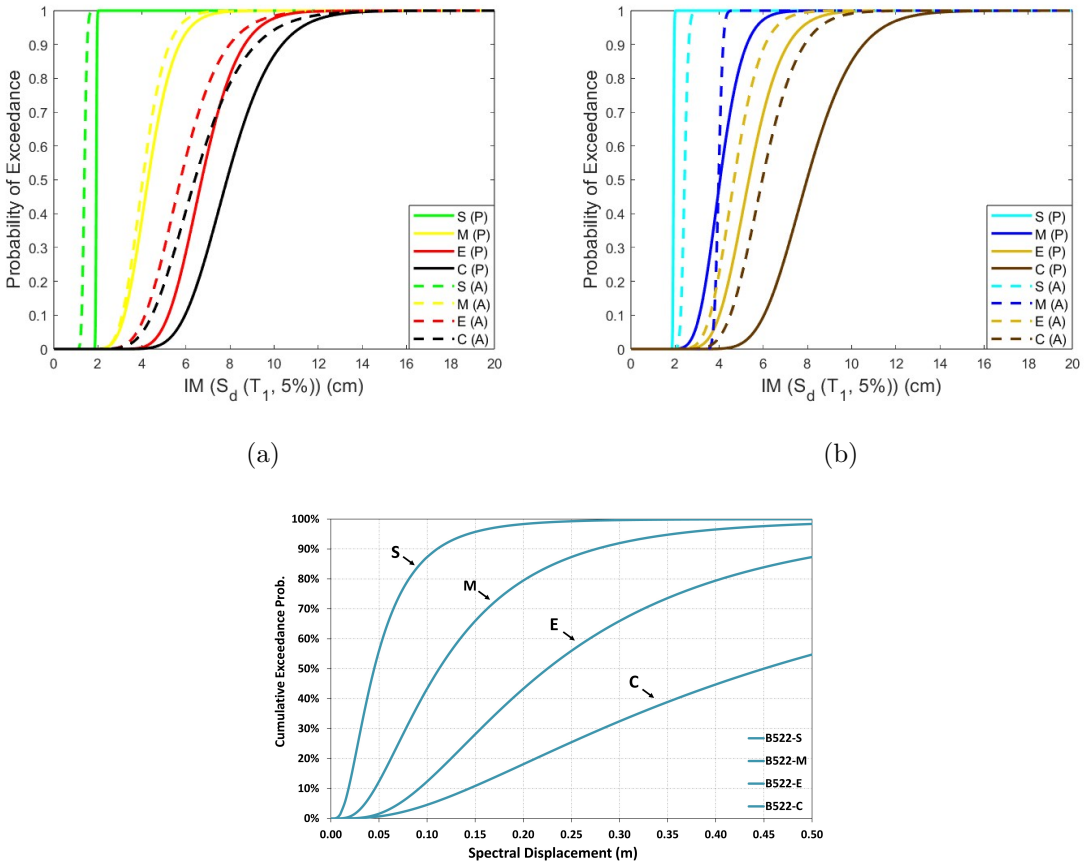

Figure 6.13. The comparison of spectral-displacement based fragility curves from this study, and probable earthquake loss estimations for Istanbul province (S=Slight, M=Moderate, E=Extensive, C=Complete) (a) 6-1975 pristine (solid) and aged (dashed) (EDP=MIDR%), (b) 6-1975 pristine (solid) and aged (dashed) (EDP=D_{Top}), (c) B522.

Figures 6.10, 6.11, 6.12, and 6.13 illustrate spectral-displacement based fragility curves that are obtained from this study and probable earthquake loss estimations for Istanbul province. Figures show that the probability of exceeding the damage states considered for different intensity measures is significantly higher in this study than for those produced for Istanbul [59]. The curves obtained from this study can be used in such studies in the future and can be an alternative to the curves obtained in the past.

Figures 6.14, 6.15, 6.16, and 6.17 present a detailed comparison. Fragility curves for buildings designed according to TBEC-75 and TBEC-97, and for probable earthquake loss estimations for Istanbul province are compared for each damage level and each engineering demand parameter.

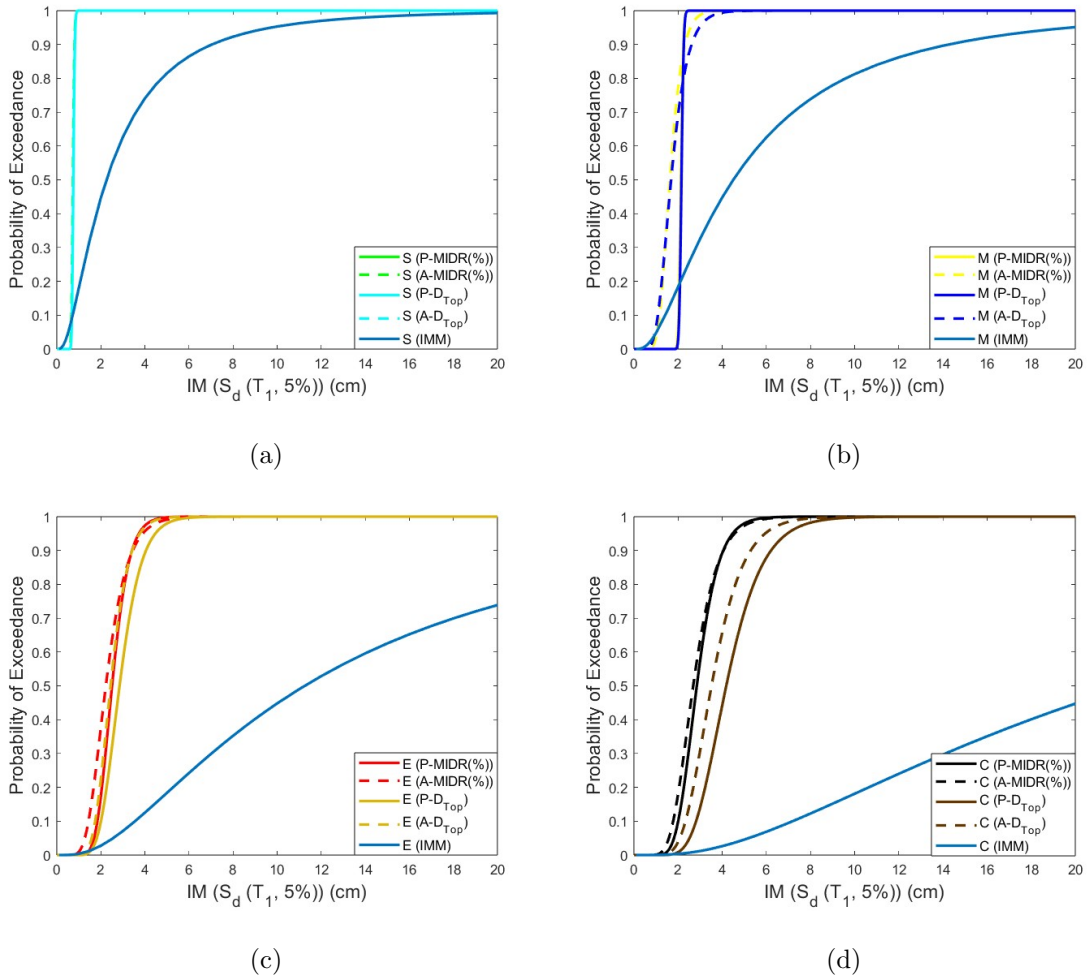

(a) (b)

(c) (d)

Figure 6.14. The comparison of spectral-displacement based fragility curves from this study, and IMM for 3-story building designed per TBEC-1975 (S=Slight, M=Moderate, E=Extensive, C=Complete) (EDP=MIDR% and D_{Top}) (a) for slight damage level, (b) for moderate damage level, (c) for extensive damage level, (d) for complete damage level.

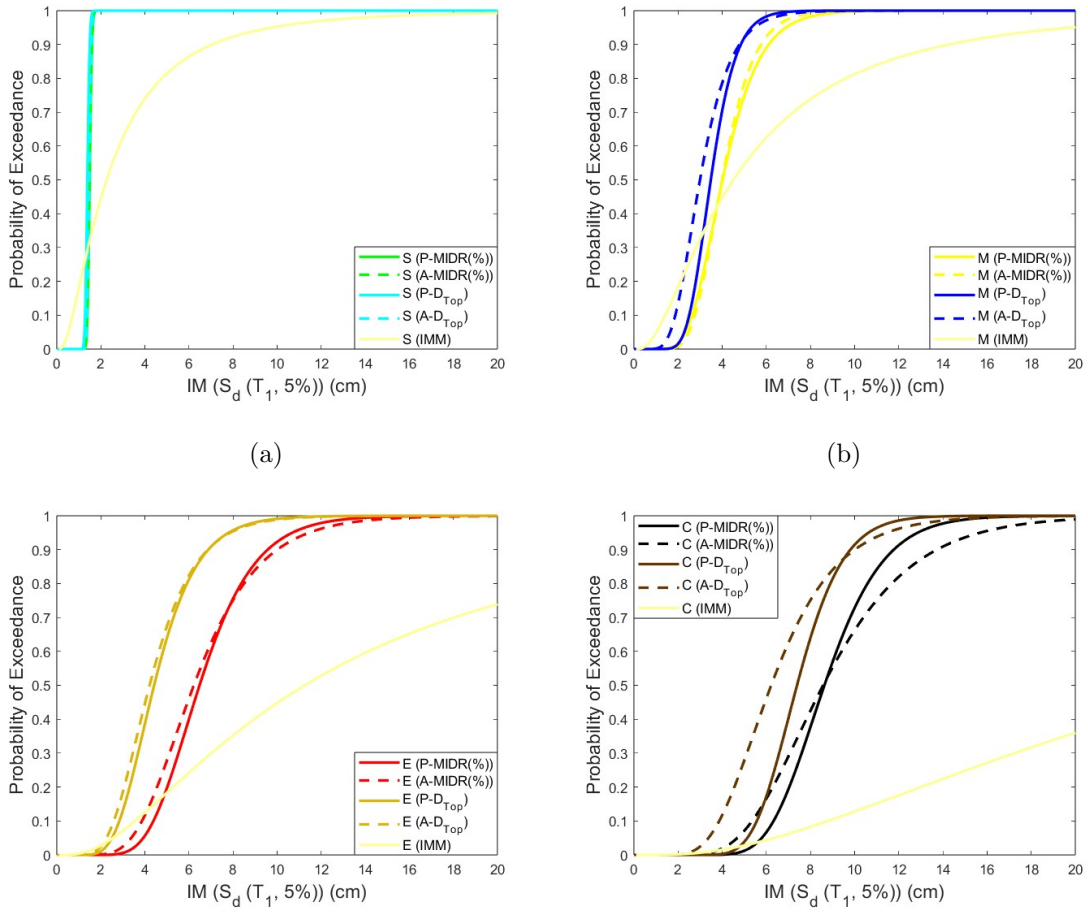

(a) (b)

(c) (d)

Figure 6.15. The comparison of spectral-displacement based fragility curves from this study, and IMM for 3-story building designed per TBEC-1997 (S=Slight, M=Moderate, E=Extensive, C=Complete) (EDP=MIDR% and D_{Top}) (a) for slight damage level, (b) for moderate damage level, (c) for extensive damage level, (d) for complete damage level.

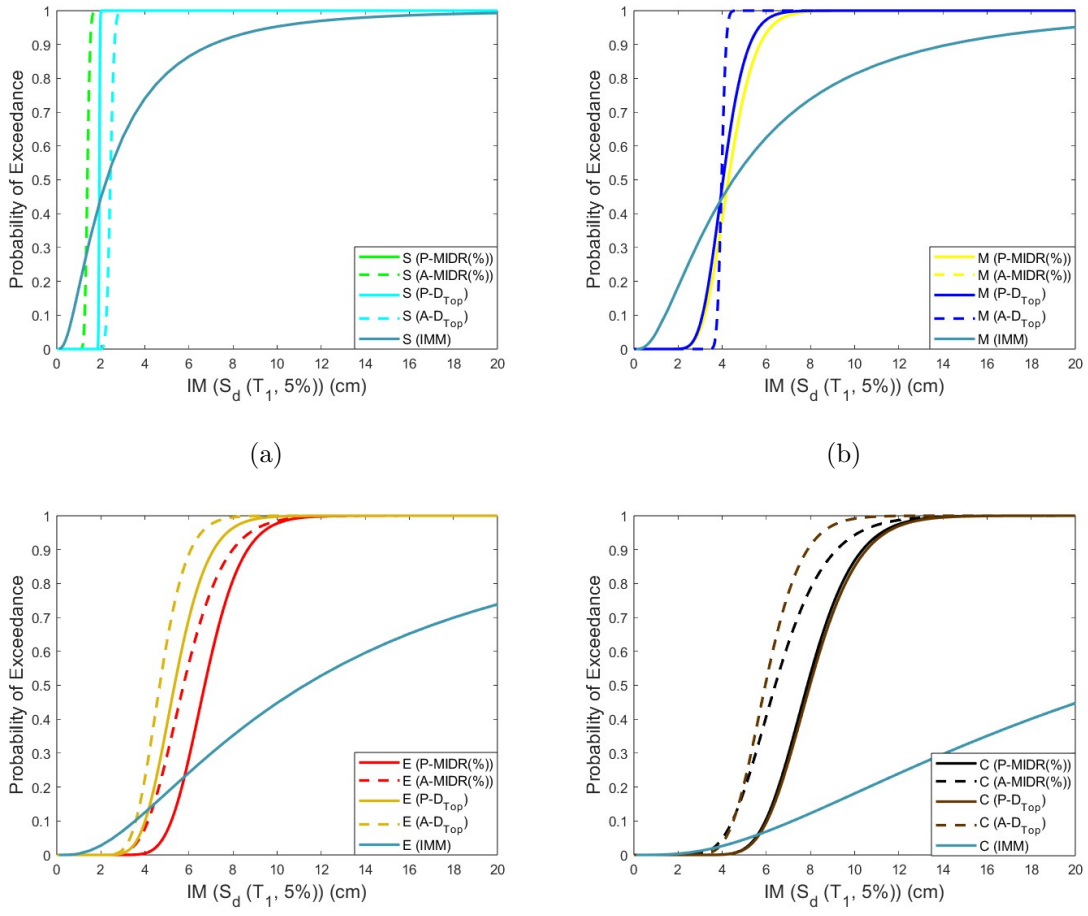

(a) (b)

(c) (d)

Figure 6.16. The comparison of spectral-displacement based fragility curves from this study, and IMM for 6-story building designed per TBEC-1975 (S=Slight, M=Moderate, E=Extensive, C=Complete) (EDP=MIDR% and D_{Top}) (a) for slight damage level, (b) for moderate damage level, (c) for extensive damage level, (d) for complete damage level.

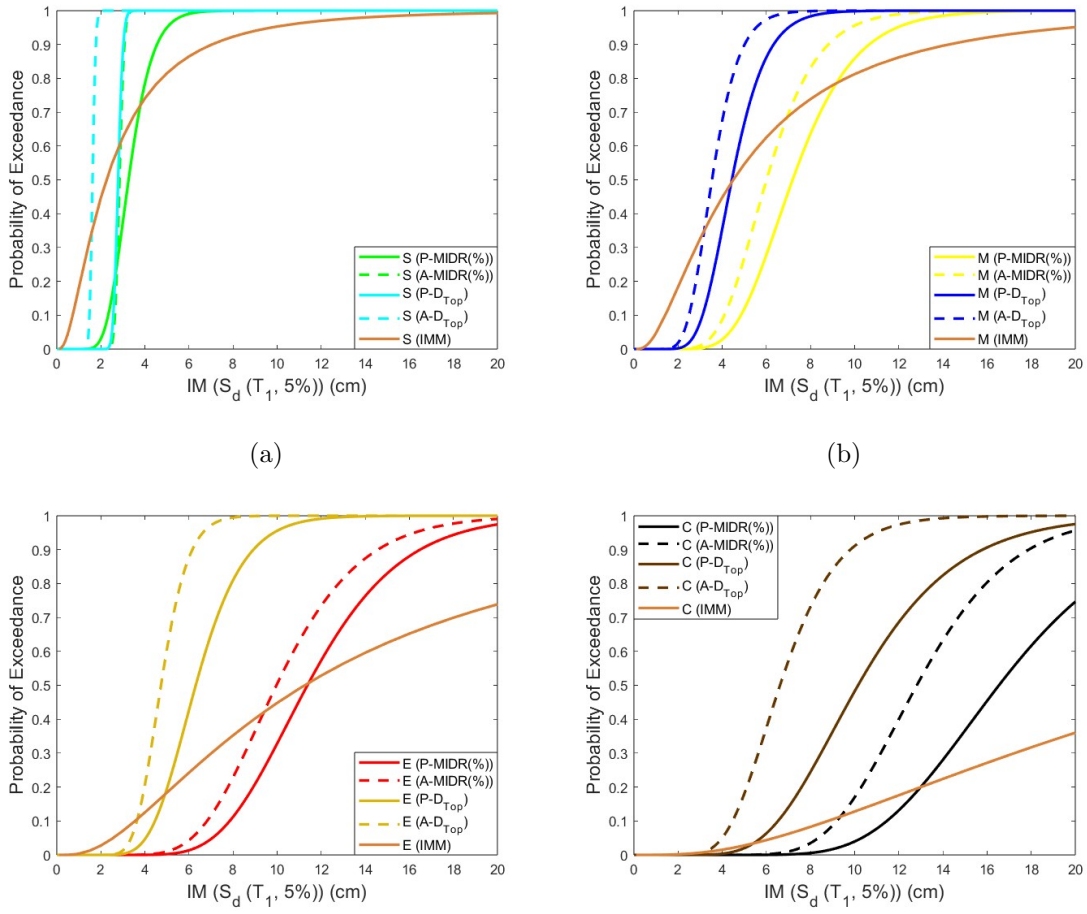

(a) (b)

(c) (d)

Figure 6.17. The comparison of spectral-displacement based fragility curves from this study, and IMM for 6-story building designed per TBEC-1997 (S=Slight, M=Moderate, E=Extensive, C=Complete) (EDP=MIDR% and D_{Top}) (a) for slight damage level, (b) for moderate damage level, (c) for extensive damage level, (d) for complete damage level.

7. CONCLUSION

7.1. Overview

In this study, two actual buildings, 3-story and 6-story, are modeled all over according to different provisions of Turkish Building Earthquake Codes linearly. To do that, equivalent static analysis procedure is conducted using the CSI ETABS software considering seismic threat at the site, and rules that are given in the codes.

For nonlinear modeling and analysis procedures, OpenSees software is used. Distributed plasticity is considered all along the structural members. Nonlinear modeling is done for pristine and aged buildings, and virgin and corroded material models are taken into account to create these models. 10% corrosion ratio is considered for materials to age buildings.

To analyze buildings, multiple-stripe analysis procedure is conducted. To do that, 11 ground motions are selected and scaled to desired spectral acceleration and displacement intensity measure levels. To understand the behavior of buildings, maximum likelihood estimation methodology is utilized for fragility assessment. Engineering demand parameters are considered as maximum inter-story drift ratio and roof displacement.

7.2. Conclusions

It is evident from the comparison of the derived fragility curves that the buildings aged by the effects of corrosion have considerably reduced capacity in their lateral load-carrying systems and thus it leads to higher damage probability estimates by the derived fragility curves.

Fragility assessment results show that the probability of failure for aged 3-story buildings if the maximum inter-story drift ratio is considered as an engineering demand

parameter, can rise to 25% higher than for new buildings, while it is 30% for 6-story buildings approximately. If roof displacement is considered as an engineering demand parameter, the probability of failure for aged 3-story buildings can rise to 45% higher than for new buildings, while it is 60% for 6-story buildings approximately.

In addition, buildings designed according to TBEC-2018 and TBEC-1997 provide a significantly lower probability of failure than structures designed per TBEC-1975, in some cases more than 3 times.

For the buildings designed based on the 1975 seismic code, the differences between the fragility curves of pristine and aged cases are not as apparent as it is for the higher-code buildings. This might be due to already poor stress-strain relationships for smooth reinforcing bars and unconfined concrete models (i.e. even if there is no corrosion).

The presented fragility functions rely on the obtained scatters of structural responses that depend on the selected ground motions and the analysis procedure used. Preliminary results are reported herein to quantify the expected effects of the reinforcing bar corrosion on structural fragility.

There are certain rooms for improvement on this subject. The initiation time of the corrosion during the service life of the building and the levels of its effects on different structural members need to be considered. Rebar slipping mechanism due to corrosion especially in smooth reinforcing bars may also be modeled in structural response analysis. Further research on the ageing of confined concrete is also needed.

REFERENCES

1. Tuutti, K., *Corrosion of Steel in Concrete*, Ph.D. Thesis, The Royal Institute of Technology, 1982.

2. Molina, F., C. Alonso and C. Andrade, "Cover Cracking as a Function of Rebar Corrosion: Part 2—Numerical Model", *Materials and Structures*, Vol. 26, pp. 532–548, 1993.

3. FIB, "Model Code for Concrete Structures", *Structural Concrete*, Vol. 14, 2010.

4. Du, Y., L. Clark and A. Chan, "Residual Capacity of Corroded Reinforcing Bars", *Magazine of Concrete Research*, Vol. 57, No. 3, pp. 135–147, 2005.

5. Du, Y., L. Clark and A. Chan, "Effect of Corrosion on Ductility of Reinforcing Bars", *Magazine of Concrete Research*, Vol. 57, No. 7, pp. 407–419, 2005.

6. Coronelli, D. and P. Gambarova, "Structural Assessment of Corroded Reinforced Concrete Beams: Modeling Guidelines", *Journal of Structural Engineering*, Vol. 130, No. 8, pp. 1214–1224, 2004.

7. Vassie, P. and TRRL, "Reinforcement Corrosion and the Durability of Concrete Bridges.", *Proceedings of the Institution of Civil Engineers*, Vol. 76, No. 3, pp. 713–723, 1984.

8. Ghosh, J. and P. Sood, "Consideration of Time-Evolving Capacity Distributions and Improved Degradation Models for Seismic Fragility Assessment of Aging Highway Bridges", *Reliability Engineering & System Safety*, Vol. 154, pp. 197–218, 2016.

9. Dizaj, E. A., R. Madandoust and M. M. Kashani, "Probabilistic Seismic Vulnerability Analysis of Corroded Reinforced Concrete Frames Including Spatial Variability

of Pitting Corrosion", *Soil Dynamics and Earthquake Engineering*, Vol. 114, pp. 97–112, 2018.

10. Baker, J. W., "Efficient Analytical Fragility Function Fitting Using Dynamic Structural Analysis", *Earthquake Spectra*, Vol. 31, No. 1, pp. 579–599, 2015.

11. "Turkish Building Earthquake Code", Turkish Earthquake Code Draft, Disaster and Emergency Management Presidency, Ankara, 2018.

12. "Turkish Building Earthquake Code", Turkish Earthquake Code Draft, Disaster and Emergency Management Presidency, Ankara, 1997.

13. "Turkish Building Earthquake Code", Turkish Earthquake Code Draft, Disaster and Emergency Management Presidency, Ankara, 1975.

14. Demircioglu, M. B., *Earthquake Hazard and Risk Assessment for Turkey*, Ph.D. Thesis, Boğaziçi University, 2010.

15. Medvedev, S. and W. Sponheuer, "Scale of Seismic Intensity", *Proc. IV World Conference of the Earthquake Engineering, Santiago, Chile, A-2*, pp. 143–153, 1969.

16. Akkar, S., T. Azak, T. Çan, U. Çeken, M. Demircioğlu Tümsa, T. Duman, M. Erdik, S. Ergintav, F. Kadirioğlu, D. Kalafat *et al.*, "Evolution of Seismic Hazard Maps in Turkey", *Bulletin of Earthquake Engineering*, Vol. 16, pp. 3197–3228, 2018.

17. "Turkish Earthquake Hazard Map", Disaster Emergency Management Presidency, 1996, `https://tdth.afad.gov.tr/`.

18. "Turkish Earthquake Hazard Map", Disaster Emergency Management Presidency, 2017, `https://tdth.afad.gov.tr/`.

19. Di-Sarno, L. and A. Elnashai, "Seismic Fragility Relationships for Structures", *Advances in Assessment and Modeling of Earthquake Loss*, pp. 189–222, Springer International Publishing Cham, 2021.

20. Silva, V., S. Akkar, J. Baker, P. Bazzurro, J. M. Castro, H. Crowley, M. Dolsek, C. Galasso, S. Lagomarsino, R. Monteiro *et al.*, "Current Challenges and Future Trends in Analytical Fragility and Vulnerability Modeling", *Earthquake Spectra*, Vol. 35, No. 4, pp. 1927–1952, 2019.

21. Jalayer, F., *Direct Probabilistic Seismic Analysis: Implementing Non-Linear Dynamic Assessments*, Stanford University, 2003.

22. Vamvatsikos, D. and C. A. Cornell, "Incremental Dynamic Analysis", *Earthquake Engineering & Structural Dynamics*, Vol. 31, No. 3, pp. 491–514, 2002.

23. "Seismic Evaluation and Retrofit of Concrete Buildings (ATC-40).", Applied Technology Council, 1996.

24. Akkar, S., H. Sucuoğlu and A. Yakut, "Displacement-Based Fragility Functions for Low-and Mid-rise Ordinary Concrete Buildings", *Earthquake Spectra*, Vol. 21, No. 4, pp. 901–927, 2005.

25. "Assesing Seismic Performance Irregularities. (FEMA-P365)", Structural Engineers Association of California (SEAOC), ATC, and CUREE Joint Venture for the Federal Emergency Management Agency, Washington, D.C, 2012.

26. "Seismic Evaluation and Retrofit of Existing Buildings (ASCE/SEI41-17).", ASCE/SEI Seismic Rehabilitation Committee, American Society of Civil Engineers, Reston, VA., 2017.

27. Giovinazzi, S. and S. Lagomarsino, "A Macroseismic Method for the Vulnerability Assessment of Buildings", 13^{th} *World Conference on Earthquake Engineering*, Vol. 896, pp. 1–6, 2004.

28. "HAZUSMH MR5-Advanced Engineering Building Module: Technical and User's Manual", Federal Emergency Management Agency, Washington DC, USA, 2003.

29. Ghobarah, A., "On Drift Limits Associated with Different Damage Levels", *International Workshop on Performance-Based Seismic Design*, Vol. 28, Department of Civil Engineering, McMaster University Ontario, Canada, 2004.

30. Silva, V., C. Casotto, D. Vamvatsikos, A. Rao and M. Villar, "Presentation of the Risk Modeller's Toolkit, the Open-Source Software for Vulnerability Assessment of the Global Earthquake Model", *16th World Conference on Earthquake Engineering. Santiago, Chile*, 2017.

31. Li, K., *Durability Design of Concrete Structures: Phenomena, Modeling, and Practice*, John Wiley & Sons, 2017.

32. Zhou, Y., B. Gencturk, K. Willam and A. Attar, "Carbonation-Induced and Chloride-Induced Corrosion in Reinforced Concrete Structures", *Journal of Materials in Civil Engineering*, Vol. 27, No. 9, p. 04014245, 2015.

33. Broomfield, J. P., *Corrosion of Steel in Concrete: Understanding, Investigation and Repair*, Crc Press, 2023.

34. Shekhar, S., J. Ghosh and J. E. Padgett, "Seismic Life-Cycle Cost Analysis of Ageing Highway Bridges Under Chloride Exposure Conditions: Modelling and Recommendations", *Structure and Infrastructure Engineering*, Vol. 14, No. 7, pp. 941–966, 2018.

35. Hancilar, U., K. Sesetyan and E. Cakti, "Comparative Damage and Economic Loss Estimations Under Design Basis Earthquake Level for Post-2000 Buildings in Istanbul", *Teknik Dergi*, Vol. 30, No. 3, pp. 9107–9123, 2019.

36. Pradhan, B. and B. Bhattacharjee, "Rebar Corrosion in Chloride Environment", *Construction and Building Materials*, Vol. 25, No. 5, pp. 2565–2575, 2011.

37. Vidal, T., A. Castel and R. François, "Analyzing Crack Width to Predict Corrosion in Reinforced Concrete", *Cement and Concrete Research*, Vol. 34, No. 1, pp. 165–174, 2004.

38. Ispir, M., A. O. Ates and A. Ilki, "Low Strength Concrete: Stress-Strain Curve, Modulus of Elasticity and Tensile Strength", *Structures*, Vol. 38, pp. 1615–1632, Elsevier, 2022.

39. Afsar Dizaj, E. and M. M. Kashani, "Nonlinear Structural Performance and Seismic Fragility of Corroded Reinforced Concrete Structures: Modelling Guidelines", *European Journal of Environmental and Civil Engineering*, Vol. 26, No. 11, pp. 5374–5403, 2022.

40. Zhang, Q., N.-H. Zheng, X.-L. Gu, Z.-Y. Wei and Z. Zhang, "Study of the Confinement Performance and Stress-Strain Response of RC Columns with Corroded Stirrups", *Engineering Structures*, Vol. 266, p. 114476, 2022.

41. Andisheh, K., A. Scott and A. Palermo, "Effects of Corrosion on Stress–Strain Behavior of Confined Concrete", *Journal of Structural Engineering*, Vol. 147, No. 7, p. 04021087, 2021.

42. Ma, J., L. Yu, B. Li and B. Yu, "Stress-Strain Model for Confined Concrete in Rectangular Columns with Corroded Transverse Reinforcement", *Engineering Structures*, Vol. 267, p. 114710, 2022.

43. Noh, H. M., Y. Sonoda, H. Tamai and I. Kuwahara, "An Analysis of Chemical-Mechanical Damage in Reinforced Concrete Beam", *International Journal of Integrated Engineering*, Vol. 10, No. 4, pp. 156–164, 2018.

44. Vu, N. S., B. Yu and B. Li, "Stress-Strain Model for Confined Concrete with Corroded Transverse Reinforcement", *Engineering Structures*, Vol. 151, pp. 472–487, 2017.

45. Şenol, E., *Development of Fragility Functions for Code Conforming Low-Rise Reinforced Concrete Buildings*, Master's Thesis, Boğaziçi University, 2021.

46. Önder, E., Z., *Epistemic Uncertainty in the Analytically Derived Fragility Functions: Multiple Stripe Analysis versus Cloud Analysis*, Master's Thesis, Boğaziçi University, 2022.

47. "ETABS v20.0.0-Extended 3D Analysis of Building Structures", Computers and Structures Inc., Berkeley, California, 2022.

48. "TS500-1984-Requirements for Design and Construction of Reinforced Concrete Structures", Turkish Standards Institute, Ankara Turkey, 1984.

49. "TS500-2000-Requirements for Design and Construction of Reinforced Concrete Structures", Turkish Standards Institute, Ankara Turkey, 2000.

50. "OpenSees v3.3.0-Open System for Earthquake Engineering Simulation", Pacific Earthquake Engineering Research Center of University of California, Berkeley, USA, 2008.

51. Neuenhofer, A. and F. C. Filippou, "Evaluation of Nonlinear Frame Finite-Element Models", *Journal of Structural Engineering*, Vol. 123, No. 7, pp. 958–966, 1997.

52. Menegetto, M. and E. Pinto, "Method of Analysis for Cyclically Loaded Reinforced Concrete Plane Frames Including Changes in Geometry and Non-Elastic Behavior of Elements Under Combined Normal Force and Bending", *Proc., IABSE Symp. on Resistance and Ultimate Deformability of Structures Acted on by Well-Defined Repeated Loads*, p. 15–22, IABSE, ETH Zurich, Zurich, Switzerland, 1973.

53. Popovic, S., "A Numerical Approach to the Complete Stress-Strain Curve for Concrete.", *Cement and Concrete Research*, Vol. 5, No. 3, pp. 583–599, 1973.

54. "Next Generation Attenuation-West2", Pasific Earthquake Engineering Research

Center, accesed at 2023, http://ngawest2.berkeley.edu/.

55. Cornell, A. and F. Jalayer, "Factored Nonlinear Displacement Demand Estimation Methods for Probability-Based Safety Assessment", *Annual Meeting Research Digest*, 2002-7, 2002.

56. Park, R., "Ductility evaluation from laboratory and analytical testing", *Proceedings of the 9th World Conference on Earthquake Engineering*, Vol. 8, pp. 605–616, Tokyo-Kyoto Japan, 1988.

57. De Luca, F., D. Vamvatsikos and I. Iervolino, "Near-optimal Piecewise Linear Fits of Static Pushover Capacity Curves for Equivalent SDOF Analysis", *Earthquake Engineering & Structural Dynamics*, Vol. 42, No. 4, pp. 523–543, 2013.

58. Vamvatsikos, D., "Quadrilinear Near-Optimal Fitting of Static Pushover Capacity Curves", , 2013, http://users.ntua.gr/divamva/software.html.

59. "Probable Earthquake Loss Estimations for Istanbul Province", Istanbul Metropolitan Municipality, 2019.

APPENDIX A: STRUCTURAL PLANS

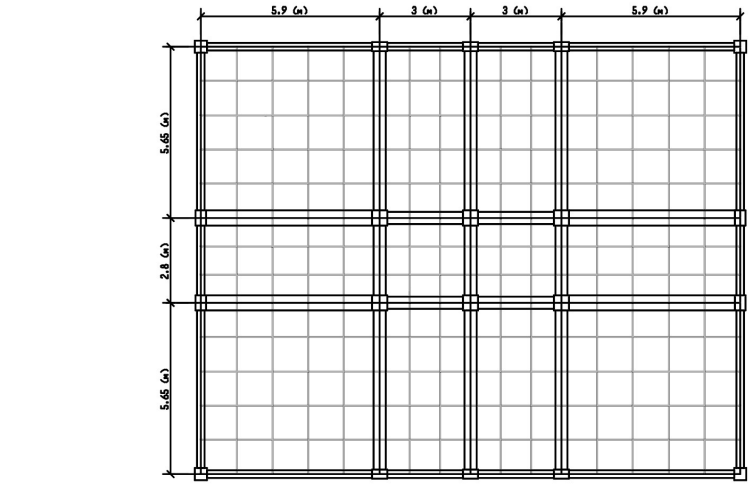

(a)

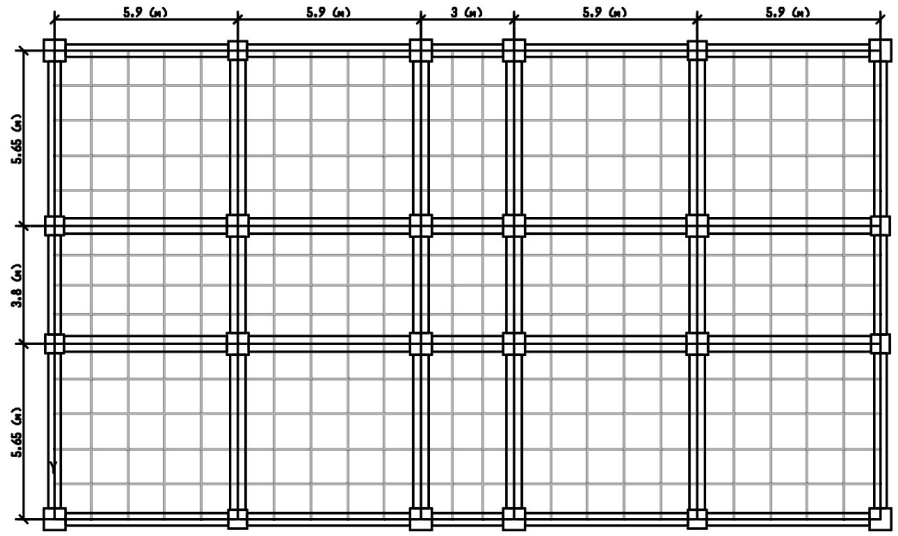

(b)

Figure A.1. Structural plans for study buildings (a) 3-story, (b) 6-story.